



If you have discovered material in AURA which is unlawful e.g. breaches copyright, (either yours or that of a third party) or any other law, including but not limited to those relating to patent, trademark, confidentiality, data protection, obscenity, defamation, libel, then please read our [Takedown Policy](#) and [contact the service](#) immediately

SIMULATION AND CONTROL OF
A STEPPING MOTOR

MICHAEL JUSTICE B.Sc

Ph.D THESIS

THE UNIVERSITY OF ASTON IN BIRMINGHAM
DEPARTMENT OF ELECTRICAL ENGINEERING

OCTOBER 1977

SIMULATION AND CONTROL OF

A STEPPING MOTOR

MICHAEL JUSTICE

Ph.D.

1977

SUMMARY

Open-loop operation of the stepping motor exploits the inherent advantages of the machine. For near optimum operation, in this mode, however, an accurate system model is required to facilitate controller design. Such a model must be comprehensive and take account of the non-linearities inherent in the system. The result is a complex formulation which can be made manageable with a computational aid.

A digital simulation of a hybrid type stepping motor and its associated drive circuit is proposed. The simulation is based upon a block diagram model which includes reasonable approximations to the major non-linearities. The simulation is shown to yield accurate performance predictions.

The determination of the transfer functions is based upon the consideration of the physical processes involved rather than upon direct input-output measurements. The effects of eddy currents, saturation, hysteresis, drive circuit characteristics and non-linear torque displacement characteristics are considered and methods of determining transfer functions, which take account of these effects, are offered.

The static torque displacement characteristic is considered in detail and a model is proposed which predicts static torque for any combination of phase currents and shaft position. Methods of predicting the characteristic directly from machine geometry are investigated.

Drive circuit design for high efficiency operation is considered and a model of a bipolar, bilevel circuit is proposed.

The transfers between stator voltage and stator current and between stator current and air gap flux are complicated by the effects of eddy currents, saturation and hysteresis. Frequency response methods, combined with average inductance measurements, are shown to yield reasonable transfer functions.

The modelling procedure and subsequent digital simulation is concluded to be a powerful method of non-linear analysis.

Indexing terms : Digital simulation, Modelling,
Non-linear systems, Stepping motors, Torque

TABLE OF CONTENTS

Page

Page

1	<u>INTRODUCTION</u>	
1.1	Stepping Motors	1
1.1.1	History	1
1.1.2	Advantages	2
1.1.3	Disadvantages	2
1.1.4	Types	2
1.2	Drive Circuit	3
1.3	Static Torque Displacement Characteristic	4
1.4	Voltage to Flux Transfer	5
1.5	Simulation of Motor and Drive	6
1.6	Control Aspects	6
2	<u>THE HYBRID STEPPING MOTOR</u>	
2.1	General Description	7
2.2	Machine Model	7
2.2.1	Description of model	11
2.2.2	Linearised model	14
2.3	Discussion	14
3	<u>DRIVE CIRCUIT</u>	
3.1	Introduction	16
3.2	Aspects of Circuit Design	19
3.2.1	State generation	19
3.2.2	Stator winding time constant	23
3.2.3	Stator winding copper loss	24
3.2.4	Power amplifier	25
3.2.5	Magnitude of voltage overdrive	27

	Page
3.2.6 Choice of winding resistance	27
3.3 Circuit Description	29
3.4 Modelling	31
3.5 Conclusions	32
4 <u>STATIC TORQUE DISPLACEMENT CHARACTERISTIC</u>	
4.1 Introduction	34
4.2 Measurement	37
4.3 Analysis of Measured Characteristics	38
4.3.1 Harmonic analysis of measured characteristics	38
4.3.2 Direct addition of phase torque	42
4.3.3 Comparison of measured and predicted harmonic torques	44
4.3.4 Conclusions	44
4.4 Static Torque Model Due to Chai	45
4.4.1 Single phase	48
4.4.2 Two phase	49
4.4.3 Conclusions	49
4.5 Extensions to Chai's Static Torque Model	51
4.5.1 Conclusions	55
4.6 Modelling and Parameter Estimation	56
4.6.1 Estimation of permeance coefficients from measured data	57
4.6.2 Estimation of permeance coefficients from machine geometry	66
4.6.3 Comparison of permeance coefficients	73
4.6.4 Numerical results and discussion	73
4.7 Conclusions	87

	Page
5	<u>VOLTAGE TO FLUX TRANSFER</u>
5.1	Introduction 89
5.2	Frequency Response Tests 92
5.3	Formulation of Transfer Function 92
5.4	Prediction of Transfer Function 96
5.4.1	Measurement of inductance 99
5.4.2	Determination of time constants 100
5.5	Calculation of Transient Current and Flux 102
5.6	Conclusions 103
6	<u>SIMULATION OF MOTOR AND DRIVE</u>
6.1	Introduction 104
6.2	Digital Simulation 105
6.2.1	Drive circuit and generated e.m.f. 108
6.2.2	Voltage to flux transfer 110
6.2.3	Torque production 117
6.2.4	Rotor dynamics 118
6.3	Prediction of Rotor Dynamics 119
6.4	Measurement of Rotor Dynamics 119
6.5	Typical Results 121
6.5.1	Discussion 137
6.6	Conclusions 138
7	<u>CONTROL ASPECTS</u>
7.1	Open-Loop 140
7.2	Closed-Loop 142
7.3	Conclusions 143
8	<u>CONCLUSIONS</u>
8.1	General 145
8.2	Suggestions for Further Work 148

APPENDICESA SIMULATION SOFTWARE

A.1	Introduction	150
A.2	Main Program	150
A.3	Subroutine RECAL2	159
A.4	Subroutine CURCAL	163
A.4.1	Subroutine derivatives	168
A.5	Subroutine TRIGTQ	169
A.6	Subroutine PLOTGR	171
A.7	Subroutine PLOTTR	174

B PROGRAM LISTINGS

B.1	Subroutine RECAL2	177
B.2	Subroutine CURCAL	178
B.3	Subroutine TRIGTQ	180

<u>REFERENCES</u>	181
-------------------	-----

<u>PUBLISHED WORK</u>	188
-----------------------	-----

LIST OF TABLES

TABLE		Page
I	Wave Drive Truth Table	21
II	Two Phase Drive Truth Table	21
III	Half Step Drive Truth Table	22
IV	Analysis of 4 A Characteristics	41
V	Comparison of Harmonic Torques	44
VI	Comparison of Harmonic Torques	50
VII	Estimated Values of P_0 and P_1	60
VIII	Estimated Values of P_3	63
IX	Estimated Values of P_2	65
X	Estimated Values of P_4	67
XI	Straight Line Arc Estimates of Permeance Coefficients	70
XII	Conformal Transformation Estimates of Permeance Coefficients	72
XIII	Moment Estimates of Permeance Coefficients	73
XIV	Comparison of Estimates of Permeance Coefficients	74
XV	Comparison of Estimates of Permeance Coefficients	81
XVI	Summary of Transfer Function	102
XVII	Drive Circuit Simulation Variables	111
XVIII	Voltage-to-Current Transfer Simulation Variables	116
XIX	Current-to-Flux Transfer Simulation Variables	117
XX	Rotor Dynamics Simulation Variables	119
XXI	Input Variables Required for Simulation	120
XXII	Simulation Output Parameters	120
XXIII	Simulation Input Data	121
XXIV	Parameters Available as Outputs	151
XXV	COMMON Statement RES	160

TABLE		Page
XXVI	COMMON Statement REC2	160
XXVII	COMMON Statement CURR	167
XXVIII	Subroutine CURCAL Arguments	167
XXIX	COMMON Statement TRIG	171
XXX	Subroutine TRIGTQ Arguments	171
XXXI	Subroutine PLOTGR Arguments	174
XXXII	Subroutine PLOTTR Arguments	176

LIST OF ILLUSTRATIONS

Page

FIGURE		Page
2.1	Cross Section of Stepping Motor Parallel to Shaft	8
2.2	Cross Section of Stepping Motor Perpendicular to Shaft	8
2.3	Block Diagram Model of Hybrid Stepping Motor	12
3.1	Block Diagram of Stepping Motor Drive Circuit	20
3.2	Switching Time as a Function of Overdrive Voltage	28
3.3	Simplified Drive Circuit (One Phase)	30
4.1	Static Torque Displacement Characteristic	34
4.2	Measurement of Static Torque Displacement Characteristic	37
4.3	Static Torque Displacement Characteristic Single Phase 2 A	39
4.4	Static Torque Displacement Characteristic Two Phase 6 A	40
4.5	Simplified PM Stepping Motor	46
4.6	Magnetic Equivalent Circuit (Thevenin)	47
4.7	Magnetic Equivalent Circuit (Norton)	47
4.8	Variation of Permeance Coefficients with Phase Current	60
4.9	Variation of Permeance Difference with the Product of Equal Phase Currents	61
4.10	Variation of Permeance Coefficients with Phase Current	64
4.11	Variation of Permeance Coefficient P_4 with Phase Current	68
4.12	Toothed Structure of Rotor and Stator	68
4.13	Approximation of Tooth Structure for Straight Line Arc and Conformal Transformation Methods	69

FIGURE		Page
4.14	Approximation of Tooth Structure for Moment Method	72
4.15	Prediction of 0.5 A, Single Phase, Static Torque Displacement Characteristic Using Permeance Coefficients Estimated from Measured Data	76
4.16	Prediction of 3 A, Two Phase, Static Torque Displacement Characteristic Using Permeance Coefficients Estimated from Measured Data	77
4.17	Prediction of 7 A, Two Phase, Static Torque Displacement Characteristic Using Permeance Coefficients Estimated from Measured Data	77
4.18	Prediction of 3 A, Single Phase, Static Torque Displacement Characteristic Using Permeance Coefficients Estimated from Measured Data	78
4.19	Prediction of 7 A, Single Phase, Static Torque Displacement Characteristic Using Permeance Coefficients Estimated from Measured Data	78
4.20	Prediction of 3 A, Two Phase, Static Torque Displacement Characteristic Using Permeance Coefficients Estimated from Machine Geometry	82
4.21	Prediction of 7 A, Two Phase, Static Torque Displacement Characteristic Using Permeance Coefficients Estimated from Machine Geometry	83
4.22	Prediction of 0.5 A, Two Phase, Static Torque Displacement Characteristic Using Permeance Coefficients Estimated by the 'Moment' Method	84
4.23	Prediction of 2 A, Two Phase, Static Torque Displacement Characteristic Using Permeance Coefficients Estimated by the 'Moment' Method	84
4.24	Prediction of 4 A, Two Phase, Static Torque Displacement Characteristic Using Permeance Coefficients Estimated by the 'Moment' Method	85
4.25	Prediction of 0.5 A, Single Phase, Static Torque Displacement Characteristic Using Permeance Coefficients Estimated by the 'Moment' Method	85

FIGURE	Page
4.26 Prediction of 2 A, Single Phase, Static Torque Displacement Characteristic Using Permeance Coefficients Estimated by the 'Moment' Method	86
4.27 Prediction of 4 A, Single Phase, Static Torque Displacement Characteristic Using Permeance Coefficients Estimated by the 'Moment' Method	86
5.1 Stator V/I Gain Response (0.2 A p-p)	93
5.2 Stator V/I Phase Response (0.2 A p-p)	93
5.3 Stator V/I Gain Response (4.0 A p-p)	94
5.4 Stator V/I Phase Response (4.0 A p-p)	94
5.5 Circuit Representation of Stator	95
5.6 Block Diagram Representation of Stator	96
5.7 Flux Linkage-Current Loop (3.8 A p-p)	98
5.8 Flux Linkage-Current Loop (0.17 A p-p)	98
5.9 D.C. Inductance Bridge	99
5.10 Average Inductance as a Function of Peak-to-Peak Current	101
6.1 Block Diagram Model of Hybrid Stepping Motor and Drive	107
6.2 Single Step Response of Unloaded Rotor	122
6.3 Prediction of Torque and Displacement in Response to a Single Step Demand	123
6.4 Prediction of 'a' Phase Current and Flux in Response to a Single Step Demand	124
6.5 Predictions of Single Step Response of Unloaded Rotor	125
6.6 Predictions of Torques in Response to a Single Step Demand	126
6.7 Single Step Response of Unloaded Rotor	128
6.8 Predictions of Torque in Response to a Single Step Demand	129

FIGURE		Page
6.9	Prediction of 'a' Phase Current and Flux in Response to a Single Step Demand	130
6.10	Single Step Response of Loaded Rotor	131
6.11	Prediction of Torque and Displacement in Response to a Single Step Demand	132
6.12	Multi-Stepping Response of Unloaded Rotor	133
6.13	Prediction of Torque in Response to a Multi-Stepping Demand	134
6.14	Multi-Stepping Response of Unloaded Rotor	135
6.15	Prediction of Torque in Response to a Multi-Stepping Demand	136
A.1	Main Program Flow Chart - Part 1	152
A.2	Main Program Flow Chart - Part 2	153
A.3	Main Program Flow Chart - Part 3	154
A.4	Main Program Flow Chart - Part 4	155
A.5	Main Program Flow Chart - Part 5	156
A.6	Main Program Flow Chart - Part 6	157
A.7	Main Program Flow Chart - Part 7	158
A.8	Subroutine RECAL2 Flow Chart - Part 1	161
A.9	Subroutine RECAL2 Flow Chart - Part 2	162
A.10	Subroutine CURCAL Flow Chart - Part 1	164
A.11	Subroutine CURCAL Flow Chart - Part 2	165
A.12	Subroutine TRIGTQ Flow Chart	170
A.13	Subroutine PLOTGR Flow Chart - Part 1	172
A.14	Subroutine PLOTGR Flow Chart - Part 2	173
A.15	Subroutine PLOTTR Flow Chart	175

ACKNOWLEDGEMENTS

I would like to thank Dr. R. C. Johnson for his advice, assistance and encouragement so freely given. I am also indebted to Mr. D. Paul for his help in obtaining equipment and components and to my wife, Berenice, for her sustained encouragement and support throughout and her supreme effort in the final months at the typewriter.

Financial support was provided by the U.K. Science Research Council.

1 INTRODUCTION

1.1 Stepping Motors

A stepping motor is an electromagnetic incremental actuator which converts digital pulse inputs to analogue motion. It is a device which, when energised by a voltage or current in a prescribed sequence, indexes in given angular or linear increments. The stepping motor operates in discrete steps of essentially uniform magnitude. When correctly used and controlled the output steps are always equal in number to the input pulses. At each pulse the output shaft advances one increment where it is magnetically or mechanically latched. Most stepping motors can operate bidirectionally as a result of changing the sequence in which windings are switched.

1.1.1 History

The first known electrical stepping motors were used by the British Royal Navy in the early 1930's in a remote positioning system for transmitting shaft rotations, with a bidirectional stepping motor operating in conjunction with a mechanically driven stepping transmitter (1). Such systems were developed and used successfully during the Second World War. However, during the same period continuous, closed-loop, servo systems were undergoing rapid development. Continuous systems possessed clear advantages over existing stepping systems in size, speed, accuracy and resolution. At this time the available technology did not support the development of stepping based control systems. By 1957 modest improvements had been made in stepping motor performance, and one machine tool application was reported using a stepping motor of large size and good performance (2).

In the last 20 years new interest has been focused on the stepping motor as a result of rapid developments in the field of electronics, particularly solid state electronics and digital computers. The stepping motor is an ideal prime mover for digital control systems since it readily interfaces with their outputs.

1.1.2 Advantages

The major advantage of a stepping motor is that it is usable as a prime mover in a position control system that does not require output measurement or the closure of the loop. Consequently the problem of instability associated with feedback systems is eliminated.

Other advantages of note are :-

- (i) No accumulative error
- (ii) Easily adapted to computer control
- (iii) The motor can be stalled without damage
- (iv) Bidirectional rotation

1.1.3 Disadvantages

The major difficulties associated with stepping motors arise from its under-damped single-step response. Other possible disadvantages are low efficiency and fixed step angle. However, by using a well designed controller, incorporating a high efficiency drive circuit, it is possible to overcome the majority of its limitations.

1.1.4 Types

There are six principal types of stepping motor :-

- (i) Solenoid

- (ii) Electromechanical
- (iii) Variable Reluctance
- (iv) Permanent-Magnet Stator
- (v) Permanent-Magnet Rotor
- (vi) Hybrid (synchronous-inductor)

The machine used as a subject for the work presented in this thesis is of the hybrid type and is described in Chapter 2. Many of the conclusions and results, however, are applicable to most types with particular relevance to the variable reluctance, permanent-magnet stator and permanent-magnet rotor machines.

1.2 Drive Circuit

The overall performance of a stepping motor system is influenced, to a considerable extent, by the type of drive circuit employed. For this reason a system simulation must include drive circuit modelling if accurate performance predictions are to be made. A constant current drive circuit is required if optimum performance of the motor is to be achieved. However, in practice, drive circuits cannot supply constant current when switching inductive loads. Thus, if true constant current is assumed, over simplification of the system model results leading to considerable error.

The contributions by Beling^{10,11,12}, on the subject of drive circuits, are comprehensive. He considers the problems of driving stepping motors and provides a range of circuit solutions together with their advantages and disadvantages.

A drive circuit of the bipolar type is described in Chapter 3. This circuit ensures high efficiency by fully utilising the motor

windings. Near constant current is achieved by using the bilevel principle. A model of this circuit is included in the system simulation, thus ensuring the effects of the winding time constants are taken into account.

Aspects of circuit design are considered in Chapter 3 with the object of presenting a general design philosophy for high efficiency systems.

1.3 Static Torque Displacement Characteristic

The accurate prediction of the flux to torque transfer function is an essential feature of a stepping motor model. The key to this prediction is a mathematical representation of torque production which will account for the observed form of the characteristic with one phase excited and with both phases excited. Most authors assume the static torque displacement characteristic to be linear which limits accurate predictions, of rotor dynamics, to small displacement angles about the null point; a result of little practical significance. Snowdon and Madsen³ were the first to attempt to derive a more accurate model of the static torque displacement characteristic. However, they obtain the torque available in the two phase case by adding the torque produced in one phase to the torque produced in the other phase shifted by 90 electrical degrees. This procedure is shown to be erroneous.

The most comprehensive analysis on the formulation of static torque has been contributed by Chai⁴. The two phase result does not rely on the erroneous use of superposition and the method predicts results which are observable in practice. The static

torque model due to Chai⁴ is extended to take account of an increased number of Fourier components of permeance which enables a higher degree of prediction accuracy to be achieved. A further extension allows the prediction of torque for any combination of phase currents which removes the restriction of either having equal currents in each phase or one phase current set to zero. In this form the model is used to predict time varying torque from time varying flux.

It is shown that, for fields which do not tend to saturate the machine iron, it is feasible to predict the static torque displacement characteristic directly from the machine geometry.

1.4 Voltage to Flux Transfer

Many authors have reported successful prediction of the stator current transient based upon a single time constant transfer function between stator voltage and current, estimates of the transfer function having been based upon inductance yielded by a.c. bridge measurements. Such a procedure failed in the case of the machine under investigation; the actual current rise being many times slower than that predicted. Investigation has shown that the effects of eddy currents and hysteresis are responsible for this discrepancy.

The voltage to flux transfer function can be estimated using frequency response tests. It is shown, however, that when using this method alone magnetic hysteresis of the machine iron can seriously affect transfer function predictions.

A method is proposed in Chapter 5 which uses a combination of average inductance measurements and frequency response tests to

deduce the voltage to flux transfer function of the machine.

1.5 Simulation of Motor and Drive

The dynamic performance of a stepping motor is, in general, highly non-linear, in consequence, mathematical models, that adequately describe these non-linearities, are complex and will, in general, require a computing aid to facilitate their solution.

A digital simulation is presented in Chapter 6 which uses the FORTRAN programming language. A block diagram of the stepping motor and drive is used as the basis of the simulation. The function blocks, and the links between them, are translated into computer software. In general the functional blocks are written as subroutines, or parts of subroutines, with linking being achieved by calls to the subroutines from a main program or subprogram.

1.6 Control Aspects

The main advantage of a stepping motor is realised when it is used in open-loop. However, near optimum performance of the machine, in this mode, is only possible with a controller designed on the basis of an accurate system model. Such a model must take account of eddy currents, hysteresis, non-linear aspects of the static torque displacement characteristic and drive circuit operation if accurate predictions of the system performance are to be made. Aspects of the open-loop and closed-loop operation of the stepping motor are considered in Chapter 7.

2 THE HYBRID STEPPING MOTOR

2.1 General Description

The construction of the stepping motor used as the subject of the work presented in this thesis is shown in Figures 2.1 and 2.2. This type of machine originated as a synchronous inductor motor. With the stator energised by a.c. it is a slow speed, self starting device. If the alternating excitation is replaced by direct excitation which is capable of being switched in a four step sequence, then the machine can be operated as a stepping motor. When used in this way the machine is usually known as a hybrid stepping motor or a hybrid vernier stepping motor.

The stator has eight salient poles and is two phase, four pole, bifilar wound. The stator teeth are at a pitch of 40 for a full circle, with four actual teeth per salient pole. The rotor has two soft iron discs each with 42 teeth, one disc being offset by half a rotor tooth pitch on the other. The discs are separated by a cylindrical permanent magnet, magnetised in the axial direction, such that one disc is a north pole and the other a south. The arrangement is effectively two machines on the same shaft; the offsetting of one rotor disc by half a tooth pitch with respect to the other ensures that torque produced by each half machine is additive.

2.2 Machine Model

Most authors have concentrated on predicting the single step transient (index) response with the philosophy that, if this response can be accurately predicted then it is a simple matter

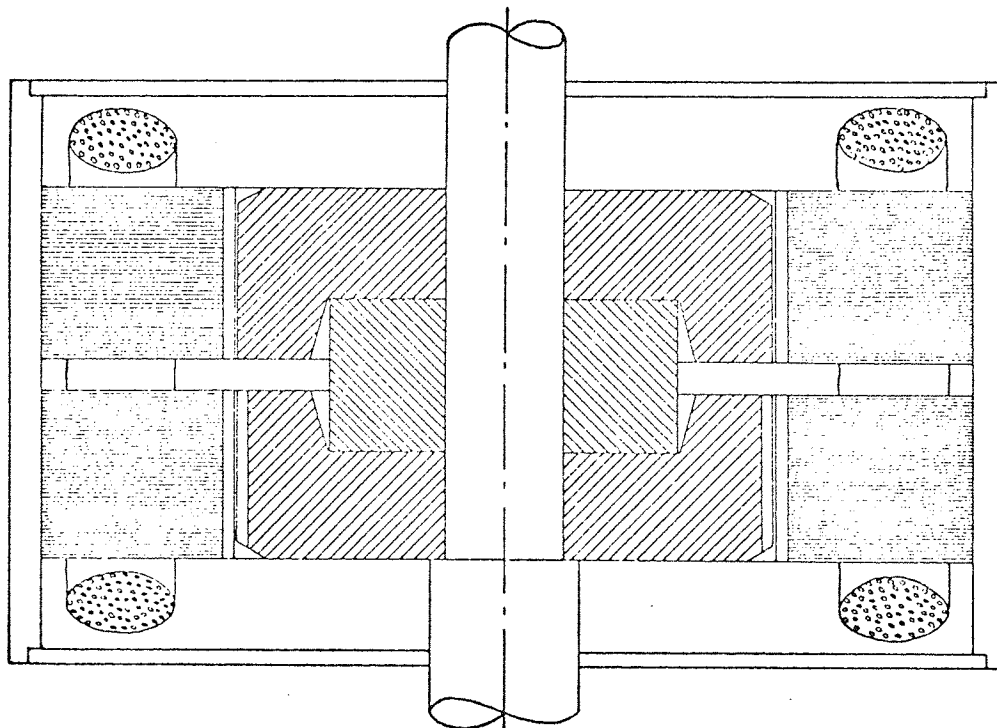


FIGURE 2.1 Cross Section of Stepping
Motor Parallel to Shaft

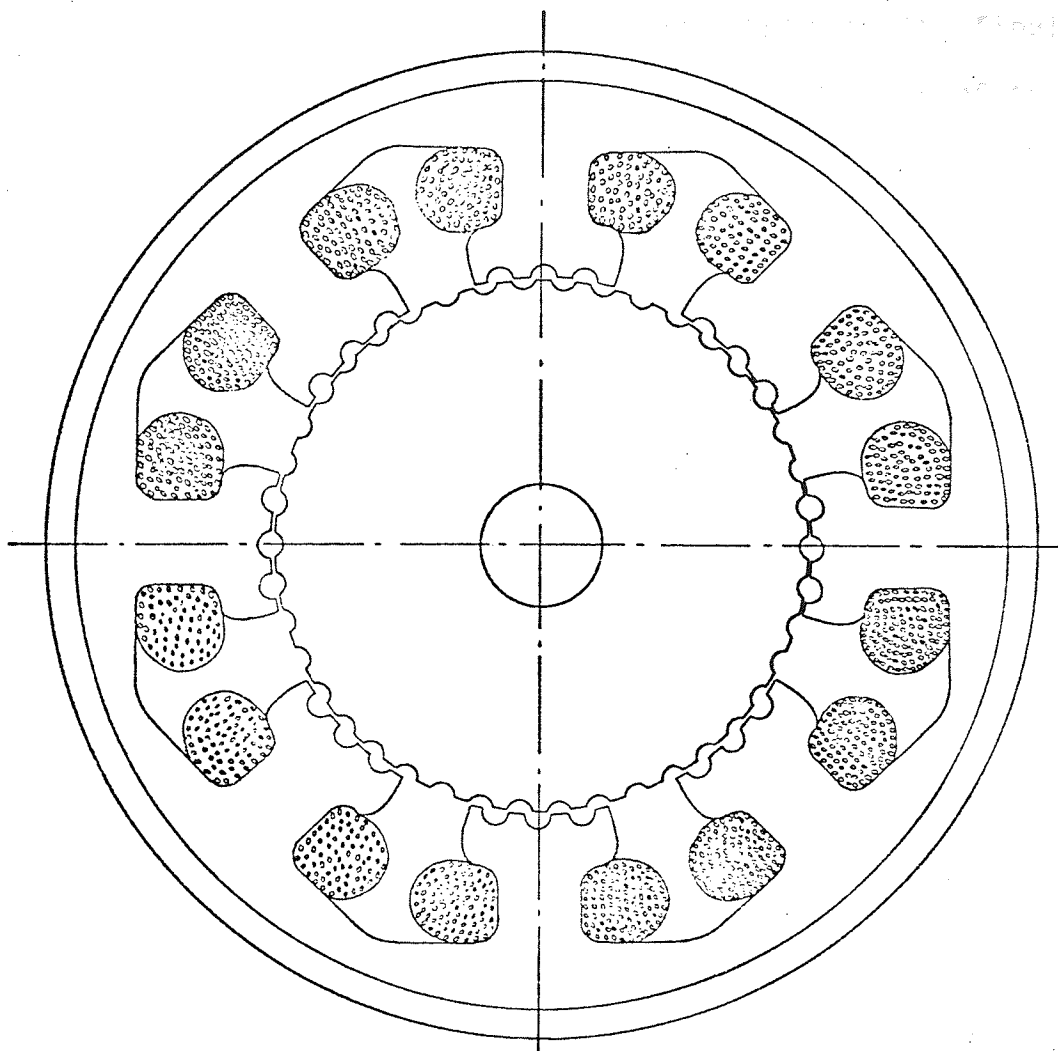


FIGURE 2.2 Cross Section of Stepping
Motor Perpendicular to Shaft

to predict the multi-stepping response by using the final conditions from one step as the initial conditions of the next. This philosophy does depend on the model being accurate for large displacement angles. Therefore, equations linearised on the basis of small displacements about the null are not suitable for such extensions.

O'Donohue⁵ was the first author to attempt to model the stepping motor and to predict its single step transient response. His approach is to apply classic servomotor treatment to the stepping motor. His object is to yield a linear second order differential equation expressed in terms of natural frequency and damping factor. He considers the effects of back e.m.f. but not the effects of inductance which leads to the erroneous conclusion that the response is second order when operated from a constant voltage source. The second order equation yielded should, however, be usable for predicting the rotor dynamics when it is displaced by a small angle and then released but he erroneously relates the voltage constant with displacement and does not correctly formulate the model. Consequently, the second order expression yielded is incorrect, in particular it implies that the magnitude of the machine step is directly proportional to the magnitude of the voltage applied.

Kiebertz⁶ follows closely the approach of O'Donohue⁵ but correctly defines the voltage constant. He yields a second order linear differential equation by defining linear torque and voltage constants and neglecting the effects of inductance. The expressions given for natural frequency and damping factor are misleading since they imply independence of current; it is assumed that the torque constant is defined for one particular current.

As in O'Donohue's⁵ contribution the result implies that the magnitude of the machine step is directly proportional to the voltage applied.

Robinson and Taft⁷ have contributed a comprehensive analysis of the dynamics of stepping motors. They start by including effects of inductance, back e.m.f. and a non-linear torque displacement characteristic. They linearise the equation for a small deviation at the end of the step and, by considering the current to be constant, yield a linear second order differential equation to describe the dynamics of the rotor for small displacements about the null. Multi-stepping operation is investigated by using the simplifying assumption that the machine is operated from a constant current source. The torque displacement characteristic is assumed to be a sinusoid whose magnitude is proportional to current. The resulting non-linear differential equation is analysed using phase plane techniques.

Pickup and Tipping⁸ recognise the importance of accounting for eddy currents when modelling the stepping motor. Although their work is specifically associated with a variable reluctance machine their conclusions are applicable to other classifications of motor, in particular to machines with solid rotors. They show that eddy currents delay the growth of magnetic flux and thus retard the motion of the rotor.

The analysis of Hughes and Lawrenson⁹ is similar to that of Robinson and Taft⁷ with the important difference that constant current is not assumed when linearising the equations. The solution is third order and is useful to illuminate the mechanisms of electromagnetic damping. To extend this analysis to the

single step transient response must be approached with caution. The mechanism leading to the third order response proposed by Hughes and Lawrenson⁹ is due to the motion of the rotor producing an e.m.f. in the stator windings which produces a disturbance of stator current when supplied from a constant voltage source. Such an analysis is strictly only valid for predicting the dynamics when the rotor is displaced by a small angle and then released. The third order type of response that may be observed when the stator is supplied with a voltage step is due to second order dynamics superimposed upon the exponential current (and therefore torque) increase.

2.2.1 Description of model

Figure 2.3 illustrates, in block diagram form, the proposed model of the hybrid stepping motor.

The notation used in the block diagram is as follows :-

N_r	number of rotor teeth
θ_e	rotor angle (electrical) (rad)
θ_m	rotor angle (mechanical) (rad)
ω_r	angular velocity of rotor (rad/s)
J	total inertia on motor shaft (kg m^2)
B	viscous friction coefficient of motor and load (N m s)
T_F	coulomb friction torque of motor and load (N m)
T	torque developed by the motor (N m)
I_a	current in 'a' phase winding (A)
I_b	current in 'b' phase winding (A)
e_{b_a}	generated e.m.f. in 'a' phase (V)
e_{b_b}	generated e.m.f. in 'b' phase (V)
s	Laplace operator

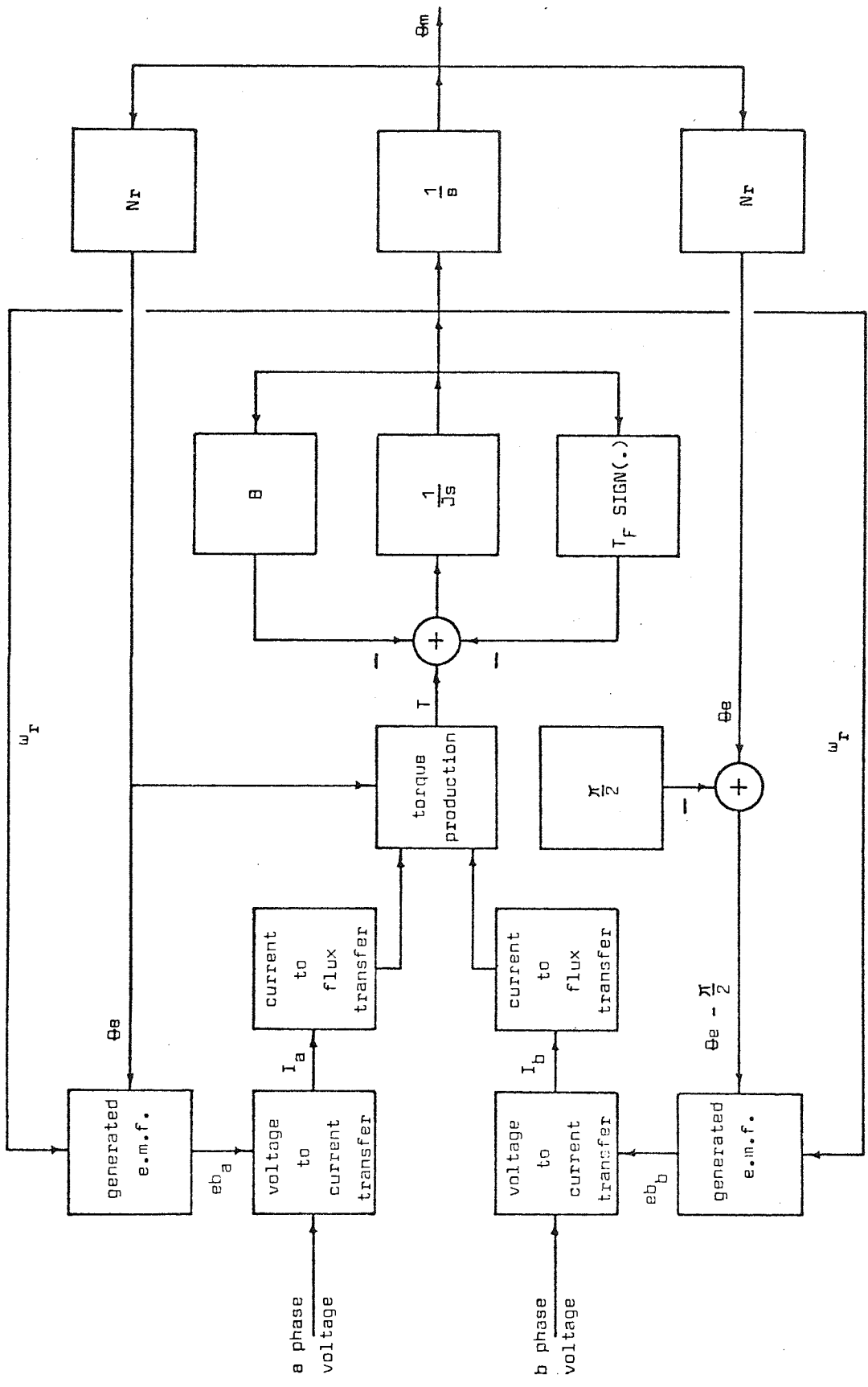


FIGURE 2.3 Block Diagram Model of Hybrid Stepping Motor

For accurate prediction of the rotor dynamics all the aspects included in the block diagram must be taken into account. The non-linear representation is not amenable to analysis but is solvable with the aid of a digital computer. For a complete system simulation the characteristics of the drive circuit must be included. Details of the digital simulation of the motor and drive are contained in Chapter 6.

The voltage to flux transfer function is complicated by eddy currents which are shown to be important (8). Consequently, the function contains more than one time constant. Further details of this function, including a method for its estimation, are to be found in Chapter 5.

The stator input voltages are modified by e.m.f.s, when the rotor is in motion, due to the permanent magnet field cutting the stator coils. These generated e.m.f.s are a function of electrical angle and the angular velocity of the rotor. There is a 90 electrical degree ($\pi/2$ radians) displacement between the e.m.f.s in each phase due to the two phase construction of the machine stator.

For an accurate prediction of torque, particularly at large displacement angles, a complex formulation is required. The model should yield torque as a function of displacement angle and the two phase fluxes and not rely on superposition of one phase torque upon the other. A model of this type is presented in Chapter 4.

When torque is applied to the rotor it moves under the constraints of inertia, coulomb friction and viscous friction. In general a second order type of response is executed by the rotor, the

values of B and J are such that the response is underdamped. The conversion between mechanical angle (θ_m) and electrical angle (θ_e) is performed by the factor N_r (number of rotor teeth) which, in the machine under investigation, is 42.

2.2.2 Linearised model

It is sometimes useful to consider a linearised and simplified form of the model presented in Figure 2.3. The linearisation is accomplished by considering small displacements about the null and therefore the results yielded by the analysis are only applicable for this condition. The use of such a procedure may be justified by the simple result yielded which can give an insight into the mechanisms of the motion and how the values of certain parameters influence that motion. Many such linearisations and simplifications are to be found in the literature with good examples being Robinson and Taft⁷ who assume constant current which leads to a second order equation, and Hughes and Lawrenson⁹ who assume constant voltage leading to a third order equation.

2.3 Discussion

Simplified, linear representations of the model presented in Figure 2.3 are frequently encountered in the literature. Such representations have a limited use since their results are confined to small deviations about the null with a disturbance injected into the system by a mechanical displacement of the rotor whilst the stator is connected to a constant current or constant voltage source. There are some optimistic extensions of this procedure which, having made the linearisation, seek to use the result to predict the single step transient with a

voltage or current step applied to the stator.

For successful prediction of the single step transient response, and hence the multi-stepping performance, of a stepping motor a comprehensive model of the type presented in Figure 2.3 should be employed together with the characteristics of the associated drive circuit. Such a model takes account of the effects of eddy currents, generated e.m.f. and the non-linear torque displacement characteristic, all of which have a considerable influence upon the rotor dynamics. A disadvantage of such a model is that, for it to yield results, it requires some form of computing aid to solve the complex representation. Analogue computers, digital computers or a hybrid arrangement, may be used for such a task.

3 DRIVE CIRCUIT

3.1 Introduction

The overall performance of a stepping motor system is influenced, to a considerable extent, by the type of drive circuit employed. For this reason a system simulation must include drive circuit modelling if accurate performance predictions are to be made. The drive circuit is an exceedingly important part of the system with parameters such as efficiency, power dissipation and cost being largely dependent upon it.

Developments in the fields of solid state electronics and power electronics are rapid. This fact makes it impossible to present an optimum design for a drive circuit since, such a design rapidly becomes obsolete. It is possible, however, to consider a general design philosophy that can be applied using 'state of the art' devices.

Snowdon and Madsen³ consider, briefly, the problems of switching an inductive load. They advocate the use of external resistance, to reduce the time constant, and the increase of the applied voltage. They report an improvement in torque output at higher stepping rates but fail to recognise the poor efficiency of such an arrangement. They favour the use of bifilar windings to allow single ended power supplies to be used. Bifilar windings are not, however, an absolute necessity when single ended power supplies are to be employed. A full bridge circuit of the type to be described, drives a full winding from a single ended supply. They erroneously propose the use of a small wire gauge to increase the ratio of resistance to inductance, thereby decreasing

the time constant. It is not, however, possible to change the time constant by changing the winding resistance when the winding space is fixed. Kieburtz⁶ repeats, exactly, the contribution on the subject, including the erroneous statement on winding time constant, made by Snowden and Madsen³.

Beling^{10,11,12} has provided a very comprehensive contribution to the subject of drive circuits. His early publication (10) discusses wave drive, two phase drive and half step drive systems giving their advantages and disadvantages. The provision of a high voltage to move current into and out of the windings is recognised as the basic problem of drive circuit design for high speed operation of the stepping motor. A range of circuit solutions are presented and their advantages and disadvantages clearly stated. His later publications (11,12) bring up to date his earlier contribution. The driving of a high power stepping motor is considered in (11) where efficiency is of considerable importance. He observes that voltages between 80 V and 100 V, and currents between 10 A and 15 A are the limitations imposed by present day (1976) semi-conductor technology. He concludes that a bipolar chopper, using a transistor bridge to provide reversible current to each winding, yields an optimum design solution. In (12) the interaction of stepping motors and drive circuits in producing extraneous shaft motions, described as resonances, is considered. He reports that there is a trend towards high efficiency drive circuits of the chopper type with high chopping rates employing optical isolators to drive the transistor bridge. Such high efficiency drive circuits do, however, emphasise resonance effects.

Maginot and Oliver¹³ discuss various types of logic and power circuitry that have been used to successfully drive stepping motors. Whilst this is a comprehensive paper it has little to add to the contributions of Beling^{10,11,12}. Several methods of suppressing the voltage spike when switching off the inductive current are considered. The use of fast recovery diodes, to isolate the high and low voltage supplies in bilevel circuits, is advocated.

Kordik and Senica¹⁴ consider how different types of voltage spike suppression technique affect the stepping motor performance. As is expected, they show that, as the damping provided by the suppression network increases, the rate of current change at switch off decreases, giving rise to a less oscillatory single step response and a lower pull-in rate.

Lawrenson et al.¹⁵ present a simple voltage multiplying circuit which is used to increase the drive voltage for the first few steps when starting and the last few steps when stopping. Using this technique together with optimally timed drive pulses, improvements of starting/stopping rates by as much as 300% are claimed. The circuit is useful for applications requiring high starting/stopping rates with a modest high speed performance. Improvements in high speed performance are only possible with a circuit that can provide full drive current from a high voltage supply for 100% of the time.

Some authors have considered the use of thyristors as power switching elements in drive circuits. Beling¹⁰ considers their use in a phase control mode to maintain the current at a set value. The slow response time of such a system is given as a

disadvantage that drastically limits the starting and stopping rates. Johnson and Steele¹⁶ present a thyristor cyclo-inverter with a high commutating frequency. Such an arrangement is capable of a much faster response than the phase control method. The circuit described is claimed to have a particular advantage when driving power stepping motors due to its high power handling capability. Present trends, however, suggest that power transistors will replace thyristors in this role.

3.2 Aspects of Circuit Design

A block diagram of a stepping motor drive circuit for driving a two phase stepping motor is given in Figure 3.1. Depending upon the type of circuit used the phase winding represented as 1 and 2 may be the two halves of a bifilar winding or, alternatively, the same winding driven by two separate power amplifiers; one amplifier drives current in one direction, the other amplifier drives current in the opposite direction. The object of the power amplifier is to switch currents, in the inductive load, as rapidly as possible. This can be achieved by increasing the supply voltage and by decreasing the circuit time constant. The state generator is a logic circuit which switches the power amplifiers in a prescribed combination at a rate set by the incoming pulses and a sequence set by the direction demand. There are three basic combinations of phase currents in general use known as, wave drive, two phase drive, and half step drive.

3.2.1 State generation

Logic circuits for state generation are of standard form and are well documented in the literature (10,13). Truth tables for wave drive, two phase drive and half step drive are given in

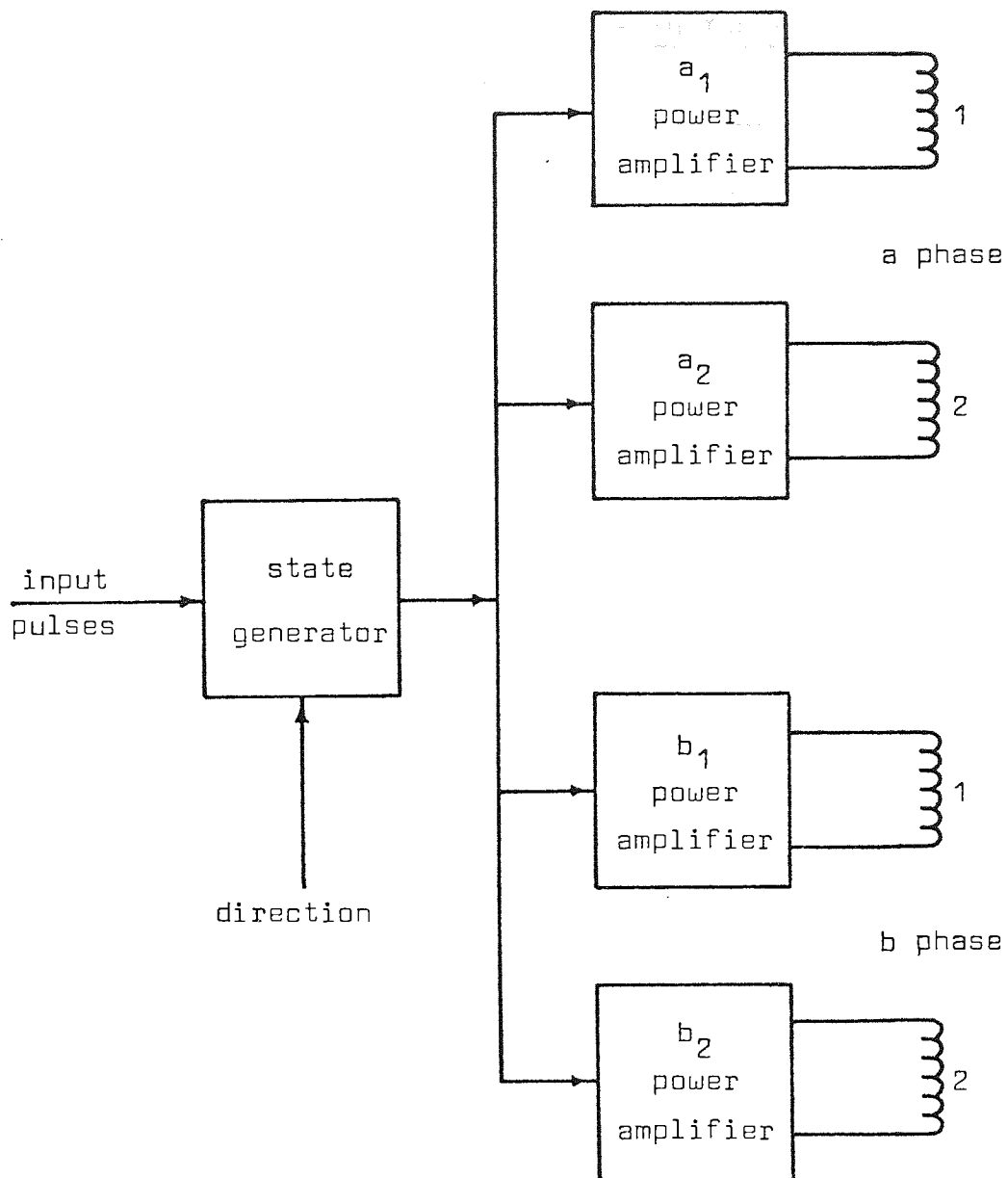


FIGURE 3.1 Block Diagram of Stepping Motor Drive Circuit

Table I, II and III respectively.

In the truth tables, the logic '1' state represents the winding switched on to the energising supply and conversely, the logic '0' state represents the off condition. For configurations using bifilar windings suffix 1 and 2 indicate the two halves of each winding with the understanding that the energisation of one produces the opposite m.m.f. to the energisation of the other.

TABLE I Wave Drive Truth Table

Input Pulse	Phase			
	a_1	b_1	a_2	b_2
1	1	0	0	0
2	0	1	0	0
3	0	0	1	0
4	0	0	0	1

TABLE II Two Phase Drive Truth Table

Input Pulse	Phase			
	a_1	b_1	a_2	b_2
1	1	0	0	1
2	1	1	0	0
3	0	1	1	0
4	0	0	1	1

For configurations using the complete phase winding suffix 1 and 2 should be taken to indicate energisation of the winding in opposite senses. Two phase drive is normally preferred to wave drive since, in two phase drive, both phases are energised at the same time whereas, in wave drive only one phase is energised. Thus, for a given machine, more output torque is possible with two phase drive than with wave drive. Torque production with

TABLE III Half Step Drive Truth Table

Input Pulse	Phase			
	a ₁	b ₁	a ₂	b ₂
1	1	0	0	1
2	1	0	0	0
3	1	1	0	0
4	0	1	0	0
5	0	1	1	0
6	0	0	1	0
7	0	0	1	1
8	0	0	0	1

both phases energised is a complex mechanism (Chapter 4). However, if it is possible to approximate the static torque displacement characteristic to a sinusoid, the maximum torque output, when two phase driven, will increase by a factor of $\sqrt{2}$ over that when wave driven. It should be observed that the rotor position at the stable equilibrium points is different for wave and two phase drive, there being a displacement of 45 electrical degrees (half step) between the two methods of energisation. In some applications the de-energised detent torque (cogging torque) available in permanent magnet stepping motors is an important feature. It should be noted, therefore, that the stable equilibrium points when de-energised align with the stable equilibrium points when energised only when wave driven. There will be 45 electrical degrees (half step) displacement between energised and de-energised equilibrium when two phase driven.

Half step drive is, effectively, a combination of two phase drive and wave drive, changing from one method to the other at successive input pulses. Thus, the equilibrium point moves 45 electrical degrees (half step) on the receipt of an input pulse. A disadvantage of this method of drive is that the torque changes between adjacent positions giving alternate 'weak' and 'strong' steps. An advantage claimed by Beling¹⁰ for half step drive is that the method can reduce resonance problems.

3.2.2 Stator winding time constant

The resistance of the stator coil, R_c , is proportional to the total length of the conductor, l , and inversely proportional to the cross-sectional area of the conductor, a .

$$R_c \propto \frac{l}{a}$$

If the mean length of one turn in the winding space is l_c , the total winding cross-sectional area available in the winding space is a_c , and the number of stator turns is N , it is clear that

$$l = N l_c \quad \text{and} \quad a = \frac{a_c}{N}$$

$$R_c \propto \frac{l_c}{a_c} N^2$$

Thus, for a given winding space

$$R_c \propto N^2$$

and

$$R_c = K_r N^2$$

where K_r is a constant of the machine and conductor material.

It can also be shown that

$$L_c = K_i N^2$$

where L_c is the inductance of the stator and K_i a constant of the machine.

But time constant $\tau = \frac{L}{R}$

Therefore, $\tau = \frac{K_i}{K_r}$

Thus, for a given winding space, excluding the extremes of very large and very small diameter conductors, the winding time constant is fixed.

3.2.3 Stator winding copper loss

For a given machine a fixed maximum value of m.m.f. will be required to be supplied by the stator coils.

$$\text{m.m.f.}_m = I_m N$$

also

$$R_c = K_r N^2$$

$$\text{Maximum stator winding copper loss} = I_m^2 R_c = K_r \text{m.m.f.}_m^2$$

Thus, for a given machine, the maximum stator winding copper loss is not a function of the resistance of the winding, it is a constant of the machine.

3.2.4 Power amplifier

For machines with bifilar windings each half may be switched in turn to produce a reversal of m.m.f. A drive circuit that uses this method is known as unipolar. A drive circuit that uses the complete phase winding and reverses the current in that winding is known as bipolar. Bipolar drive circuits are to be preferred since this method makes full use of the machine winding space and is capable of a theoretical increase in torque of 100% over unipolar drive circuits. Saturation effects and a non-linear torque displacement characteristic, limit the torque gain to a value somewhat below the theoretical maximum.

The power amplifier is required to switch current, as rapidly as possible, into, and out of, the inductive stator windings of the stepping motor. One method by which fast switching may be achieved is by the reduction of the circuit time constant. This can be effected, for a given winding space, by the addition of external resistance. The supply voltage is then increased so that the rated current is carried by the stator winding in the steady state. As the external resistance and supply voltage is increased the closer the approximation to constant current; the ideal condition. However, a considerable proportion of the total power is dissipated in the external resistance causing the overall system efficiency to be exceedingly low. Such circuits are of use only when speed and torque requirements are small and efficiency is not important.

It is clear that the ideal drive circuit will provide a step of stator current to the appropriate winding when demanded by the input conditions. Since the stator windings are generally highly inductive, with a small d.c. resistance, a step of current can only be established by a voltage which is an impulse superimposed on a small step. Circuits approximating to this ideal state are known as bilevel since, during the switching transient, the stator winding is switched to a high voltage and when the current has reached the set value the high voltage is switched off and the stator is left connected to a low voltage supply which maintains the current until the next switch demand. Such circuits are capable of establishing stator currents very rapidly and have the advantage that they are much more efficient than configurations employing added resistance.

A development of the bilevel principle is achieved by discarding the low voltage supply. Such a configuration, known as a chopper circuit, can only supply high voltage pulses. The stator winding is switched to the high voltage supply until the current reaches a set value, the voltage is then switched off. The current decays until it falls to a slightly lower set value at which point the high voltage is restored. The high voltage is, therefore, switched on and off at a rate which is dependent upon, for a given machine, the switching hysteresis and the switching rates of the drive transistors. The chopper circuit is potentially more efficient than the bilevel circuit since, being continually in the switching mode, little power is dissipated. The bilevel circuit, on the other hand, dissipates some power in the low voltage circuit where some transistors are generally in the active state. A disadvantage of chopper circuits is that the

switching frequencies can often exacerbate resonance problems and generate objectionable audio noise. High speed switches and a small switching hysteresis can be employed in an attempt to overcome this problem.

3.2.5 Magnitude of voltage overdrive

Drive circuits of the bilevel and chopper type rely on the principle of switching on a high voltage supply until the current has reached a set value. It is important to consider the magnitude of this overdrive since, semi-conductor technology imposes a restriction on the maximum voltage usable, but the resistance to which the stator is wound, and thus the minimum steady state voltage for rated current, can be changed.

Figure 3.2 presents a plot of normalised switching time against normalised overdrive voltage. Switching time is normalised against stator time constant and overdrive voltage is normalised against stator rated voltage. The graph shows that there is no great advantage in exceeding an overdrive voltage of ten times stator rated voltage, giving a switching time of approximately one tenth of the stator time constant.

3.2.6 Choice of winding resistance

As has been shown (para. 3.2.3), the stator winding copper loss is a constant for a given machine. Consequently, as far as the machine losses are concerned, the stator can be wound to any resistance. Losses in the drive circuit, however, will be a function of the volt drop between the collectors and the emitters of saturated drive transistors ($V_{ce(sat)}$) since, in well designed circuits, rated stator current will be passed by saturated transistors. This consideration indicates that drive circuit losses are minimised by increasing the winding resistance.

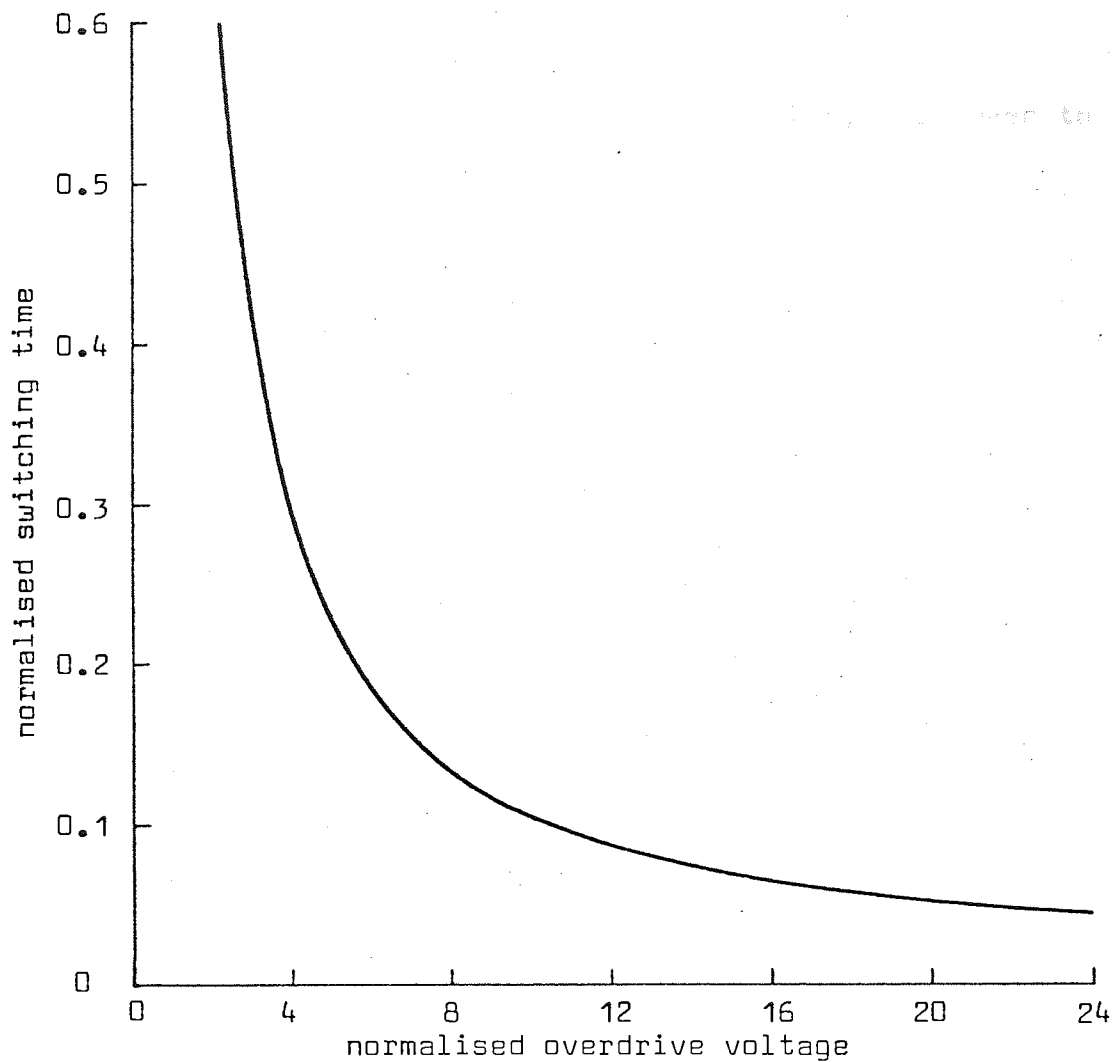


FIGURE 3.2 Switching Time as a Function of Overdrive Voltage

On the other hand, if winding resistance is increased too far, the requirement for ten times voltage overdrive may not be possible due to the voltage breakdown characteristics of the transistors employed. Thus, the stator should be wound with the maximum number of turns such that a ten times overdrive voltage will not cause the breakdown characteristics of available transistors to be exceeded.

3.3 Circuit Description

A high efficiency drive circuit of the bilevel type is used to drive the stepping motor. Although the machine under consideration is bifilar wound the circuit is bipolar to ensure optimum use of the machine winding space. Bipolar working is achieved by a full bridge circuit powered by two single ended supplies.

A simplified circuit diagram, for one phase, is presented in Figure 3.3. The switching circuit is designed such that when transistors Tr_3 and Tr_4 are on, transistors Tr_1 and Tr_2 are off, and vice versa. The voltage drop across resistor R_1 is fed back and subtracted from the reference to achieve current control. When the loop has a large error, i.e., the current has not reached the set point, it is arranged that transistor Tr_{10} is switched on, applying a high voltage to the winding during the current transient. When the set point is reached, Tr_{10} is switched off and current is drawn from the low voltage supply.

Consider that, initially, current is passing from A to B, in the stator winding, at its set value. Switch inputs G and F are negative holding transistors Tr_1 and Tr_2 off. Switch inputs E and H are positive which, with the circuit values chosen, causes transistor Tr_3 to saturate and transistor Tr_4 to be active, holding the current at the set value. A comparator circuit is used to activate the high voltage switch, Tr_{10} . The system error is compared against a preset value and it is arranged that, when the system error is small, switch input C is negative holding transistor Tr_{10} off. Thus, stator current is drawn from the low voltage supply via diode D_3 , which isolates the two voltage

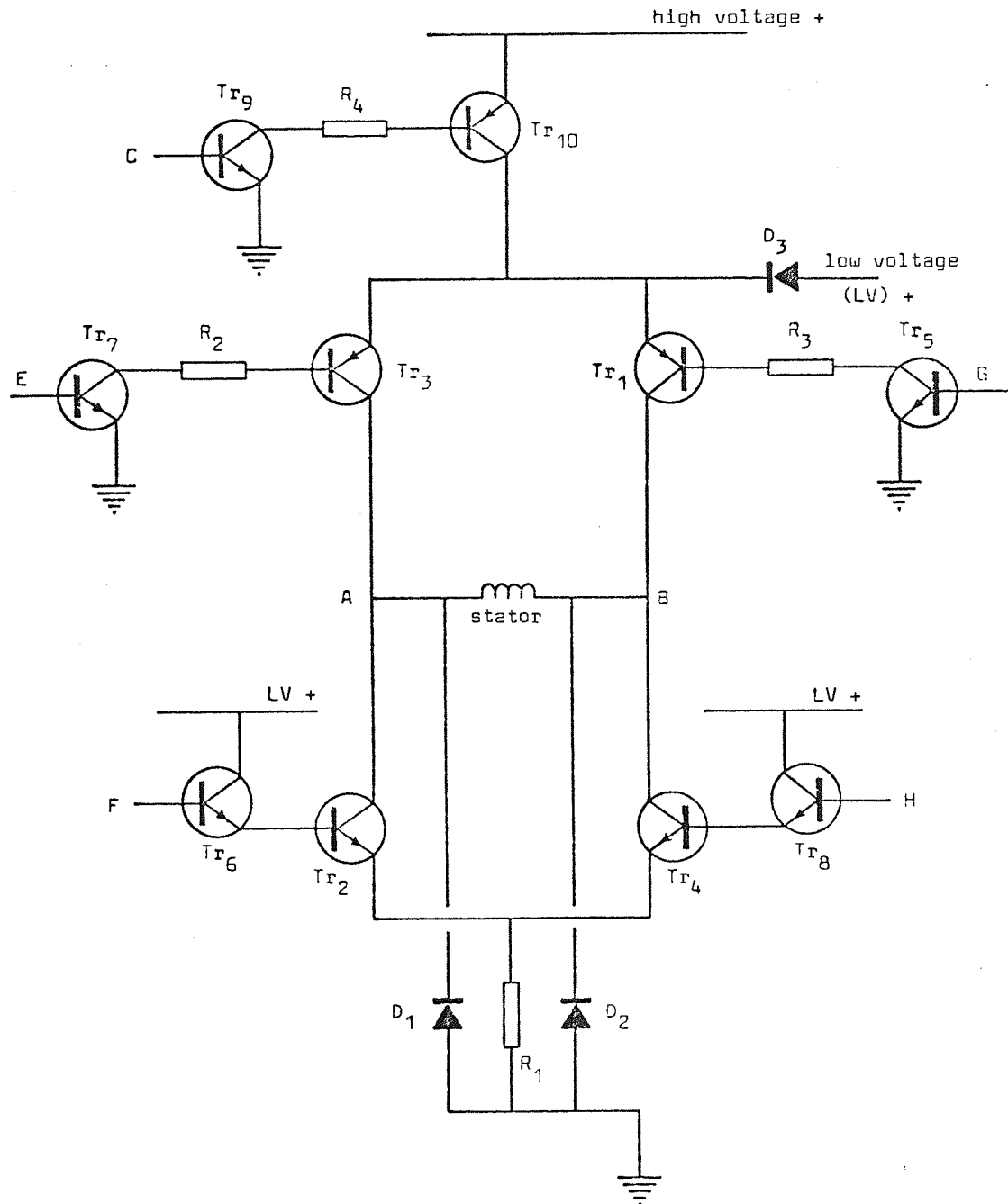


FIGURE 3.3 Simplified Drive Circuit (One Phase)

supplies.

When a current reversal is demanded switch inputs E and H go negative switching off transistors Tr_3 and Tr_4 . Switch inputs F and G go positive saturating transistors Tr_1 and Tr_2 and, because the system error is large, switch input C goes positive switching on transistor Tr_{10} , thus supplying high voltage to the circuit. The stator inductive current continues to flow in the original direction. Point A is clamped to earth by diode D_1 and the potential at point B rises sharply. Current now passes from collector to base of transistor Tr_1 , through R_3 and transistor Tr_5 , to earth. Current flow continues via this path until it has fallen to zero. The rate of current fall is rapid since, the discharge path impedance is high and the potential at point B must rise above the high voltage rail to enable transistor Tr_1 to conduct in the reverse mode. After falling to zero, the current rises in the opposite direction, flowing from B to A via saturated transistors Tr_{10} , Tr_1 and Tr_2 . When the current reaches the set value switch input C goes negative, switching off transistor Tr_{10} . Thus the high voltage is removed from the winding and current is drawn from the low voltage supply. At the same time Tr_2 becomes active, holding the current at the set value.

3.4 Modelling

To model the drive circuit it is necessary to predict the voltage applied across the stator winding as a function of time. The operation of the circuit can be split into three distinct states. By determining which one of these states the circuit is operating in, it is possible to predict the stator voltage. The three

possible conditions that the drive circuit can be in are :-

- (a) Stator current in the opposite sense to that demanded.
- (b) Stator current in the same sense to that demanded but less than the set value.
- (c) Stator current at set value.

In case (a) the voltage applied to the stator winding will require to be determined by measurement, since it is a function of the characteristics of transistors Tr_1 and Tr_5 , the value of resistor R_3 and the level of the high voltage supply. In case (b) the voltage across the winding is the high voltage supply less the voltage drop of three saturated transistors; and in case (c) the voltage across the winding is simply calculated from its d.c. resistance. Details of the digital simulation of the drive circuit are contained in Chapter 6.

3.5 Conclusions

The performance of a stepping motor system is largely dependent upon the drive circuit employed to power the motor. For high speed, high efficiency systems it is necessary to use a bipolar circuit of either the bilevel or chopper type, switched by a two phase drive state generator.

For a given machine, the time constant and copper losses of the stator winding are independent of the number of turns in the winding space. Power losses in the drive circuit, on the other hand, are inversely proportional to the number of stator turns. It is shown that the overdrive voltage, in bilevel and chopper circuits, gives little advantage when it exceeds a level

of ten times the rated stator voltage. For high system efficiency, therefore, stator windings should be wound with as many turns as possible consistent with not exceeding the voltage breakdown characteristics of the drive transistors at ten times overdrive.

Modelling of drive circuits is straightforward and should not be neglected if stepping motor systems are to be successfully simulated.

4 STATIC TORQUE DISPLACEMENT CHARACTERISTIC

4.1 Introduction

The general form of the static torque displacement characteristic for the type of machine under consideration is shown in Figure 4.1.

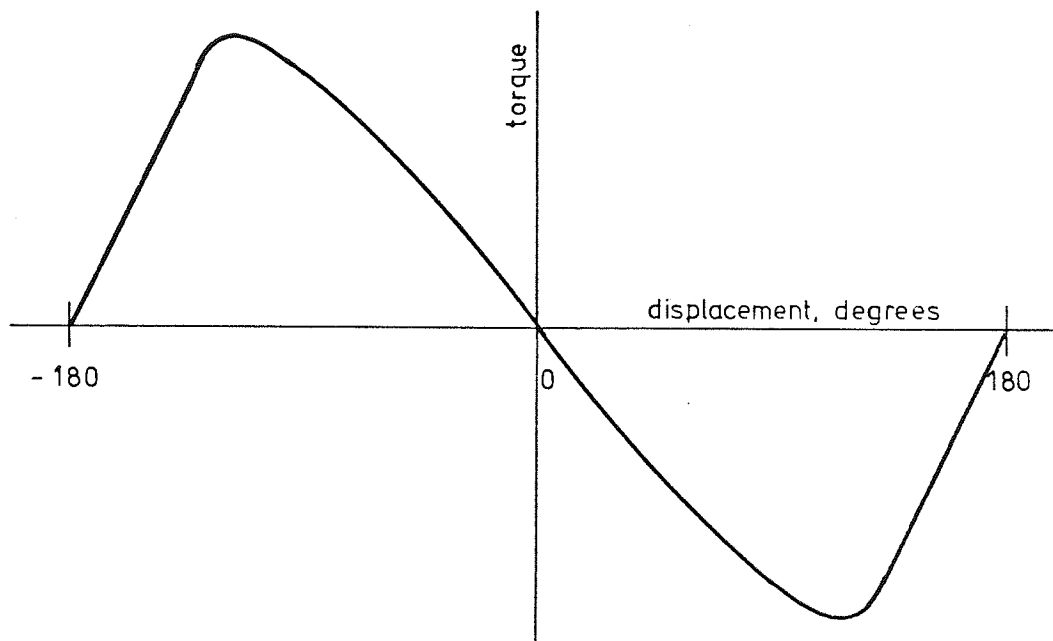


FIGURE 4.1 Static Torque Displacement Characteristic

The zero degree position shown on the torque curve represents the stable equilibrium point of the rotor and the +180 and -180 degree positions represent unstable equilibrium points. This characteristic is frequently approximated to a sinusoid or a linear function passing through the stable equilibrium point. The magnitude of torque at a given displacement angle, for both approximations, is assumed to be directly proportional to current. Extensions based on these simple approximations can be used to

predict the torque when two phases are excited and when the current is time varying. The incorporation of these approximations into the overall machine model, however, generally yields poor predictions of the rotor dynamics. Improved results are achieved, in the case of single phase excitation, by representing the static torque displacement characteristic as a set of data points and linearly interpolating between them. It is difficult to extend this method to two phase excitation since torque produced by one phase cannot simply be added to torque produced by the other. For two phase predictions, therefore, it is necessary to consider the physical methods of torque production in order that a mathematical model can be evolved which will predict, accurately, the torque at any displacement angle for any combination of the phase currents.

The majority of authors have assumed the static torque displacement characteristic to be linear. This is, in most cases, a reasonable approximation for small displacements with the important advantage that it is more amenable to analysis than the sinusoidal form. The usefulness of such an approximation is, however, confined to predicting the dynamics when the rotor is displaced by a small angle and then released. If the machine is to be modelled for normal operating conditions it is essential to predict the torque accurately for large displacement angles. Such a condition exists when the machine is started from rest and generally exists when the machine is slewing under well designed operating conditions. If large displacement angles are to be accommodated then it is clear that the sinusoidal form is superior to the linear form. However, serious discrepancies can arise since, in general, static torque displacement characteristics

contain a significant proportion of spacial harmonics.

Bailey¹⁷, O'Donohue⁵, Kieburz⁶, and Robinson and Taft⁷ all assume the torque to be linearly related to displacement. Robinson and Taft⁷ do, however, postulate a sinusoidal characteristic but later linearise the equations. Snowdon and Madsen³ were the first to attempt to derive a more accurate model of the static torque displacement characteristic. They start with the premise that the expression for permeance comprises a constant term plus a term which varies with the cosine of the electrical displacement angle (fundamental component). They conclude that the torque for single phase excitation is periodic in space containing both fundamental and second harmonic terms. However they erroneously obtain the torque available in the two phase case by adding the torque produced in one phase to the torque produced in the other phase shifted by 90 electrical degrees, thus cancelling the second harmonic term. It is shown later that superposition should not have been assumed. Singh¹⁸ obtains a torque equation which is sinusoidal in space. His assumption that the winding distribution around the stator is sinusoidal leads to this simplified result. The most comprehensive analysis on the formulation of static torque has been contributed by Chai⁴. He assumes an expression for permeance that comprises a constant term, a fundamental term and a fourth harmonic term. He derives an expression for static torque with one phase excited and with two phases excited with equal m.m.f.s. The two phase result does not rely on the erroneous use of superposition and it predicts results that are observable in practice.

4.2 Measurement

The apparatus was set up as shown in Figure 4.2. The pointer length was calculated to give a movement at its end of 3 mm for 5 electrical degrees of rotation of the machine rotor. Current was supplied to the machine stator windings from a constant current source set at 0.5 A, 1 A and then every 1 A to 8 A. At each current setting a static torque displacement characteristic was measured by adding weights to the scale pans and noting the corresponding displacement; one pan for each half of the characteristic.

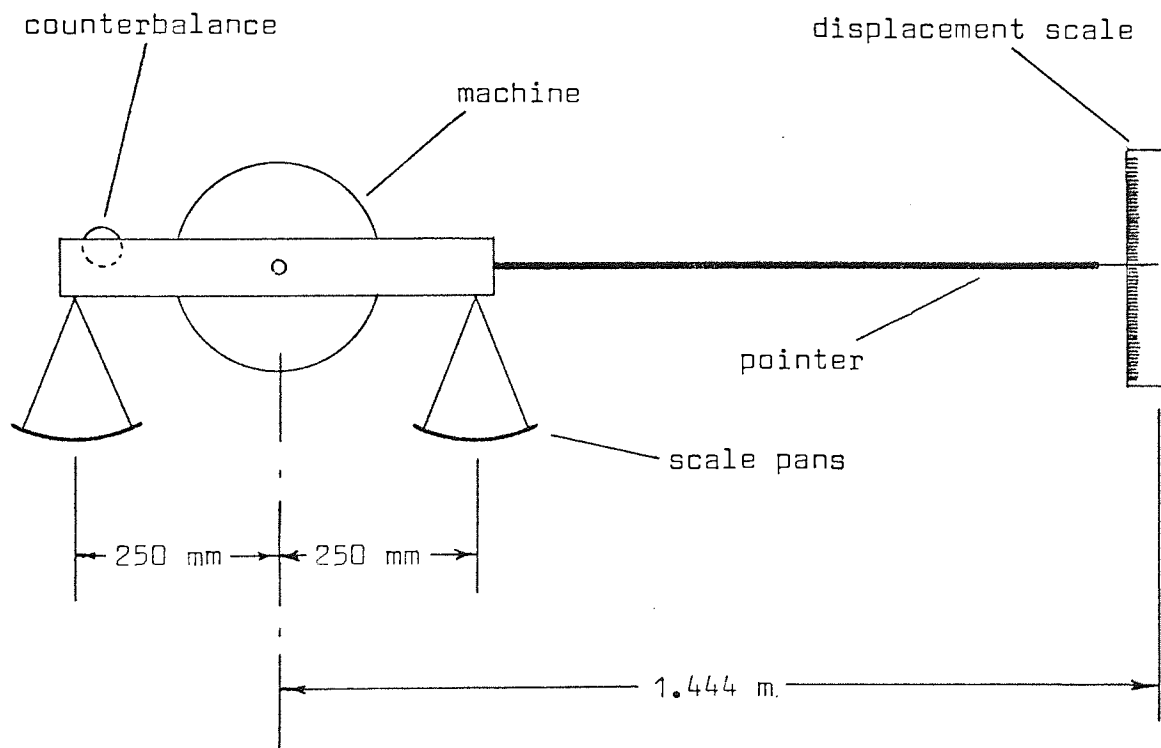


FIGURE 4.2 Measurement of Static Torque Displacement Characteristic

The measurements were repeated for reducing torque by subtracting weights from the scale pans. Characteristics were obtained for

each phase excited in turn and both phases excited together. The characteristic obtained for single phase excitation at 2 A is presented in Figure 4.3. Figure 4.4 presents a two phase characteristic obtained at 6 A, the continuous line being the result of adding the contribution of one phase to the contribution of the other shifted by 90 electrical degrees.

4.3 Analysis of Measured Characteristics

It is clear from Figures 4.3 and 4.4 that the static torque displacement characteristics contain spacial harmonics and that the two phase characteristic is not obtainable by adding the torque produced by one phase to the torque produced by the other. An insight into the problem of how the individual phase contributions combine to produce two phase torque may be obtained by subjecting the characteristics to harmonic analysis and comparing the results obtained in practice to those predicted by direct addition.

4.3.1 Harmonic analysis of measured characteristics

Harmonic analysis was carried out on the measured static torque displacement characteristics using a Fast Fourier Transform (FFT) subroutine. A computer program provided thirty-six samples from measured data held on magnetic tape and the subroutine returned the magnitude and phase of the eighteen harmonics.

The results are presented in the form :-

$$T_n = T_{m_n} \sin n(\theta_e - \phi)$$

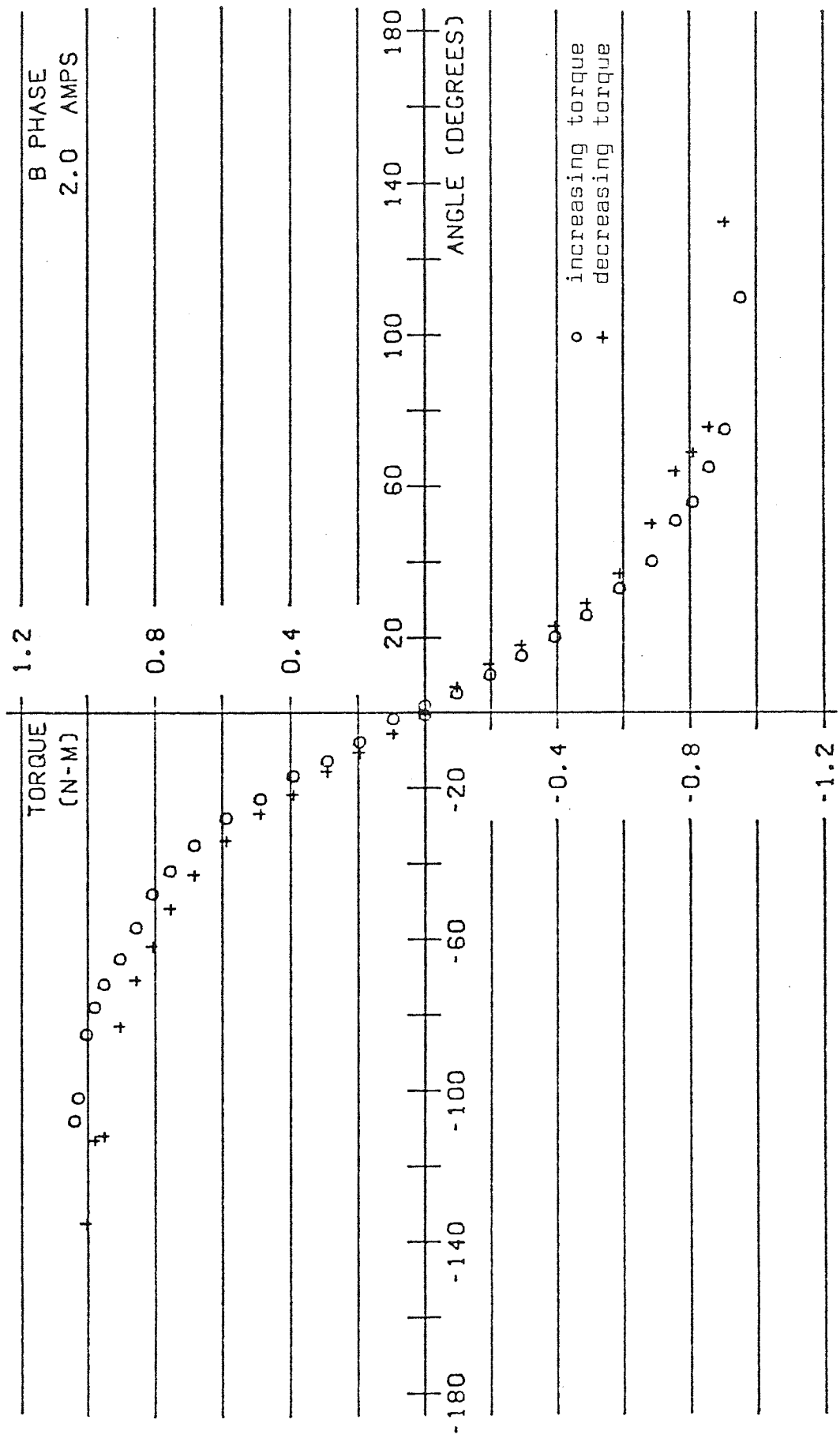


FIGURE 4.3 Static Torque Displacement Characteristic Single Phase 2 A

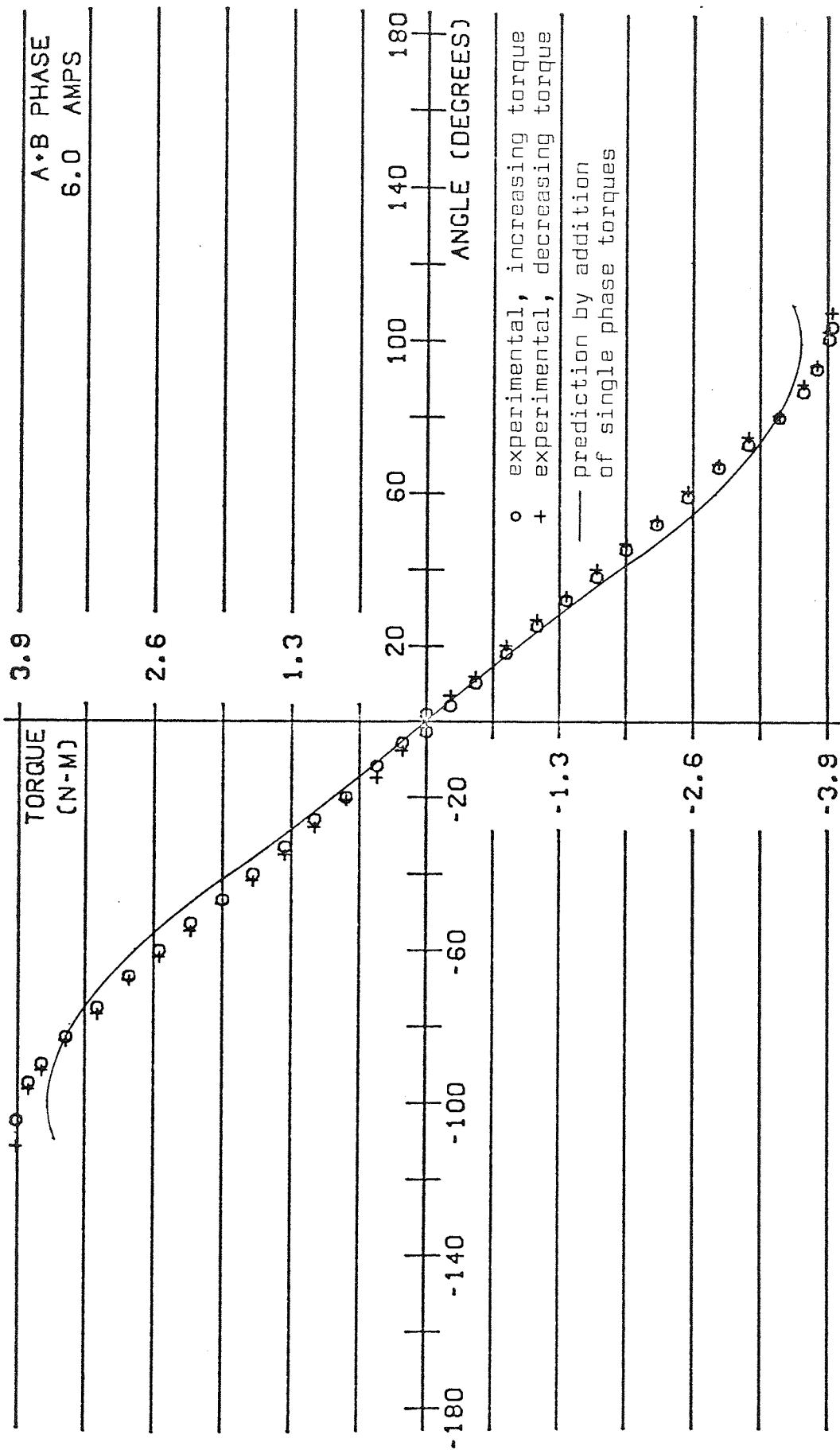


FIGURE 4.4 Static Torque Displacement Characteristic Two Phase 6 A

Where :-

T_n = instantaneous value of the nth Fourier component of torque

T_{m_n} = magnitude of the nth Fourier component of torque

θ_e = electrical angle

The sign of T_{m_n} is adjusted to keep the phase angle ϕ the same as the spacial relationship between the phases. Thus :-

$$\phi_a = 0^\circ, \quad \phi_b = 90^\circ \quad \text{and} \quad \phi_{ab} = 45^\circ$$

The results of analysis on the characteristics obtained at an excitation current of 4 A are presented in Table IV.

TABLE IV Analysis of 4 A Characteristics

Harmonic	Harmonic Torque (N m)		
	a Phase	b Phase	ab Phase
1	- 1.674	- 1.733	- 2.514
2	0.113	0.148	0.243
3	- 0.0404	- 0.0367	0.246
4	- 0.0613	- 0.0598	- 0.0598
5	0.0217	0.0388	- 0.0261
6	- 0.00346	- 0.00289	0.0342
7	- 0.0152	- 0.0127	0.00442
8	0.0193	0.0265	- 0.0121

4.3.2 Direct addition of phase torque

Consider two phase torque to be the summation of two periodic functions representing the single phase torques :-

$$T = \sum_{n=1}^{\infty} \left\{ A_n \sin n(\theta_e - \phi_a) + B_n \sin n(\theta_e - \phi_b) \right\}$$

Since 'a' phase and 'b' phase are separated by 90 electrical degrees put

$$\phi_a = 0^\circ \quad \text{and} \quad \phi_b = 90^\circ$$

and taking the case of equal excitation currents put

$$A_n = B_n = C_n$$

The function then becomes

$$T = \sum_{n=1}^{\infty} \left\{ C_n \sin n\theta_e + C_n \sin n(\theta_e - 90^\circ) \right\}$$

$$\sum_{n=\text{odd}}^{\infty} C_n (-1)^{\frac{n+1}{2}} \cos n\theta_e$$

$$T = \sum_{n=1}^{\infty} C_n \sin n\theta_e +$$

$$\sum_{n=\text{even}}^{\infty} C_n (-1)^{\frac{n}{2}} \sin n\theta_e$$

When n = 1

$$T_1 = C_1 \sin \theta e + C_1 \cos \theta e$$

$$T_1 = \sqrt{2}C_1 \sin (\theta e - 45^\circ)$$

$$Tm_1 = \sqrt{2}C_1$$

When n = 2

$$T_2 = C_2 \sin 2\theta e - C_2 \sin 2\theta e$$

$$T_2 = 0$$

$$Tm_2 = 0$$

When n = 3

$$T_3 = C_3 \sin 3\theta e + C_3 \cos 3\theta e$$

$$T_3 = \sqrt{2}C_3 \sin (3\theta e + 45^\circ)$$

$$T_3 = -\sqrt{2}C_3 \sin 3(\theta e - 45^\circ)$$

$$Tm_3 = -\sqrt{2}C_3$$

When n = 4

$$T_4 = C_4 \sin 4\theta e + C_4 \sin 4\theta e$$

$$T_4 = 2C_4 \sin 4\theta e$$

$$T_4 = -2C_4 \sin 4(\theta e - 45^\circ)$$

$$Tm_4 = -2C_4$$

4.3.3 Comparison of measured and predicted harmonic torques

The 4 A, two phase, harmonic torques predicted by the direct addition of the single phase harmonic torques are compared in Table V, with the results of harmonic analysis carried out on the two phase characteristic.

TABLE V Comparison of Harmonic Torques

Harmonic	Two Phase Harmonic Torque (N m)	
	Direct Addition	Harmonic Analysis
1	- 2.409	- 2.514
2	0	0.243
3	0.0545	0.246
4	0.121	- 0.0598

4.3.4 Conclusions

The comparison of the Fourier components obtained by analysis of a practical, two phase, static torque displacement characteristic with the components obtained by direct addition of the corresponding single phase characteristics demonstrates clearly that the single phase characteristics do not combine linearly to produce torque when both phases are excited simultaneously. Table V shows that only the fundamental component of the practical characteristic has a result which corresponds to direct addition. It is concluded that a model based on direct addition is very likely to produce large errors especially when the single phase static torque displacement characteristic is rich in harmonics. An improved model for torque production is therefore necessary

and such a model will be a key factor in providing an improvement in the prediction of machine dynamics.

4.4 Static Torque Model Due to Chai

Chai⁴ starts by considering a simplified permanent magnet stepping motor (Figure 4.5) from which Thevenin and Norton type equivalent circuits are derived (Figure 4.6 and Figure 4.7).

Where :-

$P_1 - P_4$ = air gap permeances at the stator poles (Wb/A t)

P_n = magnitude of the nth Fourier component of permeance at the stator poles (Wb/A t)

P_m = permanent magnet permeance (Wb/A t)

$F_1 - F_4$ = excitation m.m.f.s in the stator poles (A t)

F_m = permanent magnet m.m.f. (A t)

F_0 = m.m.f. drop across the stator-rotor gap including the excitation source

N_r = number of rotor teeth

θ_m = mechanical angle = $\frac{\theta_e}{N_r}$

Chai shows that :-

$$\text{Torque } T = \frac{N_r}{2} \sum_{i=1}^4 (F_i - F_0)^2 \frac{dP_i}{d\theta_e} \quad \text{-----} \quad 4.1$$

$$\text{Where } F_0 = \frac{\sum_{i=1}^4 P_i F_i + P_m F_m}{\sum_{i=1}^4 P_i + P_m}$$

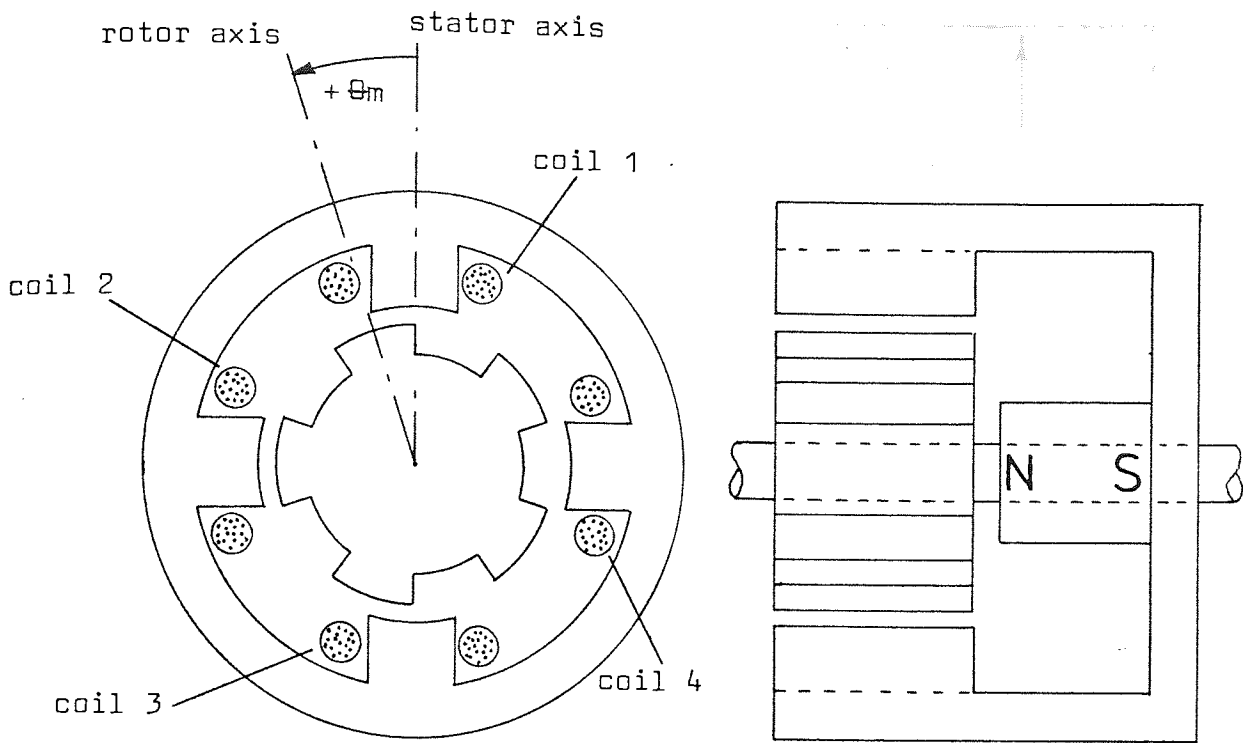


FIGURE 4.5 Simplified PM Stepping Motor

The gap permeance, P_i , is periodic with respect to θ_e (electrical angle). Chai assumes a periodic permeance function comprising a constant term, a fundamental term and a fourth harmonic term while ignoring the possibility of a second and third harmonic term. He has no justification for this assumption other than it is the fourth harmonic that is responsible for detent (cogging) torque.

It is useful, at this point, to consider a simplified permeance function, i.e. a function that contains a constant term and a fundamental term only. The simplification enables the method to be demonstrated clearly while allowing useful conclusions to be drawn. The four permeances can therefore be represented as :-

$$P_1 = P_0 + P_1 \cos \theta_e$$

$$P_2 = P_0 + P_1 \cos (\theta_e - 90^\circ)$$

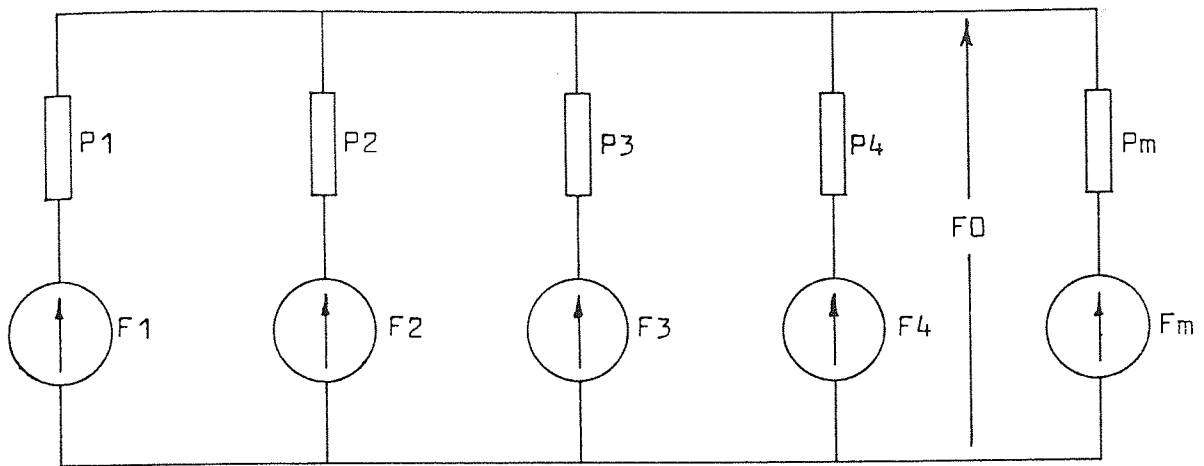


FIGURE 4.6 Magnetic Equivalent Circuit (Thevenin)

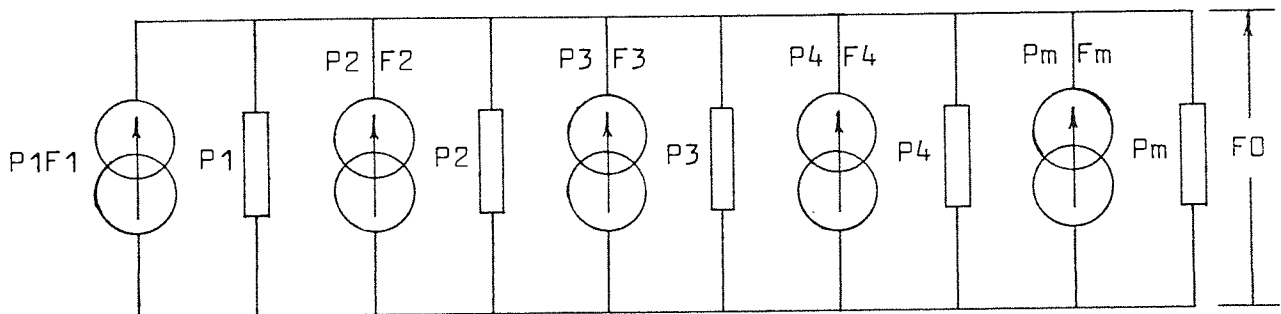


FIGURE 4.7 Magnetic Equivalent Circuit (Norton)

$$P_3 = P_0 + P_1 \cos (\theta_e - 180^\circ)$$

$$P_4 = P_0 + P_1 \cos (\theta_e - 270^\circ)$$

Simplifying

$$P_1 = P_0 + P_1 \cos \theta_e$$

$$P_2 = P_0 + P_1 \sin \theta_e$$

$$P_3 = P_0 - P_1 \cos \theta_e$$

$$P_4 = P_0 - P_1 \sin \theta_e$$

Therefore

$$\frac{dP_1}{d\theta_e} = -P_1 \sin \theta_e$$

$$\frac{dP_2}{d\theta_e} = P_1 \cos \theta_e$$

$$\frac{dP_3}{d\theta_e} = P_1 \sin \theta_e$$

$$\frac{dP_4}{d\theta_e} = -P_1 \cos \theta_e$$

$$\sum_{i=1}^4 P_i + P_m = 4P_0 + P_m$$

$$\approx 4P_0 \quad (\text{since } 4P_0 \gg P_m)$$

4.4.1 Single phase

With single phase excitation assume :-

$$F_1 = -F = -NI, \quad F_3 = F = NI, \quad F_2 = F_4 = 0$$

$$\sum_{i=1}^4 P_i F_i = F(-P_1 + P_3) = -2FP_1 \cos \theta_e$$

$$F_0 = \frac{P_m F_m - 2FP_1 \cos \theta_e}{4P_0}$$

Substituting in equation 4.1 and putting $i=1$ yields the following terms

$$\begin{aligned} & \frac{N_r}{2} \left(-F - \frac{P_m F_m}{4P_0} + \frac{2FP_1 \cos \theta_e}{4P_0} \right)^2 (-P_1 \sin \theta_e) \\ &= \frac{N_r}{32P_0^2} (2FP_1 \cos \theta_e - P_m F_m - 4P_0 F)^2 (-P_1 \sin \theta_e) \end{aligned}$$

Adding the terms above to the terms of equation 4.1 when $i=3$, yields

$$T = \frac{NrFP_1}{2P_0} (FP_1 \sin 2\theta_e - PmFm \sin \theta_e) \quad 4.2$$

4.4.2 Two phase

With both phases energised with the same m.m.f.

$$F_1 = F_3 = -F, \quad F_2 = F_4 = F$$

$$\sum_{i=1}^4 P_i F_i = F(-P_1 - P_2 + P_3 + P_4)$$

$$= 2P_1 F (\cos \theta_e + \sin \theta_e)$$

$$= 2\sqrt{2}P_1 F \cos (\theta_e - 45^\circ)$$

Substituting in equation 4.1 for all i it is found that

$$T = \frac{NrFP_1}{2P_0} \left[(2P_1 \sin 2(\theta_e - 45^\circ) - \sqrt{2}PmFm \sin (\theta_e - 45^\circ)) \right] \quad 4.3$$

4.4.3 Conclusions

The single phase analysis shows that, starting from an assumption of a sinusoidal variation of permeance, the expression for torque will contain a second harmonic term. The magnitude of the second harmonic is a function of the square of the m.m.f. whilst the fundamental magnitude is a linear function of m.m.f. It is clear, that in general, the static torque displacement characteristic

will contain spacial harmonics which are generated by lower order permeance harmonics. These torque harmonics being non-linear functions of m.m.f. Thus, the use of a simple approximation for the static torque displacement characteristic, over a wide m.m.f range, is very likely to yield poor results.

The two phase analysis shows that, for equal m.m.f.s in both phases, the magnitude of the fundamental torque component increases by a factor of $\sqrt{2}$ over single phase excitation whilst the second harmonic component increases by a factor of 2. The angle at which the torque is zero has shifted by 45 electrical degrees from the single phase zero. It is clear that, due to the functional non-linearity, two phase torque cannot be obtained simply by adding the single phase torques.

The analysis has used a simple representation of permeance which predicts a torque displacement characteristic comprising a fundamental and second harmonic component only. For these components it is clear that, from Table VI the Chai model predictions of the 4 A, two phase, harmonic torques from the corresponding single phase harmonic torques are in close agreement with the results yielded by harmonic analysis of the measured characteristic.

TABLE VI Comparison of Harmonic Torques

Harmonic	Two Phase Harmonic Torque (N m)		
	Direct Addition	Chai Model	Harmonic Analysis
1	- 2.409	- 2.409	- 2.514
2	0	0.261	0.243

The results of harmonic analysis given in Table IV show that the static torque displacement characteristics contain high order harmonics of significance. It is clear that a permeance function containing higher order Fourier coefficients is required to adequately describe the actual permeance displacement characteristic of the machine.

4.5 Extensions to Chai's Static Torque Model

Chai's⁴ work can be extended by considering the permeance function to contain Fourier coefficients up to, and including, the fourth and by removing the constraint that the currents in each phase are equal. The four permeances are therefore represented as follows :-

$$P_1 = P_0 + P_1 \cos \theta_e + P_2 \cos 2\theta_e + P_3 \cos 3\theta_e + P_4 \cos 4\theta_e$$

$$P_2 = P_0 + P_1 \cos (\theta_e - 90^\circ) + P_2 \cos 2(\theta_e - 90^\circ) \\ + P_3 \cos 3(\theta_e - 90^\circ) + P_4 \cos 4(\theta_e - 90^\circ)$$

$$P_3 = P_0 + P_1 \cos (\theta_e - 180^\circ) + P_2 \cos 2(\theta_e - 180^\circ) \\ + P_3 \cos 3(\theta_e - 180^\circ) + P_4 \cos 4(\theta_e - 180^\circ)$$

$$P_4 = P_0 + P_1 \cos (\theta_e - 270^\circ) + P_2 \cos 2(\theta_e - 270^\circ) \\ + P_3 \cos 3(\theta_e - 270^\circ) + P_4 \cos 4(\theta_e - 270^\circ)$$

Simplifying

$$P_1 = P_0 + P_1 \cos \theta_e + P_2 \cos 2\theta_e + P_3 \cos 3\theta_e + P_4 \cos 4\theta_e$$

$$P_2 = P_0 + P_1 \sin \theta_e - P_2 \cos 2\theta_e - P_3 \sin 3\theta_e + P_4 \cos 4\theta_e$$

$$P_3 = P_0 - P_1 \cos \theta e + P_2 \cos 2\theta e - P_3 \cos 3\theta e + P_4 \cos 4\theta e$$

$$P_4 = P_0 - P_1 \sin \theta e - P_2 \cos 2\theta e + P_3 \sin 3\theta e + P_4 \cos 4\theta e$$

Therefore

$$\frac{dP_1}{d\theta e} = -P_1 \sin \theta e - 2P_2 \sin 2\theta e - 3P_3 \sin 3\theta e - 4P_4 \sin 4\theta e$$

$$\frac{dP_2}{d\theta e} = P_1 \cos \theta e + 2P_2 \sin 2\theta e - 3P_3 \cos 3\theta e - 4P_4 \sin 4\theta e$$

$$\frac{dP_3}{d\theta e} = P_1 \sin \theta e - 2P_2 \sin 2\theta e + 3P_3 \sin 3\theta e - 4P_4 \sin 4\theta e$$

$$\frac{dP_4}{d\theta e} = -P_1 \cos \theta e + 2P_2 \sin 2\theta e + 3P_3 \cos 3\theta e - 4P_4 \sin 4\theta e$$

$$\sum_{i=1}^4 P_i + P_m = 4P_0 + 4P_4 \cos 4\theta e + P_m$$

$$\approx 4P_0 \quad (\text{since } 4P_0 \gg 4P_4 \cos 4\theta e + P_m)$$

Removing the restriction of equal phase currents the m.m.f.s may be represented as

$$F_1 = -F_a \quad F_2 = -F_b \quad F_3 = F_a \quad F_4 = F_b$$

$$\sum_{i=1}^4 P_i F_i = -F_a P_1 - F_b P_2 + F_a P_3 + F_b P_4$$

$$= F_a (P_3 - P_1) + F_b (P_4 - P_2)$$

$$= -2P_1 \sqrt{F_a^2 + F_b^2} \cos \left(\theta e - \arctan \frac{F_b}{F_a} \right)$$

$$- 2P_3 \sqrt{F_a^2 + F_b^2} \cos \left(3\theta e + \arctan \frac{F_b}{F_a} \right)$$

Substituting in equation 4.1 for all i and putting

N = number of turns per pole

produces the following 13 terms which, when summed, yields the total torque T.

$$1. - 2 \frac{N^2 N_r}{P_0^2} P_1^2 P_4 (I_a^2 + I_b^2) \cos^2 \left(\theta_e - \arctan \frac{I_b}{I_a} \right) \sin 4\theta_e$$

$$2. - 2 \frac{N^2 N_r}{P_0^2} P_3^2 P_4 (I_a^2 + I_b^2) \cos^2 \left(3\theta_e + \arctan \frac{I_b}{I_a} \right) \sin 4\theta_e$$

$$3. - \frac{N_r}{2P_0^2} P_m^2 F_m^2 P_4 \sin 4\theta_e$$

$$4. - 2N^2 N_r P_2 (I_a^2 - I_b^2) \sin 2\theta_e$$

$$5. - 4N^2 N_r P_4 (I_a^2 + I_b^2) \sin 4\theta_e$$

$$6. - 4 \frac{N^2 N_r}{P_0^2} P_1 P_3 P_4 (I_a^2 + I_b^2) \cos \left(\theta_e - \arctan \frac{I_b}{I_a} \right)$$

$$\cos \left(3\theta_e + \arctan \frac{I_b}{I_a} \right) \sin 4\theta_e$$

$$7. 2 \frac{N N_r}{P_0^2} P_1 P_4 P_m F_m \sqrt{I_a^2 + I_b^2} \cos \left(\theta_e - \arctan \frac{I_b}{I_a} \right) \sin 4\theta_e$$

$$8. \frac{N^2 N_r}{2P_0^2} P_1^2 (I_a^2 + I_b^2) \sin 2 \left(\theta_e - \arctan \frac{I_b}{I_a} \right)$$

$$9. \frac{N^2 N_r}{P_0^2} P_1 P_3 (I_a^2 + I_b^2) \left(2 \sin 4\theta_e + \sin 2 \left(\theta_e + \arctan \frac{I_b}{I_a} \right) \right)$$

$$10. 2 \frac{N N_r}{P_0^2} P_3 P_4 P_m F_m \sqrt{I_a^2 + I_b^2} \cos \left(3\theta_e + \arctan \frac{I_b}{I_a} \right) \sin 4\theta_e$$

$$11. \quad 1.5 \frac{N^2 N_I}{P_0} P_3^2 (I_a^2 + I_b^2) \sin 2(3\theta_e + \arctan \frac{I_b}{I_a})$$

$$12. \quad - \frac{N N_I}{2P_0} P_1 P_m F_m \sqrt{I_a^2 + I_b^2} \sin (\theta_e - \arctan \frac{I_b}{I_a})$$

$$13. \quad - 1.5 \frac{N N_I}{P_0} P_3 P_m F_m \sqrt{I_a^2 + I_b^2} \sin (3\theta_e + \arctan \frac{I_b}{I_a})$$

Collecting together terms in the first four harmonics the following expressions for the components are obtained.

N.B. The common term $\frac{N N_I}{32P_0^2}$ has been taken out of all expressions.

Fundamental

$$- 16P_0 P_1 P_m F_m \sqrt{I_a^2 + I_b^2} \sin (\theta_e - \arctan \frac{I_b}{I_a})$$

Second Harmonic

$$- 64N P_0^2 P_2 (I_a^2 - I_b^2) \sin 2\theta_e$$

$$+ 16N P_0 P_1^2 (I_a^2 + I_b^2) \sin 2(\theta_e - \arctan \frac{I_b}{I_a})$$

$$+ 32N P_0 P_1 P_3 (I_a^2 + I_b^2) \sin 2(\theta_e + \arctan \frac{I_b}{I_a})$$

$$- 16N P_1^2 P_4 (I_a^2 + I_b^2) \sin 2(\theta_e + \arctan \frac{I_b}{I_a})$$

$$+ 16N P_3^2 P_4 (I_a^2 + I_b^2) \sin 2(\theta_e + \arctan \frac{I_b}{I_a})$$

$$- 32N P_1 P_3 P_4 (I_a^2 + I_b^2) \sin 2(\theta e - \arctan \frac{I_b}{I_a})$$

Third Harmonic

$$- 48P_0 P_3 P_m F_m \sqrt{I_a^2 + I_b^2} \sin (3\theta e + \arctan \frac{I_b}{I_a})$$

$$+ 32P_1 P_4 P_m F_m \sqrt{I_a^2 + I_b^2} \sin (3\theta e + \arctan \frac{I_b}{I_a})$$

Fourth Harmonic

$$64N P_0 P_1 P_3 (I_a^2 + I_b^2) \sin 4\theta e$$

$$- 32N P_1^2 P_4 (I_a^2 + I_b^2) \sin 4\theta e$$

$$- 32N P_3^2 P_4 (I_a^2 + I_b^2) \sin 4\theta e$$

$$- 128N P_0^2 P_4 (I_a^2 + I_b^2) \sin 4\theta e$$

$$- 16P_4 P_m^2 F_m^2 \sin 4\theta e$$

4.5.1 Conclusions

Terms 8 and 12, yielded by the fundamental component of permeance represent, in a more general form, the results already derived and given in equations 4.2 and 4.3. Equation 4.2 is obtained by putting I_b to zero and equation 4.3 by putting $I_a = I_b$. The second harmonic terms have no dependency on the permanent magnet and their magnitude is proportional to the square of the energising m.m.f. The fundamental and third harmonic terms,

however, are dependent upon the permanent magnet and their magnitudes are directly proportional to the energising m.m.f. The fourth harmonic is more complex since it contains four terms which are independent of the permanent magnet and are proportional to the square of the energising m.m.f. and one term which is independent of the energising m.m.f. and proportional to the square of the permanent magnet m.m.f., it is this term that gives rise to detent torque.

The inclusion of the extra Fourier components of permeance and the removal of the restriction of equal phase currents for two phase working has resulted in a complex expression. However, this expression yields torque for any combination of phase currents at any electrical angle θ_e and can be easily programmed on a digital computer and is capable of accurate results.

4.6 Modelling and Parameter Estimation

The results, yielded by measurement of the static torque displacement characteristic, show that spacial harmonics are significant and should not, therefore, be ignored. In consequence it is not possible to add the torque contributed by each phase. Chai⁴ has proposed a mathematical model for the formulation of static torque by considering a magnetic equivalent circuit of the machine (Figure 4.6) from which an expression for torque was obtained. His results are somewhat limited in that he has ignored the second and third permeance harmonics, but included the fourth, and his expression for torque, in the two phase case, is usable only for equal currents in each phase. Extensions of Chai's work, which remove these limitations, are given in para. 4.5 where a complex expression for torque is

obtained. This expression is programmed on a digital computer as a subroutine to yield torque for any combination of the two phase currents at any displacement angle. Details of the digital simulation are contained in Chapter 6.

4.6.1 Estimation of permeance coefficients from measured data

The permeance coefficients are expected to be current dependent due, in particular, to the effects of saturation and hysteresis in the machine iron. The values of the coefficients and their variation with current can be estimated by comparing the Fourier components of torque obtained by harmonic analysis of the measured static torque displacement characteristic with the expressions for the Fourier components of torque obtained in para. 4.5. A polynomial fit to the variation of permeance with current is obtained for each Fourier component by using a standard digital computer program employing the method of least squares. The polynomials obtained form part of the torque calculation subroutine (Appendix A.5).

The average value of permeance (P_0) is estimated from the single phase inductance measurements which were obtained by the method due to Jones¹⁹ (para. 5.4.1). The relationship,

$$P_0 = \frac{L}{4 N^2}$$

where N = number of turns per pole, is used to calculate P_0 .

This relationship holds for both single and two phase excitation with the understanding that P_0 is likely to have a different saturation characteristic for the two methods of excitation.

All Fourier components of permeance, except the average value,

P_0 , are due to the toothed structure of the machine rotor and stator. Since the tooth flux of a particular phase is not influenced by the tooth flux in the other, it is to be expected that the saturation characteristics of the harmonic components will be independent of the method of excitation. The same is not true of P_0 however, since, for a given phase, the iron cross section is effectively reduced by flux due to the other phase. It is therefore expected that, for a given current near to saturation, P_0 will be smaller when operated in two phase than when operated in single phase.

The fundamental component of torque is given by :-

$$T_1 = - \frac{N N_r}{2P_0} P_1 P_m F_m \sqrt{I_a^2 + I_b^2} \sin (\theta_e - \arctan \frac{I_b}{I_a}) \quad (\text{see para.4.5})$$

For single phase excitation ($I_b = 0$) this expression becomes

$$T_1(1\phi) = - \frac{N N_r}{2P_0} P_1 P_m F_m I_a \sin \theta_e$$

the signed magnitude of which is

$$T_{m_1}(1\phi) = - \frac{N N_r}{2P_0} P_1 P_m F_m I_a$$

The values of P_m , F_m , N and N_r are, for the machine under consideration, as follows :-

$$P_m \text{ (permanent magnet permeance)} = 0.201 \mu\text{Wb/A t}$$

$$F_m \text{ (permanent magnet m.m.f.)} = 6534 \text{ A t}$$

$$N \text{ (number of turns per pole)} = 40$$

$$N_r \text{ (number of rotor teeth)} = 42$$

Thus having obtained the value of P_0 for single phase excitation

from the single phase inductance measurements the values of P_1 are estimated from :-

$$P_1 = - \frac{T_{m_1}(1\phi) 2P_0}{N N_r P_1 P_m F_m I_a}$$

$$P_1 = - 0.906 \frac{T_{m_1}(1\phi) P_0}{I_a}$$

For two phase excitation with equal currents ($I_a = I_b$) the fundamental component becomes :-

$$T_{m_1}(2\phi) = - \frac{\sqrt{2} N N_r}{2P_0} P_1 P_m F_m I_a \sin(\theta_e - 45^\circ)$$

the signed magnitude of which is

$$T_{m_1}(2\phi) = - \frac{\sqrt{2} N N_r}{2P_0} P_1 P_m F_m I_a$$

Assuming that P_1 is the same in both single and two phase excitation then the value of P_0 in two phase excitation is estimated from

$$P_0 = - 1.56 \frac{P_1 I_a}{T_{m_1}(2\phi)}$$

The estimated values for the average and fundamental components of permeance at values of current in the machine operating range are given in Table VII and presented graphically in Figure 4.8. The expected dependency of P_0 on the excitation conditions is clearly shown. To account for this effect the following empirical relationship is proposed

$$P_0 = P_0(1\phi) - K \text{ abs}(I_a I_b)$$

TABLE VII Estimated Values of P_0 and P_1

Phase I	Phase L	$Tm_1(1\phi)$	$Tm_1(2\phi)$	P_1	$P_0(1\phi)$	$P_0(2\phi)$	$P_0(1\phi) - P_0(2\phi)$
A	mH	N m	N m	$\mu\text{wb}/\text{A t}$	$\mu\text{wb}/\text{A t}$	$\mu\text{wb}/\text{A t}$	$\mu\text{wb}/\text{A t}$
0.5	9.6	- 0.30	- 0.41	0.818	1.50	1.54	- 0.04
1.0	10.8	- 0.50	- 0.72	0.758	1.69	1.65	0.03
2.0	11.8	- 0.97	- 1.34	0.808	1.84	1.88	- 0.04
3.0	11.7	- 1.34	- 1.96	0.742	1.83	1.77	0.06
4.0	11.7	- 1.70	- 2.51	0.705	1.82	1.75	0.08
5.0	11.4	- 1.98	- 3.02	0.639	1.78	1.65	0.12
6.0	11.0	- 2.15	- 3.39	0.560	1.72	1.55	0.18
7.0	10.6	- 2.24	- 3.64	0.481	1.66	1.44	0.22

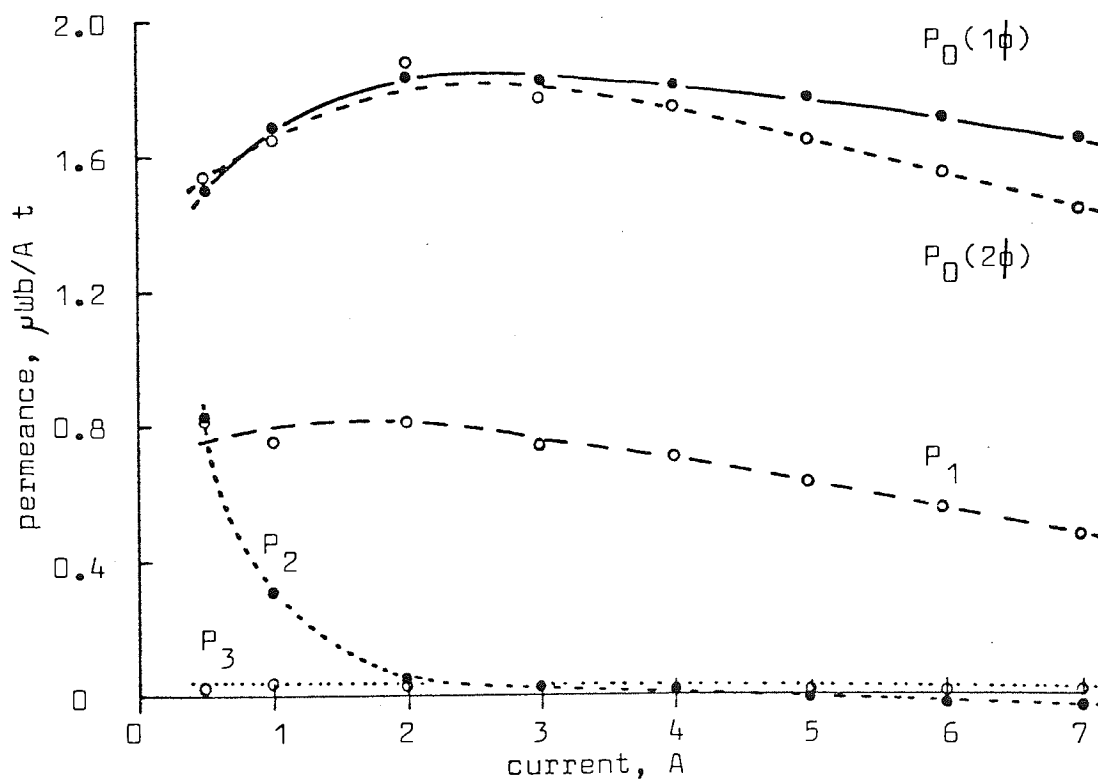


FIGURE 4.8 Variation of Permeance Coefficients with Phase Current

In two phase excitation with equal phase currents ($I_a = I_b$)

$$P_0(2\phi) = P_0(1\phi) - K I_a^2$$

$$P_0(1\phi) - P_0(2\phi) = K I_a^2$$

Permeance difference is shown plotted against the square of phase current in Figure 4.9.

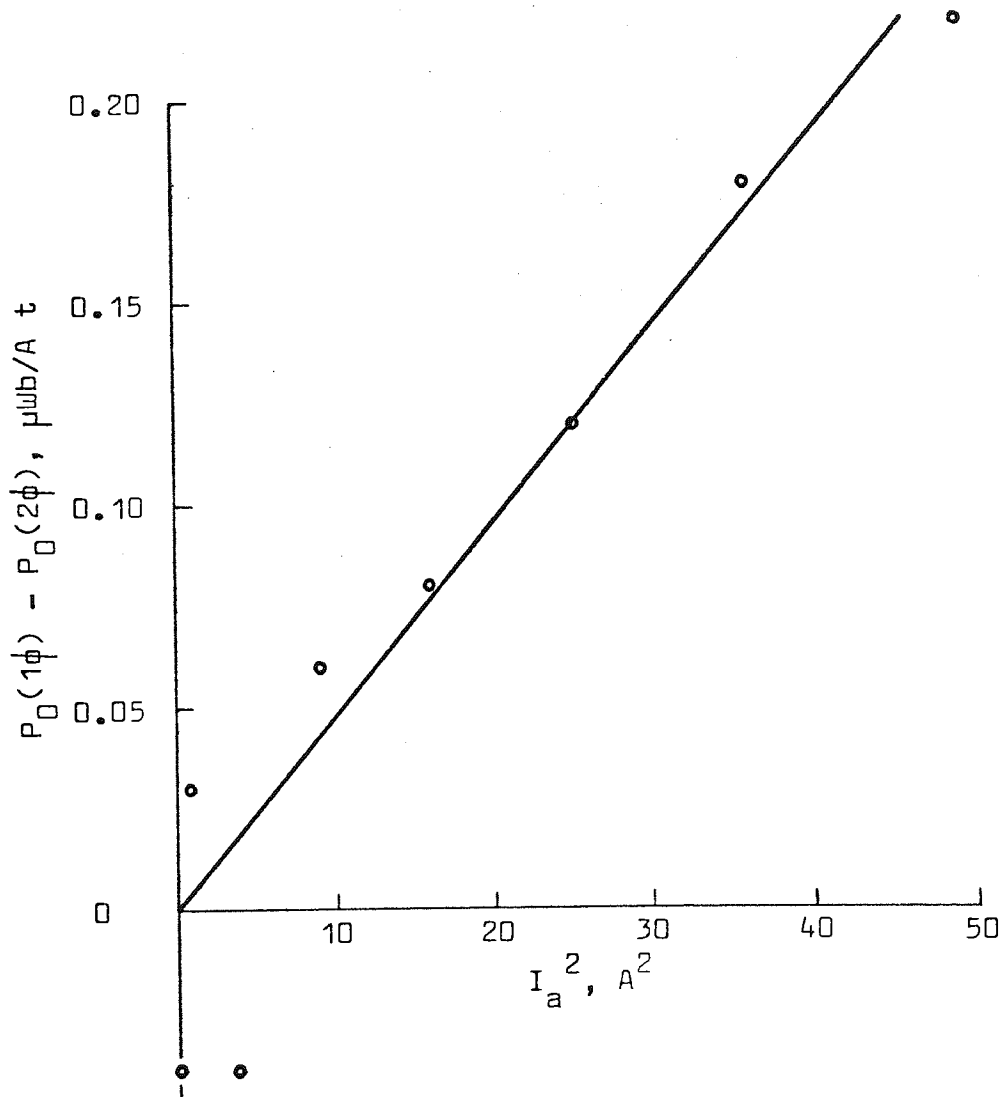


FIGURE 4.9 Variation of Permeance Difference with the Product of Equal Phase Currents

The graph shows that the relationship proposed is a good model of the interactive effect of the phase currents on the value of P_0 . The value of K for the machine under investigation is :-

$$K = 4.8 \times 10^{-9} \text{ Wb/A}^3 \text{ t}$$

The third harmonic component of torque is shown to comprise of two terms (para. 4.5). For the machine under investigation it is found that the second term is insignificant. By approximating the third harmonic torque to the first term only the values of P_3 can be estimated.

$$T_3 = - 1.5 \frac{N N_r}{P_0} P_3 P_m F_m \sqrt{I_a^2 + I_b^2} \sin(3\theta_e + \arctan \frac{I_b}{I_a})$$

For two phase excitation with equal currents ($I_a = I_b$)

$$T_3(2\phi) = - 1.5 \sqrt{2} \frac{N N_r}{P_0} P_3 P_m F_m I_a \sin(3\theta_e + 45^\circ)$$

$$T_3(2\phi) = 1.5 \sqrt{2} \frac{N N_r}{P_0} P_3 P_m F_m I_a \sin 3(\theta_e - 45^\circ)$$

The signed magnitude of which is

$$T_{m3}(2\phi) = 1.5 \sqrt{2} \frac{N N_r}{P_0} P_3 P_m F_m I_a$$

$$P_3 = \frac{T_{m3}(2\phi) P_0}{1.5 \sqrt{2} N N_r P_m F_m I_a}$$

$$P_3 = \frac{T_{m3}(2\phi) P_0}{4.68 I_a}$$

The estimated values for the third harmonic component of permeance

at values of current in the machine operating range are given in Table VIII and presented graphically in Figures 4.8 and 4.10.

TABLE VIII Estimated Values of P_3

Phase I	$T_{m_3}(2\phi)$	$P_0(2\phi)$	P_3
A	N m	$\mu\text{Wb/A t}$	$\mu\text{Wb/A t}$
0.5	0.039	1.54	0.0259
1.0	0.077	1.65	0.0273
2.0	0.160	1.88	0.0322
3.0	0.206	1.77	0.0259
4.0	0.246	1.75	0.0230
5.0	0.248	1.65	0.0175
6.0	0.285	1.55	0.0157
7.0	0.274	1.44	0.0121

The second harmonic component of torque is shown to comprise of six terms (para. 4.5). For the machine under investigation it is found that the first three terms are very much greater than the remainder. By approximating the second harmonic torque to the dominant terms the values of P_2 can be estimated

$$T_2 = N^2 N_r \left[\frac{P_1^2}{2P_0} (I_a^2 + I_b^2) \sin 2(\theta_e - \arctan \frac{I_b}{I_a}) - 2P_2 (I_a^2 - I_b^2) \right. \\ \left. \sin 2\theta_e + \frac{P_1 P_3}{P_0} (I_a^2 + I_b^2) \sin 2(\theta_e + \arctan \frac{I_b}{I_a}) \right] - 4.4$$

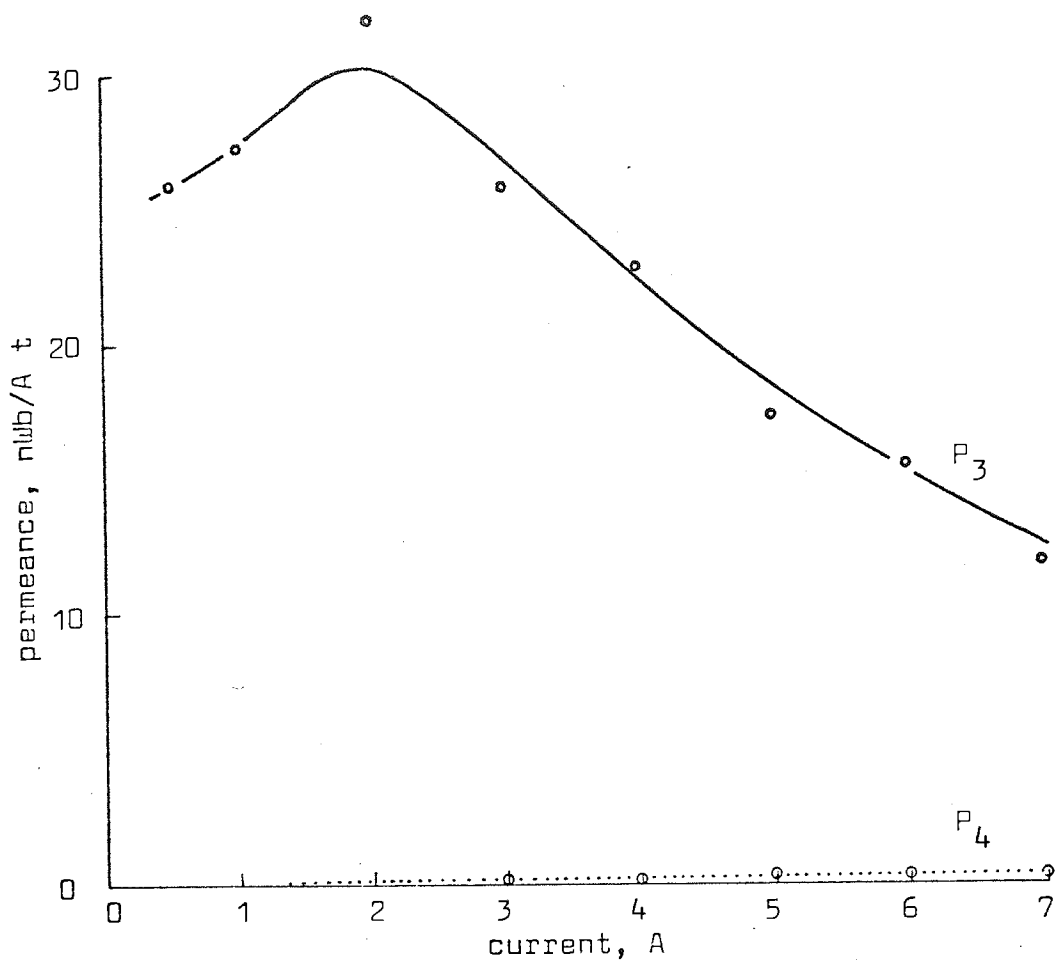


FIGURE 4.10 Variation of Permeance Coefficients with Phase Current

For single phase excitation ($I_b = 0$)

$$T_2(1\phi) = N^2 N_r \left[\frac{P_1^2}{2P_0} - 2P_2 + \frac{P_1 P_3}{P_0} \right] I_a^2 \sin 2\theta e$$

The signed magnitude of which is

$$T_{m_2}(1\phi) = N^2 N_r \left[\frac{P_1^2}{2P_0} - 2P_2 + \frac{P_1 P_3}{P_0} \right] I_a^2$$

$$P_2 = \frac{P_1^2}{4P_0} + \frac{P_1 P_3}{2P_0} - \frac{T_{m2}(1\phi)}{2N^2 N_r I_a^2}$$

$$P_2 = \frac{P_1^2}{4P_0} + \frac{P_1 P_3}{2P_0} - \frac{T_{m2}(1\phi)}{134000 I_a^2}$$

The estimated values for the second harmonic component of permeance at values of current in the machine operating range are given in Table IX and presented graphically in Figure 4.8.

TABLE IX Estimated Values of P_2

Phase I	$T_{m2}(1\phi)$	$P_0(1\phi)$	P_1	P_3	P_2
A	N m	$\mu\omega b/A t$	$\mu\omega b/A t$	$\mu\omega b/A t$	$\mu\omega b/A t$
0.5	- 0.024	1.50	0.818	0.0259	0.827
1.0	- 0.029	1.69	0.758	0.0273	0.306
2.0	0.020	1.84	0.808	0.0322	0.0580
3.0	0.063	1.83	0.742	0.0259	0.0282
4.0	0.130	1.82	0.705	0.0230	0.0119
5.0	0.245	1.78	0.639	0.0175	- 0.0124
6.0	0.328	1.72	0.560	0.0157	- 0.0198
7.0	0.396	1.66	0.481	0.0121	- 0.0235

The fourth harmonic component of torque is shown to comprise of five terms (para. 4.5). For the machine under investigation it is found that the first, fourth and fifth are very much greater than the remainder. By approximating the fourth harmonic torque

to the dominant terms the values of P_4 can be estimated

$$T_4 = \frac{N N_r}{2P_0^2} \left[4NP_0 P_1 P_3 (I_a^2 + I_b^2) - 8NP_0^2 P_4 (I_a^2 + I_b^2) - P_4 P_m^2 F_m^2 \right] \sin 4\theta_e \quad \text{--- 4.5}$$

For two phase excitation with equal currents ($I_a = I_b$)

$$T_4(2\phi) = \frac{N N_r}{2P_0^2} \left[8NP_0 P_1 P_3 I_a^2 - 16NP_0^2 P_4 I_a^2 - P_4 P_m^2 F_m^2 \right] \sin 4\theta_e$$

The signed magnitude of which is

$$T_{m4}(2\phi) = \frac{N N_r}{2P_0^2} \left[8NP_0 P_1 P_3 I_a^2 - 16NP_0^2 P_4 I_a^2 - P_4 P_m^2 F_m^2 \right]$$

$$P_4 = \frac{4N^2 N_r P_0 P_1 P_3 I_a^2 - P_0^2 T_{m4}(2\phi)}{0.5 N N_r (16NP_0^2 I_a^2 + P_m^2 F_m^2)}$$

$$P_4 = \frac{269000 P_0 P_1 P_3 I_a^2 - P_0^2 T_{m4}(2\phi)}{538000 P_0^2 I_a^2 + 0.00149}$$

The estimated values for the fourth harmonic component of permeance at values of current in the machine operating range are given in Table X and presented graphically in Figures 4.10 and 4.11.

4.6.2 Estimation of permeance coefficients from machine geometry

The geometric structure for one pole pitch, of the rotor and stator of the machine under investigation, is shown in Figure 4.12.

TABLE X Estimated Values of P_4

Phase I	$T_{m_4}(2\phi)$	$P_0(2\phi)$	P_1	P_3	P_4
A	N m	$\mu Wb/A t$	$\mu Wb/A t$	$\mu Wb/A t$	$n Wb/A t$
0.5	0.00179	1.54	0.818	0.0259	- 0.00142
1.0	0.0147	1.65	0.758	0.0273	- 0.0214
2.0	- 0.00624	1.88	0.808	0.0322	0.0499
3.0	- 0.0334	1.77	0.742	0.0259	0.128
4.0	- 0.0598	1.75	0.705	0.0230	0.207
5.0	- 0.105	1.65	0.639	0.0175	0.277
6.0	- 0.132	1.55	0.560	0.0157	0.300
7.0	- 0.173	1.44	0.481	0.0121	0.314

It is of interest to explore the feasibility of obtaining good estimates of the permeance coefficients directly from this geometry.

Chai²⁰ has proposed a 'Straight Line Arc' method to yield permeance between rectangular toothed structures. Field lines are assumed to consist of straight line segments and circular arcs, the tooth depth is assumed large compared with the air gap and tooth width is limited to lie between half the valley width and the full valley width. The toothed structure of the machine under investigation is approximated to a rectangular form as shown in Figure 4.13.

The values of permeance are calculated as the relative position of the toothed structure is varied between maximum and minimum permeance. The resulting permeance characteristic is subjected

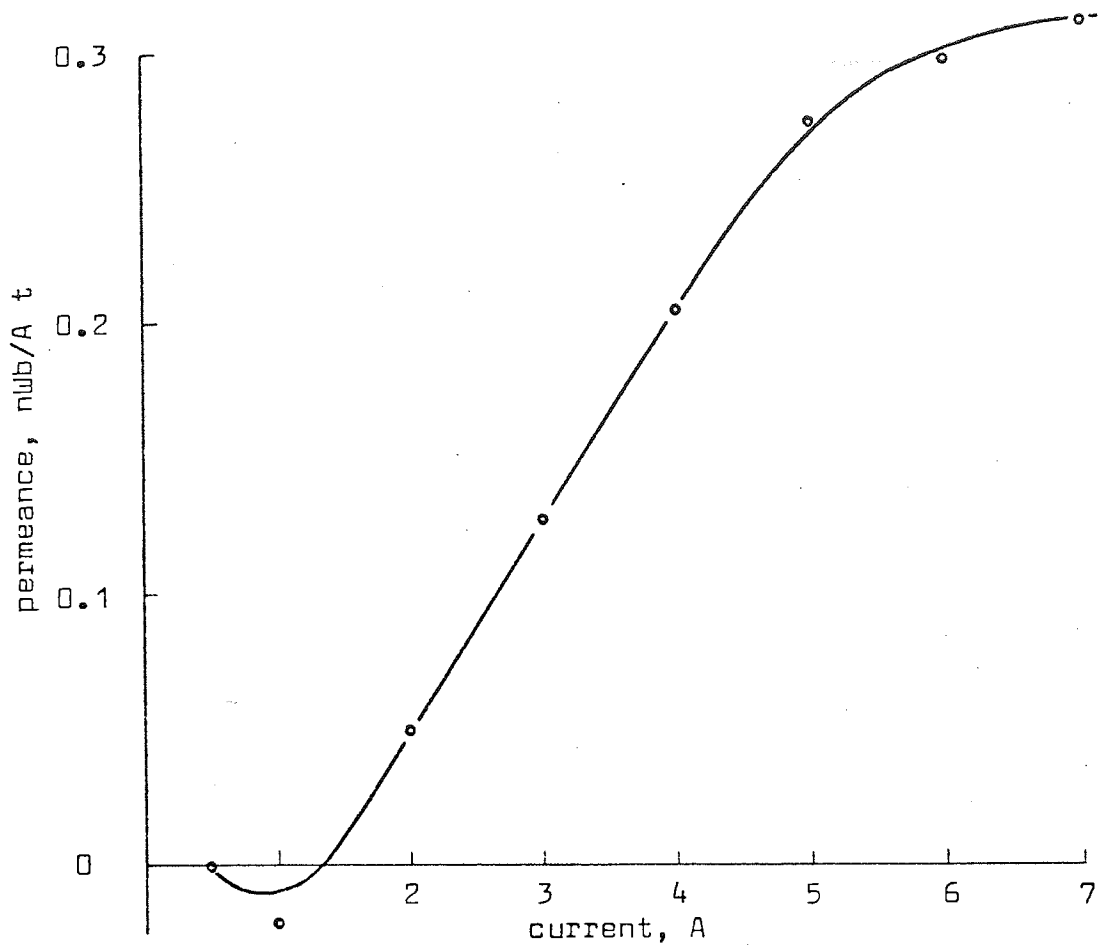


FIGURE 4.11 Variation of Permeance Coefficient P_4 with Phase Current

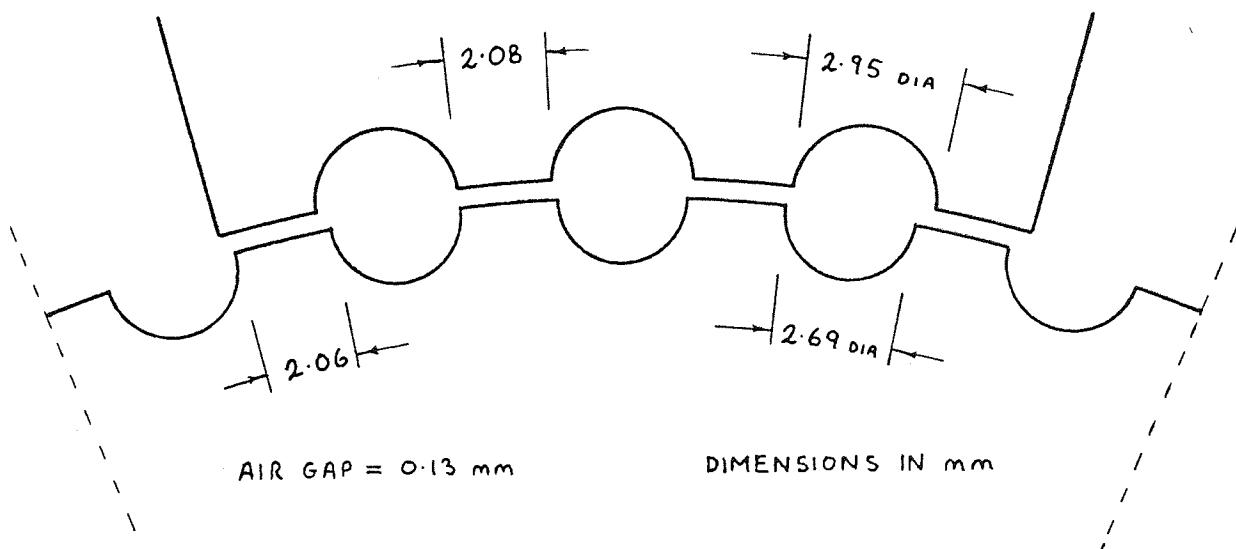


FIGURE 4.12 Toothed Structure of Rotor and Stator

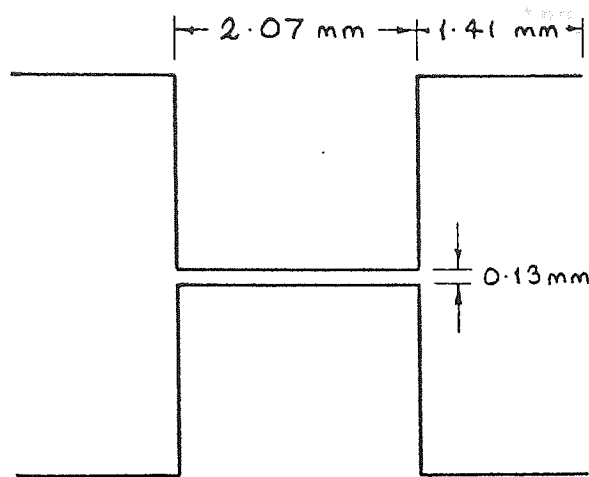


FIGURE 4.13 Approximation of Tooth Structure for Straight Line Arc and Conformal Transformation Methods

to harmonic analysis and the resulting Fourier coefficients yielded. The results are given in Table XI and were provided by Dr. Chai in the form

$$P_t = \mu_0^t C_0 + \sum_{n=1}^{\infty} C_n \cos n\theta_e$$

Where :-

P_t = permeance at each stator-rotor tooth pair

t = stack thickness

For the machine under investigation $t = 0.04$ m

To obtain the permeance at the stator poles from the permeance at each tooth pair it should be recognised that the stator pole consists of four tooth pairs; the maximum permeance position of each pair being successively displaced by 18 electrical degrees upon its adjacent pair (Figure 4.12).

TABLE XI Straight Line Arc Estimates of
Permeance Coefficients

Coefficient (n)	C_n	Pt_n $\mu\text{wb}/A t$	P_n $\mu\text{wb}/A t$
0	10.9	0.549	2.20
1	6.62	0.333	1.25
2	0.137	0.00690	0.0212
3	0.487	0.0245	0.0513
4	0.0914	0.00459	0.00459

The permeance at the stator poles is therefore :-

$$P = 4Pt_0 + \sum_{n=1}^{\infty} Pt_n \left\{ \cos n(\theta_e - 27^\circ) + \cos n(\theta_e - 9^\circ) \right. \\ \left. + \cos n(\theta_e + 9^\circ) + \cos n(\theta_e + 27^\circ) \right\}$$

Where :-

Pt_n = magnitude of the nth Fourier component of permeance at each stator-rotor tooth pair

$$P = 4Pt_0 + \sum_{n=1}^{\infty} 2Pt_n (\cos 27n^\circ + \cos 9n^\circ) \cos n\theta_e$$

Thus the relationship between the tooth and stator Fourier coefficients of permeance is given by :-

$$P_n = 2Pt_n (\cos 27n^\circ + \cos 9n^\circ)$$

Thus

$$P_0 = 4.000 Pt_0$$

$$P_1 = 3.757 Pt_1$$

$$P_2 = 3.078 Pt_2$$

$$P_3 = 2.095 Pt_3$$

$$P_4 = 1.000 Pt_4$$

Jones²¹ has proposed a 'Conformal Transformation' method to yield permeance between rectangular toothed structures. Two problems are considered, one when the teeth are almost aligned and the second when the teeth are misaligned. A different mapping is used in each case and the mapping transformation found. The simpler field problem is then solved in the mapped plane. Force on the structure is given by integrating the normal derivative of the field strength along the boundary for each problem and the total force is yielded by superposition of the forces given by the solution of the two problems. The permeance is then obtained by a truncated integral of the total force. The toothed structure of the machine under investigation is approximated as before and the resulting permeance characteristic subjected to harmonic analysis. The results, which were provided by Dr. Chai, are given in Table XII.

Chai²² has proposed a method to yield permeance between toothed structures of arbitrary shape which does not require opposing teeth to be identical. The technique is based on the 'Moment' method (23,24) which converts two-dimensional Laplace problems into matrix form. The toothed structure of the machine is approximated to the form shown in Figure 4.14. The values of permeance are calculated as the relative position of the toothed structure is moved between the maximum and minimum permeance

TABLE XII Conformal Transformation Estimates of
Permeance Coefficients

Coefficient (n)	C_n	Pt_n $\mu\omega b/A t$	P_n $\mu\omega b/A t$
0	10.9	0.547	2.19
1	6.36	0.320	1.20
2	0.183	0.00918	0.0283
3	0.432	0.0217	0.0455
4	0.121	0.00608	0.00608

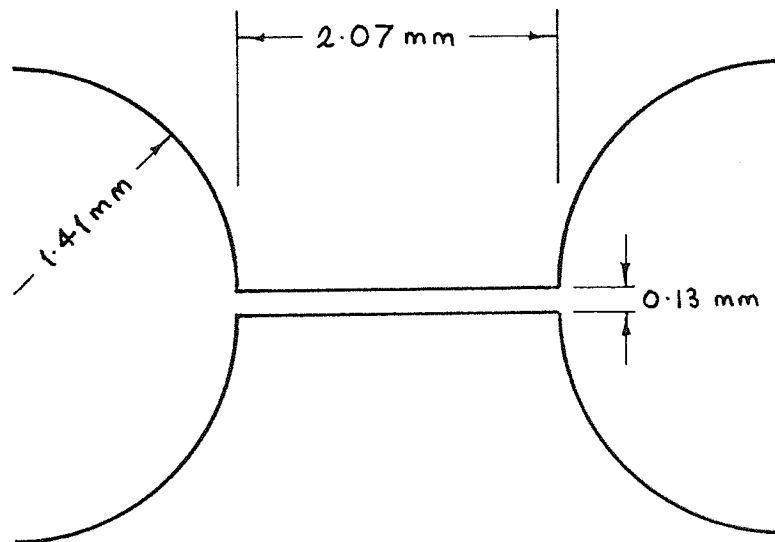


FIGURE 4.14 Approximation of Tooth Structure
for Moment Method

TABLE XIII Moment Estimates of Permeance Coefficients

Coefficient (n)	C_n	Pt_n $\mu\text{wb}/A t$	P_n $\mu\text{wb}/A t$
0	12.7	0.637	2.55
1	6.04	0.304	1.14
2	0.111	0.00557	0.0172
3	0.409	0.0205	0.0430
4	0.0227	0.00114	0.00114

positions. The results of harmonic analysis on the resulting permeance characteristic were provided by Dr. Chai and are given in Table XIII.

4.6.3 Comparison of permeance coefficients

Permeance coefficients are compared in Table XIV. The 'Measured Data' results are those estimated at a phase current of 3 A. It is considered that, at this current, the effects of saturation are minimal. The 'Measured Data' results, therefore, provide a valid comparison with the non saturating results estimated from geometric considerations.

4.6.4 Numerical results and discussion

The extension of the mathematical model for the formulation of static torque predicts that spacial harmonics in the machine permeance displacement characteristic give rise to spacial harmonics of the same and higher orders in the static torque displacement characteristic. To some degree it is a test of

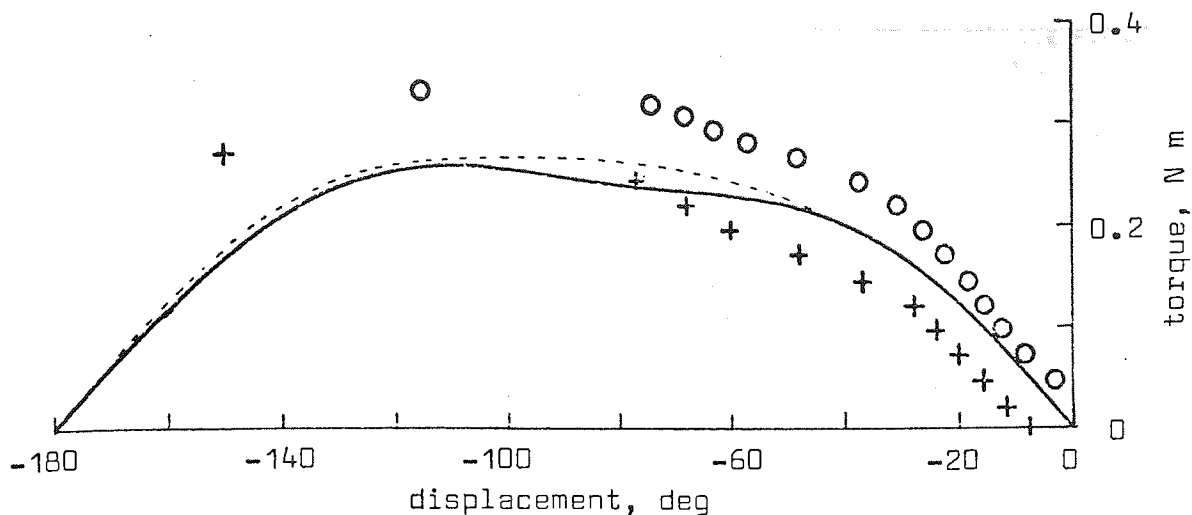
TABLE XIV Comparison of Estimates of Permeance Coefficients

	Straight Line Arc	Conformal Transformation	Moment	Measured Data
$P_0 \mu\omega b/A t$	2.20	2.19	2.55	1.83
$P_1 \mu\omega b/A t$	1.25	1.20	1.14	0.742
$P_2 \mu\omega b/A t$	0.0212	0.0283	0.0172	0.0282
$P_3 \mu\omega b/A t$	0.0513	0.0455	0.0430	0.0259
$P_4 n\omega b/A t$	4.59	6.08	1.14	0.128
$\frac{P_1}{P_0}$	0.568	0.548	0.447	0.405
$\frac{P_2}{P_0} \times 10^3$	9.64	12.9	6.74	15.4
$\frac{P_3}{P_0} \times 10^3$	23.3	20.8	16.9	14.2
$\frac{P_4}{P_0} \times 10^3$	2.09	2.78	0.447	0.0699

this model to attempt to predict the permeance characteristic from the torque characteristic and to observe if the Fourier coefficients of permeance have expected values and behave in a reasonable manner with current. Permeance coefficients P_0 , P_1 and P_3 (Figures 4.8 and 4.10), estimated from the measured torque displacement characteristic are, in all respects, reasonable having normal values and showing saturation effects with increasing phase current. Permeance coefficient P_2

(Figure 4.8), however, has a form which is unreasonable having a very large value at 0.5 A and then falling rapidly through zero to become negative at higher currents. It is considered that this characteristic is due to the uncertainty of estimating the coefficient, particularly at low current levels. P_2 appears only in the expression for second harmonic torque (equation 4.4) where it is part of a term which is small compared to the remainder of the expression. The term is zero when the phase currents are equal and thus two phase torque with equal currents is independent of P_2 . It is considered, therefore, that P_2 can, for the machine under investigation, be reduced to zero with little loss of accuracy. It is noted that the most pronounced effect, of this simplification, will be observable when one phase current is set to zero and the other phase current is set to a low value. Therefore, a comparison of predictions of single phase, low current, static torque displacement characteristics with, and then without, P_2 included, is made. The results are presented in Figure 4.15 where the single phase 0.5 A characteristic, with P_2 set to $0.827 \mu\text{Wb/A t}$, is compared with the characteristic predicted when P_2 is set to zero. The result shows, clearly, that the permeance coefficient P_2 has a negligible effect upon the prediction of the static torque displacement characteristic of the machine under investigation and can therefore be set to zero.

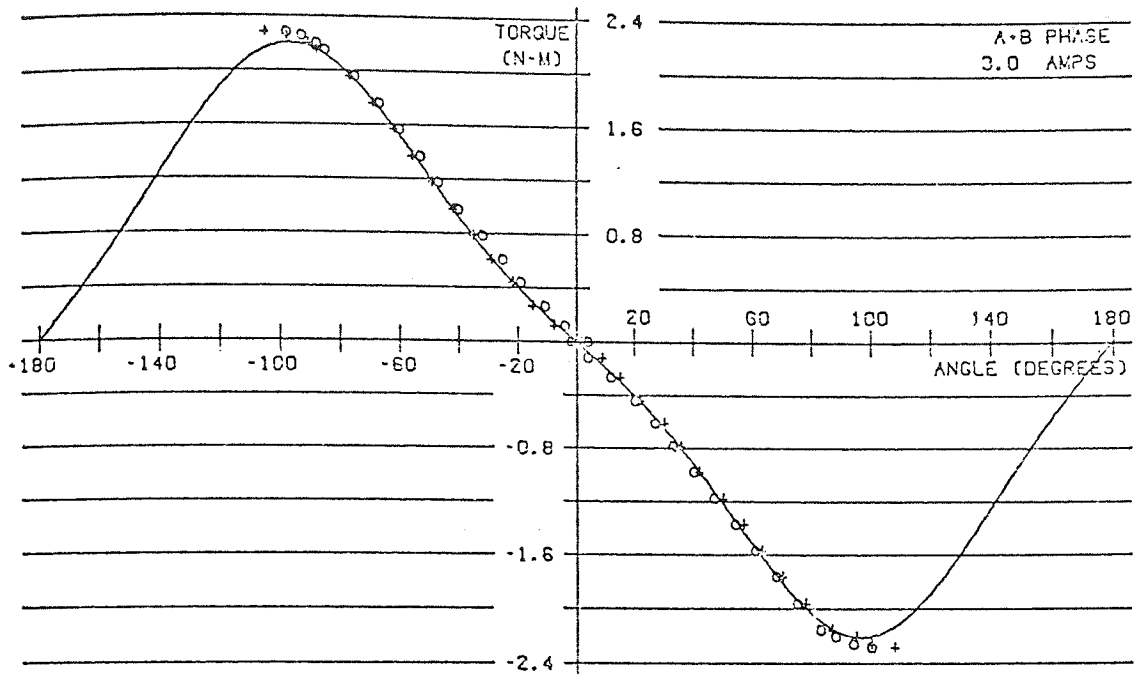
Permeance coefficient P_4 is shown to be very small (Figure 4.11). Inspection of equation 4.5 will show that, with the value of P_4 yielded, the contribution to the fourth harmonic torque made by P_4 is negligible. It is clear that, for the machine under investigation, permeance coefficient P_4 can also be set to zero.



- experimental, increasing torque
- + experimental, decreasing torque
- prediction, $P_2 = 0.827 \mu\text{Wb/A t}$
- prediction, $P_2 = 0$

FIGURE 4.15 Prediction of 0.5 A, Single Phase, Static Torque Displacement Characteristic Using Permeance Coefficients Estimated from Measured Data

A further validation of the model may be obtained by ensuring that the static torque displacement characteristic can be predicted in regions that were not used for the estimation of the permeance coefficients. All the dominant permeance coefficients are estimated from the two phase ($I_a = I_b$) static torque displacement characteristics. It is of interest, therefore, to predict the single phase ($I_b = 0$) static torque displacement characteristics using the same permeance coefficients. Two phase predictions, at phase currents of 3 A and 7 A are presented in Figures 4.16 and 4.17 respectively. The predictions are very close to the experimental values, as expected, since the permeance coefficients are estimated from these values. However, Figures 4.18



- experimental, increasing torque
- + experimental, decreasing torque
- prediction

FIGURE 4.16 Prediction of 3 A, Two Phase, Static Torque Displacement Characteristic Using Permeance Coefficients Estimated from Measured Data

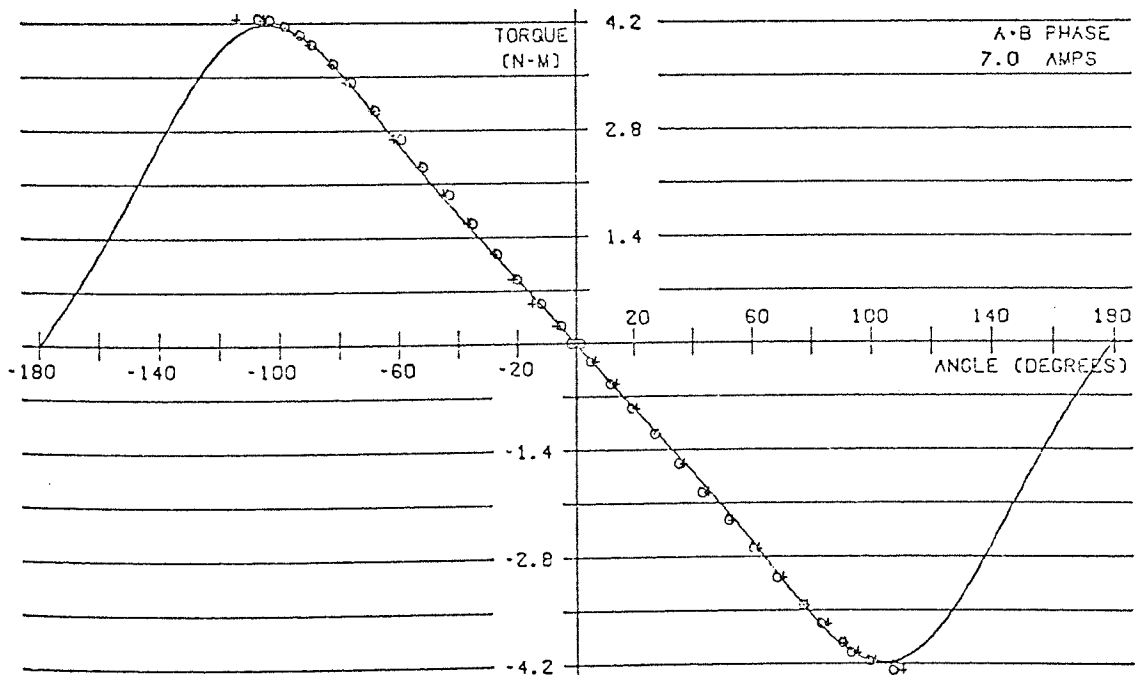


FIGURE 4.17 Prediction of 7 A, Two Phase, Static Torque Displacement Characteristic Using Permeance Coefficients Estimated from Measured Data

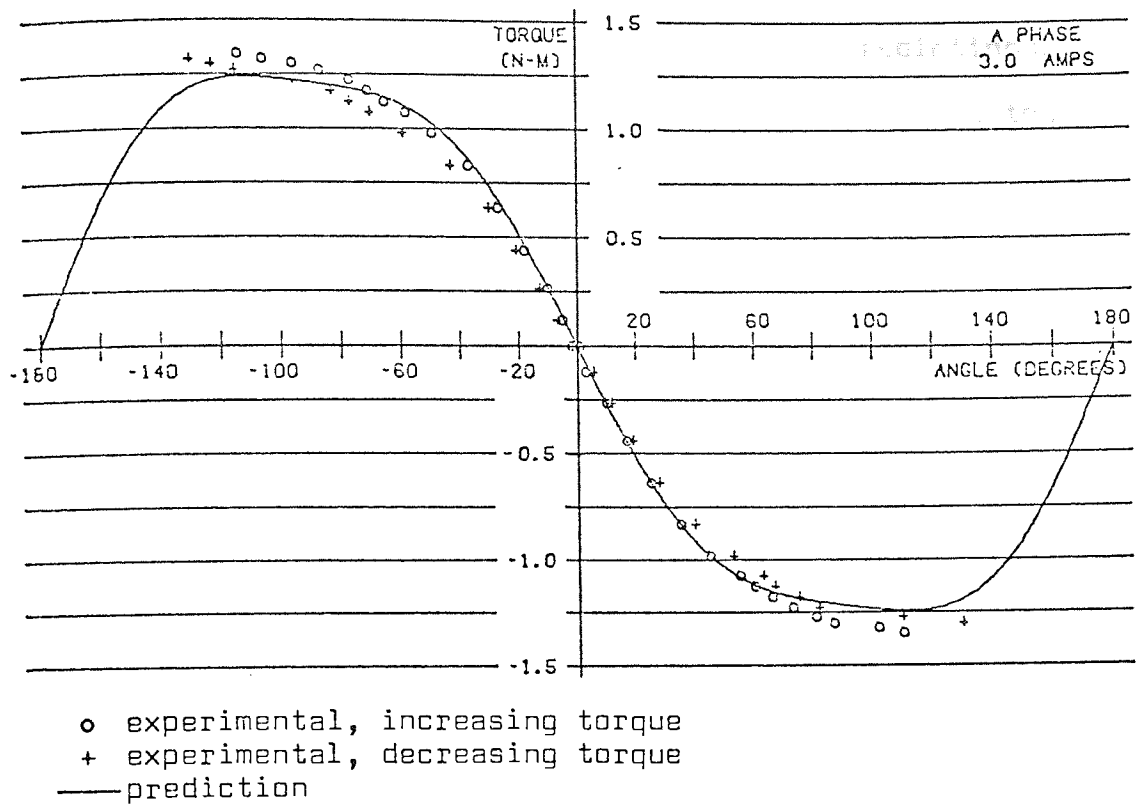


FIGURE 4.18 Prediction of 3 A, Single Phase, Static Torque Displacement Characteristic Using Permeance Coefficients Estimated from Measured Data

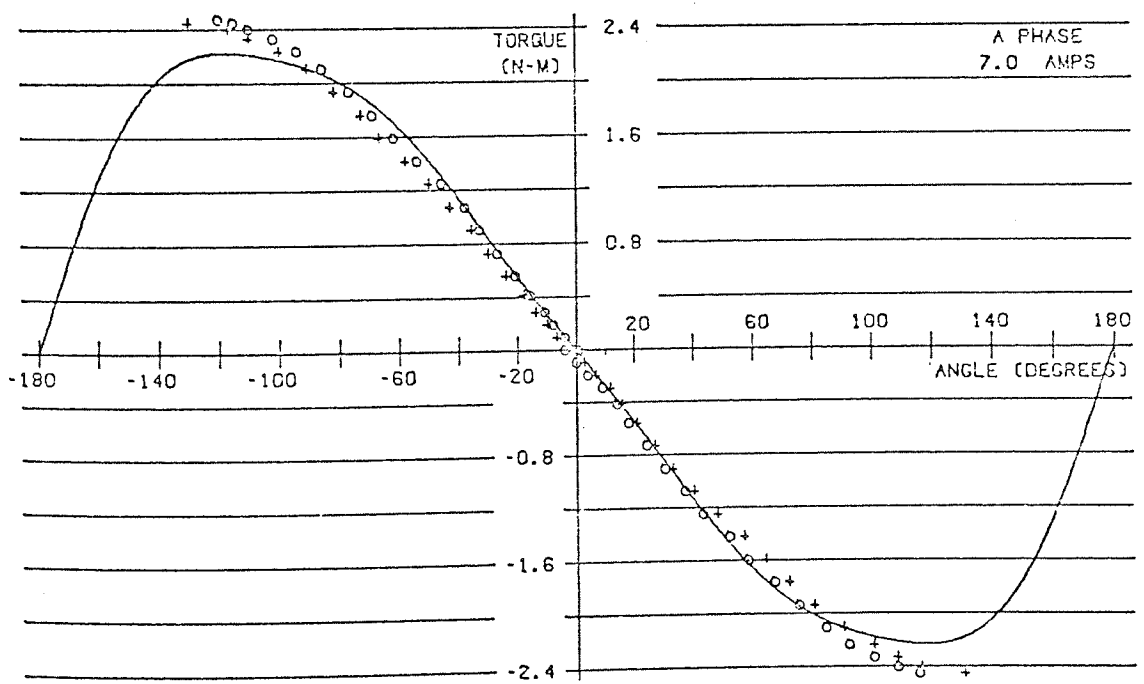


FIGURE 4.19 Prediction of 7 A, Single Phase, Static Torque Displacement Characteristic Using Permeance Coefficients Estimated from Measured Data

and 4.19 present the corresponding single phase predictions. These results are considered to be sufficiently close to the experimental values to imply that the mathematical model for the formulation of static torque is valid.

The estimation of permeance coefficients from the machine geometry is of considerable interest since, if feasible, the static torque displacement characteristic can be predicted directly from the machine structure; this in turn may give some insight into how the geometry of the machine influences the form of the torque characteristic. The 'Straight Line Arc' and 'Conformal Transformation' methods suffer from the disadvantage that they are limited to rectangular toothed structures which, for the machine under investigation, requires a considerable approximation. The 'Moment' method has the advantage that it allows permeance to be estimated between structures of arbitrary shapes but has the disadvantage that it is probable that it will yield high estimates due to its use of open boundary conditions. Chai²² suggests that the estimates may be corrected by applying a factor based on a calculation of the maximum and minimum permeance since, when opposing teeth are aligned, and when a tooth and valley are aligned, the boundary conditions are known. A further disadvantage of the 'Moment' method is the large amount of digital computer work space necessary to yield a solution. For the system used by Chai²² $17N^2$ bytes of work space is required where N is the number of boundary points used to specify the problem. The 'Straight Line Arc' method is, on the other hand, a small problem in computing terms and allows a simple sinusoidal approximation to the permeance characteristic to be made. This approximation is capable of reasonable results

and is of particular use in giving an insight into the problem of how the changes in machine geometry affect the form of the torque displacement curve.

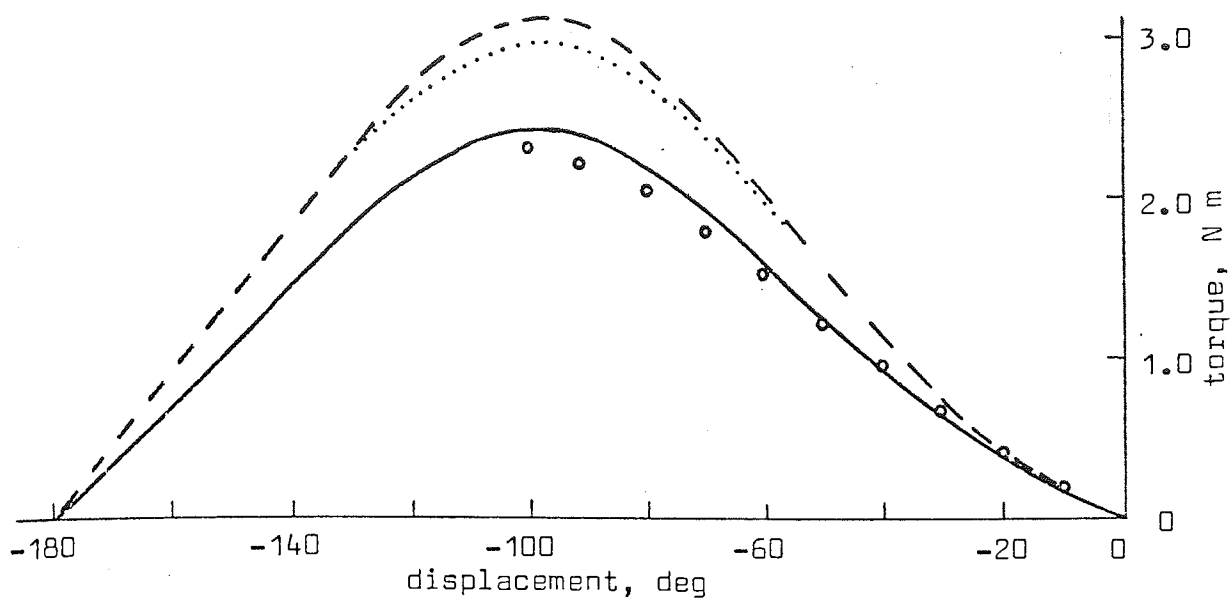
The data presented by Table XIV shows that, in general, the estimates of the permeance coefficients from machine geometry are somewhat higher than the estimates from measured data. This may be due to the rotor-stator air gap being greater than the nominal 0.13 mm. 'Straight Line Arc' estimates of permeance coefficients at air gaps of 0.13 mm and 0.15 mm are compared in Table XV. It is observed that, with the larger gap, the coefficients are much nearer to those estimated from measured data.

Predictions of the two phase torque displacement characteristic, at phase currents of 3 A and 7 A, using permeance coefficients yielded by machine geometry are presented in Figures 4.20 (3 A) and 4.21 (7 A). Figure 4.20 shows that the permeance coefficients yielded by the 'Moment' method have predicted a two phase, 3 A, static torque displacement characteristic which is very close to experimental values and is superior to other predictions based on the machine geometry. This is to be expected since only this method is capable of taking into account the non-rectangular toothed structure of the machine under investigation. The 'Moment' prediction is good even though the estimates of the permeance coefficients are high. This is so because the Fourier components of torque are dependent upon ratios of the Fourier components of permeance rather than upon absolute values. For example, the fundamental component of torque, which is the dominant term, is proportional to the ratio P_1/P_0 .

TABLE XV Comparison of Estimates of Permeance Coefficients

	Straight Line Arc		Measured Data
	Air Gap = 0.13mm	Air Gap = 0.15mm	
$P_0 \mu\text{wb/A t}$	2.20	1.92	1.83
$P_1 \mu\text{wb/A t}$	1.25	1.02	0.742
$P_2 \mu\text{wb/A t}$	0.0212	0.0160	0.0282
$P_3 \mu\text{wb/A t}$	0.0513	0.0409	0.0259
$P_4 \text{ nwb/A t}$	4.59	3.19	0.128
$\frac{P_1}{P_0}$	0.568	0.531	0.405
$\frac{P_2}{P_0} \times 10^3$	9.64	8.33	15.4
$\frac{P_3}{P_0} \times 10^3$	23.3	21.3	14.2
$\frac{P_4}{P_0} \times 10^3$	2.09	1.66	0.0699

Figure 4.21 shows that, at a phase current of 7 A, the predictions of the two phase static torque displacement characteristic are poor. This is expected since the effects of saturation of the machine iron are pronounced at this current. It is clear that, in general, any attempt to predict the static torque displacement characteristic from a permeance characteristic estimated from the machine geometry should be restricted to fields which do not tend to saturate the magnetic material.



- experimental
- straight line arc
- conformal transformation
- moment

FIGURE 4.20 Predictions of 3 A, Two Phase, Static Torque Displacement Characteristic Using Permeance Coefficients Estimated from Machine Geometry

Figures 4.22, 4.23 and 4.24 present the results of predictions of the two phase static torque displacement characteristic using permeance coefficients yielded by the 'Moment' method. The predictions are for phase currents of 0.5 A, 2 A and 4 A respectively. Figures 4.25, 4.26 and 4.27 present the corresponding single phase predictions. It is clear that, for unsaturated conditions, predictions of the static torque displacement characteristic from the machine geometry is both feasible and reasonably accurate. A criticism of the method must be that it fails when the machine iron tends to saturate.

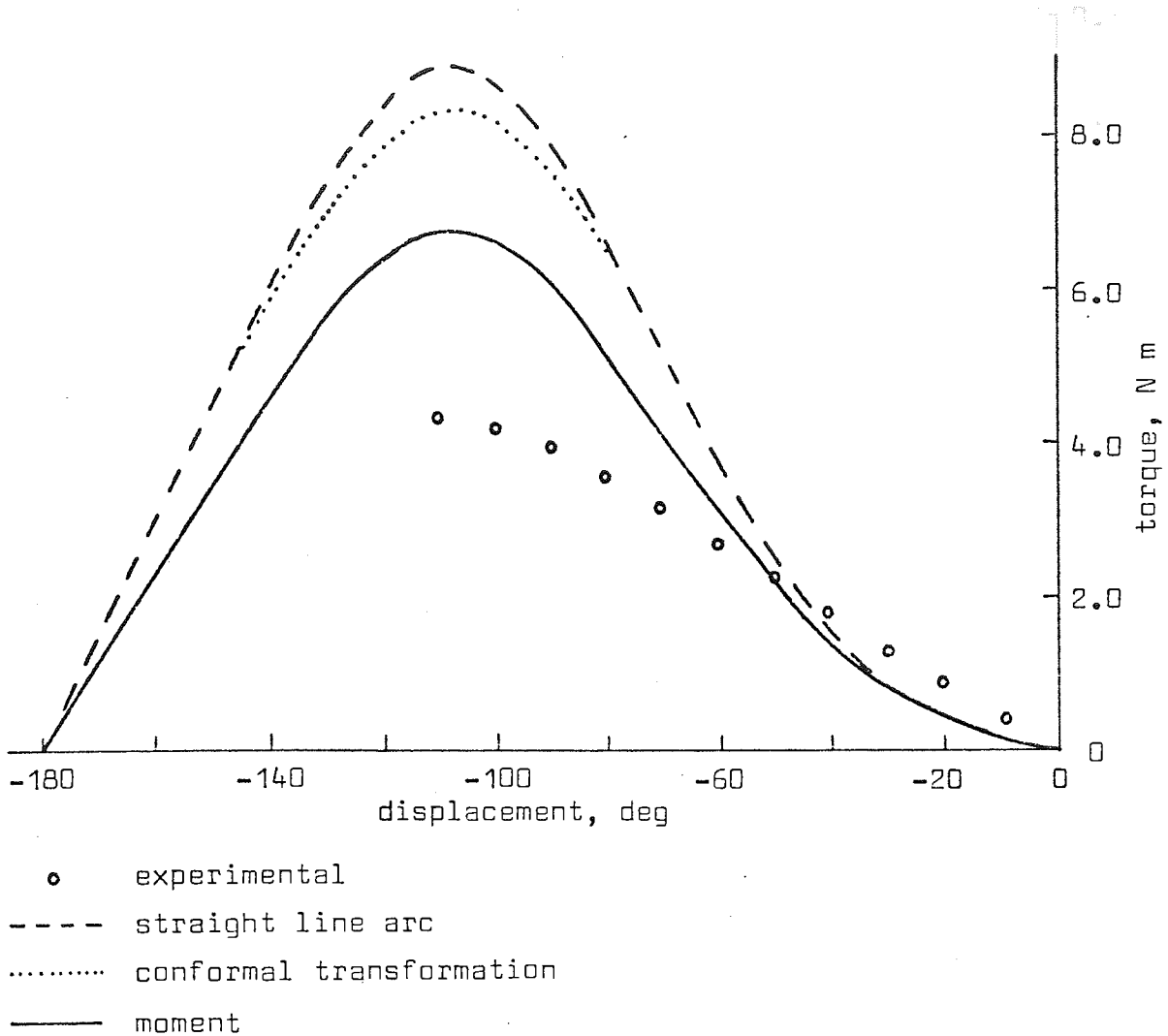


FIGURE 4.21 Prediction of 7 A, Two Phase, Static Torque Displacement Characteristic Using Permeance Coefficients Estimated from Machine Geometry

However, it may be possible to take account of these effects since, as the teeth start saturating, the magnetic boundary will deviate progressively from the mechanical boundary. It may be practical, therefore, to model the effects of saturation by changing the mechanical boundary of the structure.

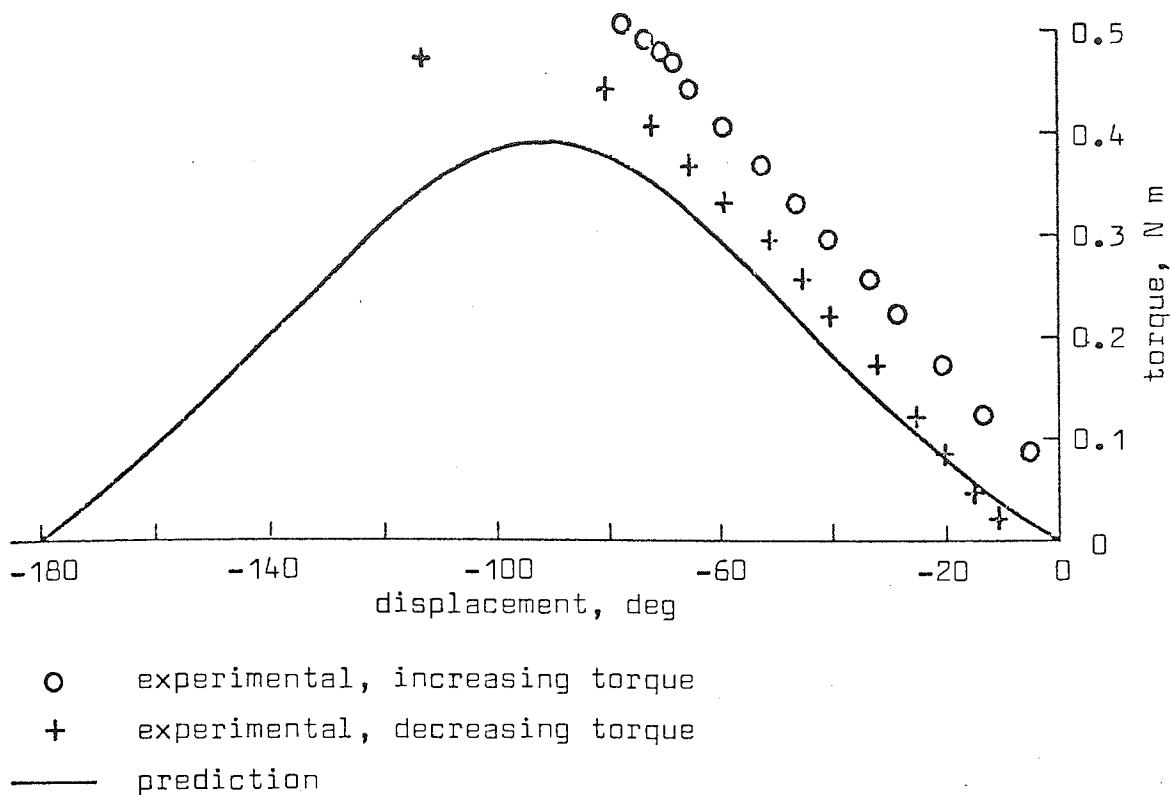


FIGURE 4.22 Prediction of 0.5 A, Two Phase, Static Torque Displacement Characteristic Using Permeance Coefficients Estimated by the 'Moment' Method

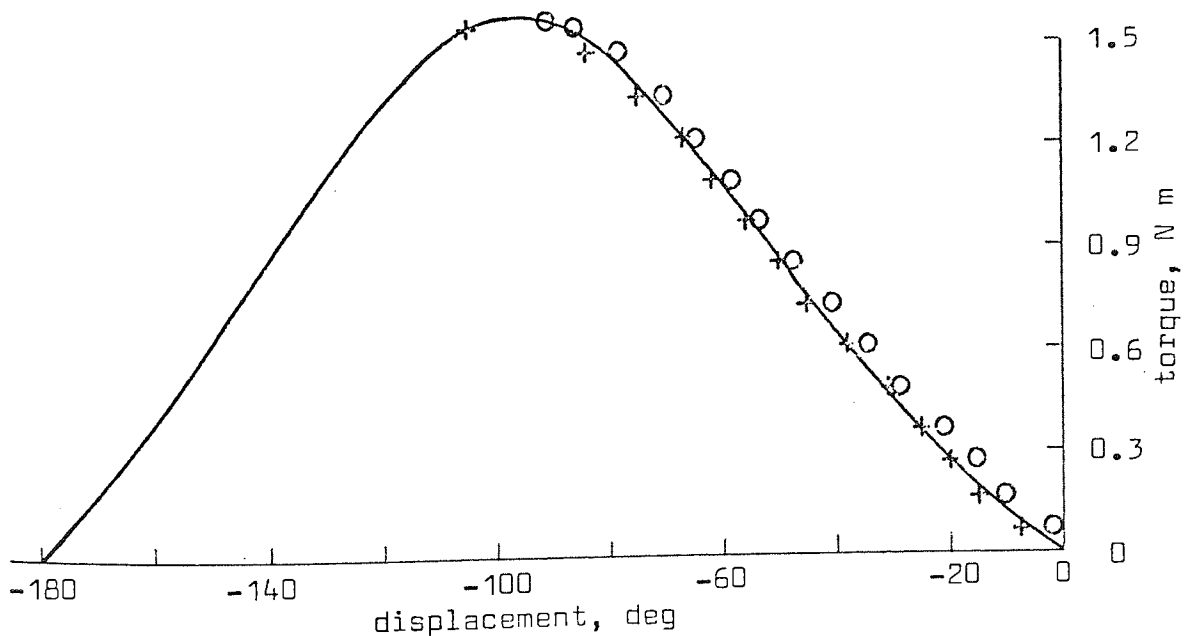


FIGURE 4.23 Prediction of 2 A, Two Phase, Static Torque Displacement Characteristic Using Permeance Coefficients Estimated by the 'Moment' Method

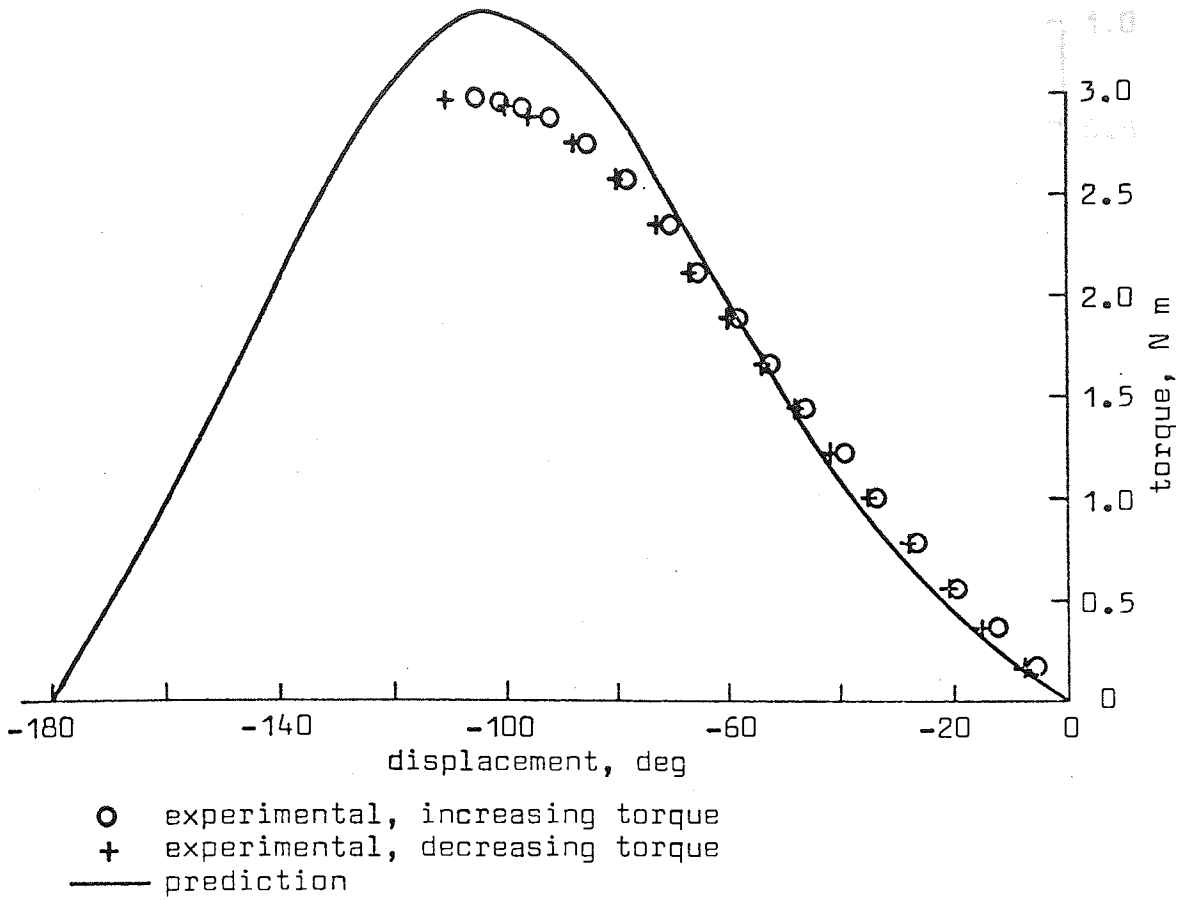


FIGURE 4.24 Prediction of 4 A, Two Phase, Static Torque Displacement Characteristic Using Permeance Coefficients Estimated by the 'Moment' Method

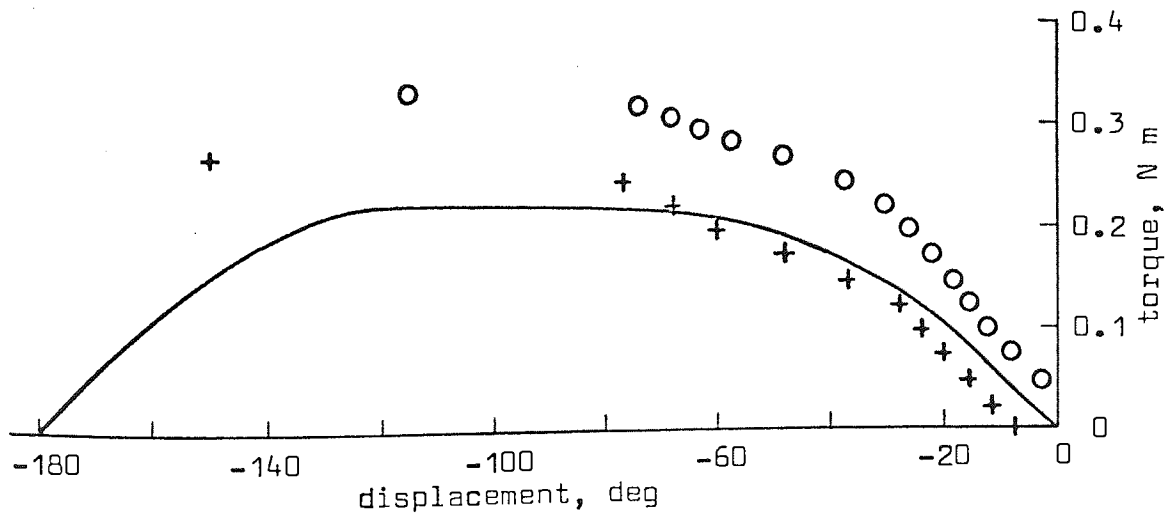


FIGURE 4.25 Prediction of 0.5 A, Single Phase, Static Torque Displacement Characteristic Using Permeance Coefficients Estimated by the 'Moment' Method

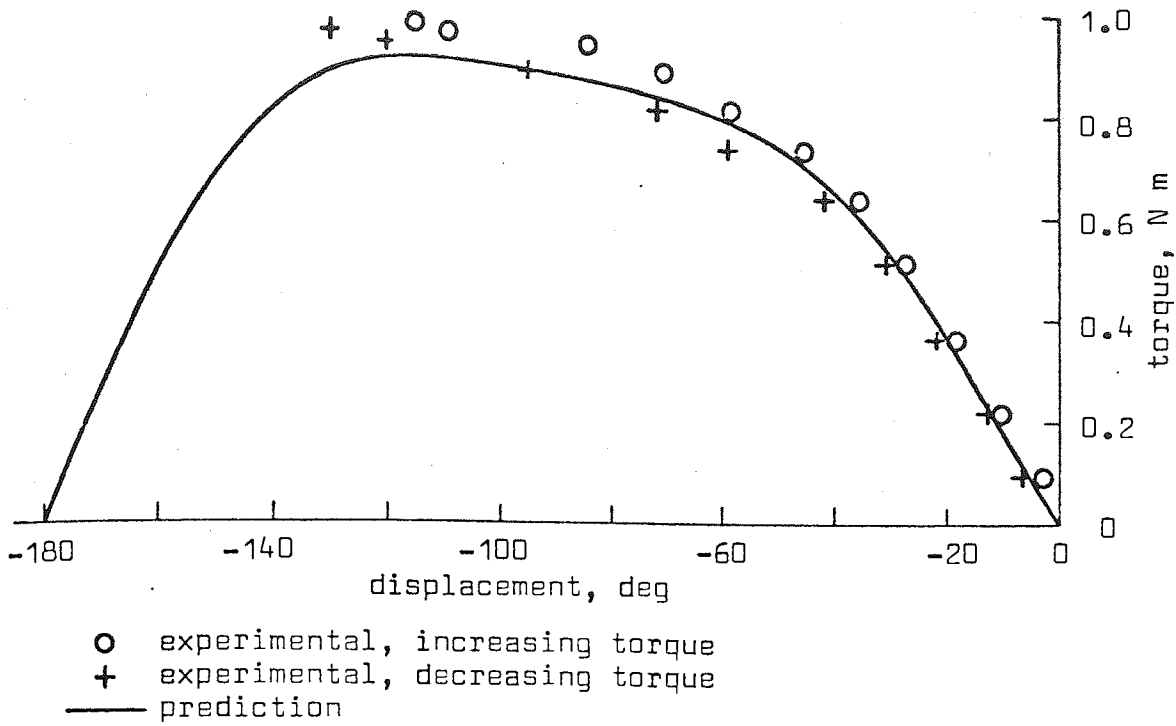


FIGURE 4.26 Prediction of 2 A, Single Phase, Static Torque Displacement Characteristic Using Permeance Coefficients Estimated by the 'Moment' Method

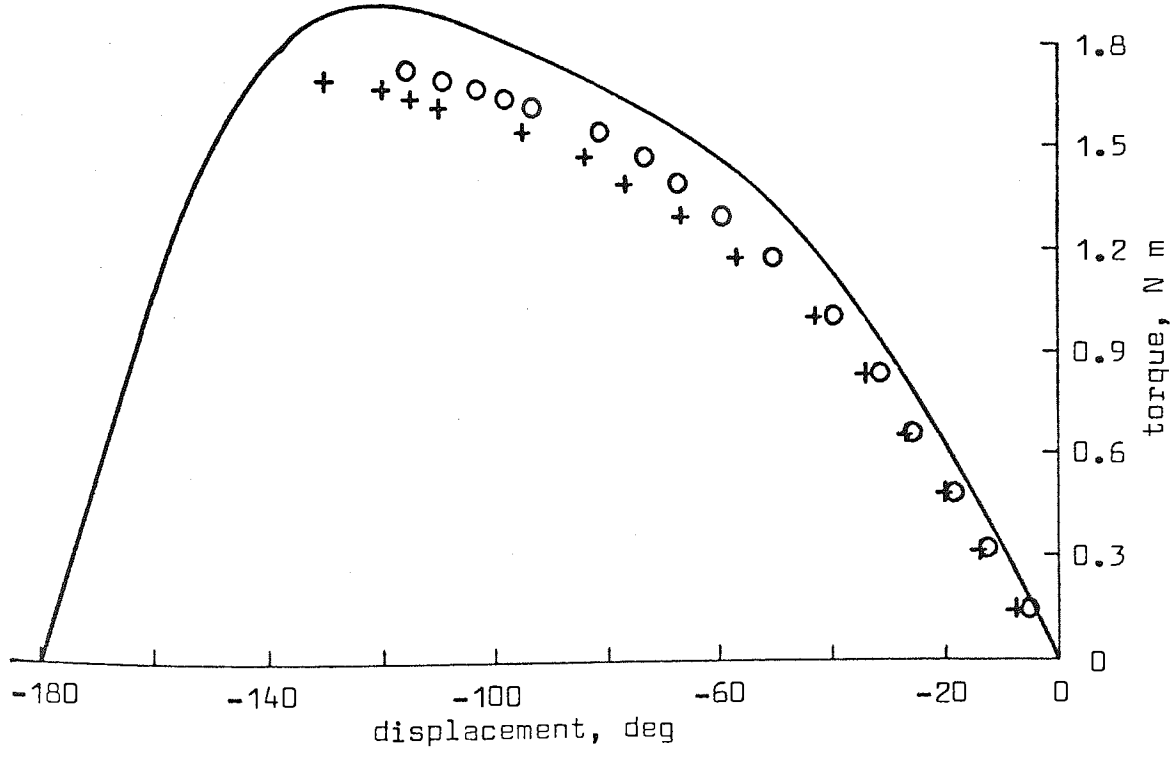


FIGURE 4.27 Prediction of 4 A, Single Phase, Static Torque Displacement Characteristic Using Permeance Coefficients Estimated by the 'Moment' Method

4.7 Conclusions

The accurate prediction of torque for any combination of the phase currents is an essential feature of a stepping motor simulation. Many models of the static torque displacement characteristic have been proposed, the majority of which are poor and of limited use. Chai's⁴ model, and the extensions thereof proposed here, do, however, predict results that are observable in practice. In general the static torque displacement characteristic of a stepping motor will contain spacial harmonics which are not insignificant and therefore the frequently used sinusoidal approximation, of this characteristic, will yield poor predictions of torque. It is shown that it is very unlikely that the static torque displacement characteristic will be a sinusoid since, even if the permeance characteristic contains no Fourier components above the first, the static torque displacement characteristic will contain a significant second harmonic component. It is also shown that, the frequently practised, direct addition of phase torque to yield the total torque with both phases energised is erroneous. The extensions to Chai's⁴ model take account of permeance harmonics, in addition to the first and fourth, and allow any combination of phase currents to be handled.

The estimation of permeance coefficients from measured data is, to some extent, unsatisfactory in that it is a circular argument. Therefore, it is certain that the characteristic that is used to estimate the coefficients is predictable. It is shown, however, that the permeance coefficients estimated from the measured static torque displacement characteristics have expected values and compare favourably with permeance parameters estimated directly

from the machine geometry. In addition, the predictions have been satisfactorily extended to regions that were not used to estimate the permeance coefficients.

The estimation of the permeance coefficients directly from the machine geometry is shown to be feasible. Coefficients yielded by the 'Moment' method are, in the case of the machine under investigation, shown to be superior to other geometric methods examined. It is considered that, for rectangular toothed structures, the 'Straight Line Arc' method has many advantages. The prediction of the torque displacement characteristic directly from machine geometry has much to offer the machine designer and control engineer with the methods being more attractive if they could be adapted to take account of saturation effects.

5.1 Introduction

The machine dynamics are affected, to a considerable extent, by the transfer function between the voltage applied to the stator winding and the magnetic flux in the stator-rotor air gap. In general, the drive circuit applies a voltage step to the stator windings, however, inductance and eddy current effects contribute time constants which cause the flux, and therefore the torque, to lag the voltage. Although the single-step transient response of the rotor is similar to a second order step response, an important difference occurs due to the fact that a step of torque cannot be applied. It is important that the initial part of the rotor response is capable of prediction if the high speed slewing performance is to be accurately simulated. For such predictions the transfer function between applied voltage and current, and between current and flux, should be accurately known.

The voltage to flux transfer function can be obtained directly by using frequency response methods. However, when using these methods, magnetic hysteresis of the machine iron can seriously affect the result. The measurement technique should take account of the presence of magnetic hysteresis in order that its effects are included, where appropriate. A combination of inductance measurements, using a d.c. bridge, and frequency response tests is found to yield a transfer function which predicts results observable in practice.

Robinson and Taft⁷ were the first to recognise that the transient response of the stator current has a significant effect upon the

dynamics of the stepping motor, especially at high stepping rates. The effects of stator inductance and resistance are considered, yielding a simple first order transfer between applied voltage and current. Eddy currents, in the solid rotor machine investigated, are neglected. To obtain results for the machine's multi-stepping performance they use the simplifying assumption of constant current drive, thus eliminating the stator time constant.

Singh¹⁸ reports that magnetic non-linearities and core losses are extremely difficult to model accurately and for this reason are often neglected. He admits that, due to this simplification, the results will be inaccurate, particularly for solid rotor machines, and advocates correction by semi-empirical methods. The effects of inductance are, however, included and he derives a model which is suitable for the prediction of multi-stepping performance. He advocates the use of an incremental inductance bridge (a.c.) for the determination of stator incremental inductance, at various values of direct current, and then using the data to determine the average inductance. This method is likely to yield very poor results due to the effects of hysteresis and eddy currents. In a later contribution Singh et al.²⁵ refer to the possibility of using a d.c. inductance bridge as a method of yielding average inductance directly and eliminating the effects of eddy currents on the measurement.

Pickup and Tipping⁸ have shown the effects of eddy currents on the single-step transient response of the stepping motor. Eddy currents are detected by observing the delay in the rise of the flux linking the exciting coil relative to the rise of the input current when a voltage step is applied, with the rotor clamped.

They propose an equivalent circuit to account for eddy currents in which fictitious resistive elements couple with parts of the total core flux. They use the observed current and step responses, together with d.c. tests, to determine the values of the components in the equivalent circuit. Predictions, using this circuit, of switch on current and resulting rotor dynamics are shown to be in close agreement with experimental results whilst results presented, neglecting eddy current effects, are shown to have unacceptable errors. In a later contribution (27) they turn their attention to predicting multi-stepping performance using the same model to account for eddy currents. Predictions of pull-in rate and settling-time show a satisfactory level of agreement with experimental values.

Kordik²⁶ addresses himself to the problem of measuring stepping motor stator inductance with the justification that, to predict the performance of a stepping motor an accurate knowledge of the self inductance is required. The d.c. bridge, a.c. bridge and observation of the stator current, in response to a voltage step, are described and considered as measurement methods. He recognises that a.c. bridge methods will be in error if eddy currents are significant and advocates the use of low frequency, small amplitude a.c. to minimise the error. This is only correct in the unlikely event that the machine iron does not exhibit hysteresis effects. Modest hysteresis will cause the error in inductance measurements to be particularly high if small amplitude current perturbations are used since, with these conditions, the average slope of the minor B-H loop is much smaller than the slope of the major B-H loop at that point. For the same reason, the method does not give the true value of

incremental inductance when hysteresis is present. Inductance determination by the observation of the response of the stator current to a step input of voltage assumes, as does the a.c. bridge method, a simple first order transfer between voltage and current. However, the presence of eddy currents add pole-zero pairs to the transfer function causing the method to be in error when their effects are significant.

5.2 Frequency Response Tests

Initial attempts to predict the form of the stator current transient by assuming a single time constant transfer function, between voltage and current, failed. The actual current rise is many times slower than that predicted. Frequency response measurements were taken to investigate this transfer and revealed that the function was indeed more complex. A set of results were obtained between 0.1 A peak-to-peak and 8 A peak-to-peak using a symmetrical current perturbation, whose amplitude was held constant for each response. The results for peak-to-peak current perturbations of 0.2 A and 4.0 A are presented in Figures 5.1 to 5.4. It is evident that any attempt to predict the current and flux transient or to make measurements upon the winding, assuming a single time constant, will lead to unacceptable errors. The form of the frequency response is accounted for by the presence of eddy currents in the solid rotor causing a lag of the flux upon the current.

5.3 Formulation of Transfer Function

Inspection of the frequency response measurements leads to the conclusion that the transfer between voltage and current at each

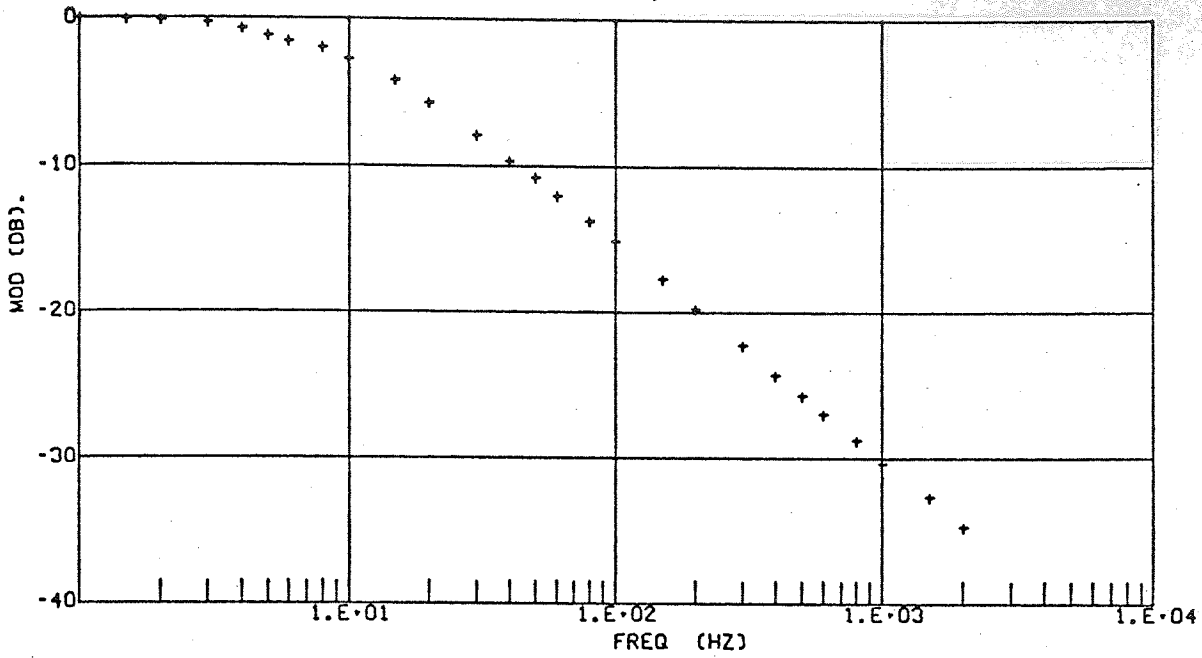


FIGURE 5.1 Stator V/I Gain Response (0.2 A p-p)

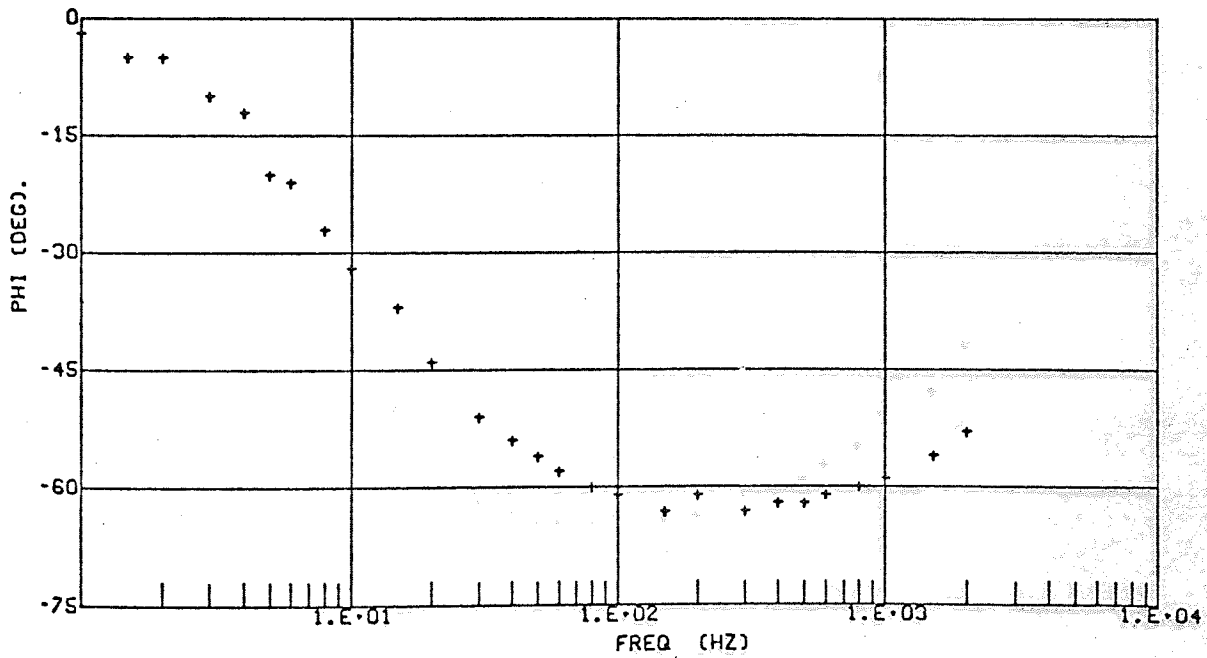


FIGURE 5.2 Stator V/I Phase Response (0.2 A p-p)

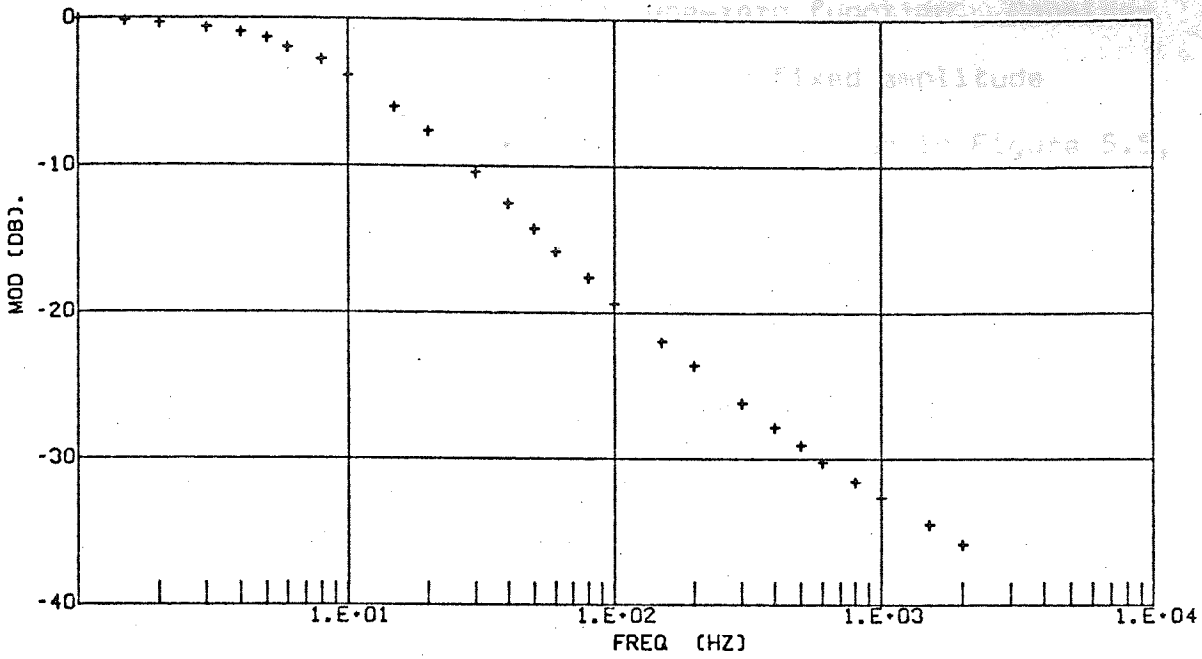


FIGURE 5.3 Stator V/I Gain Response (4.0 A p-p)

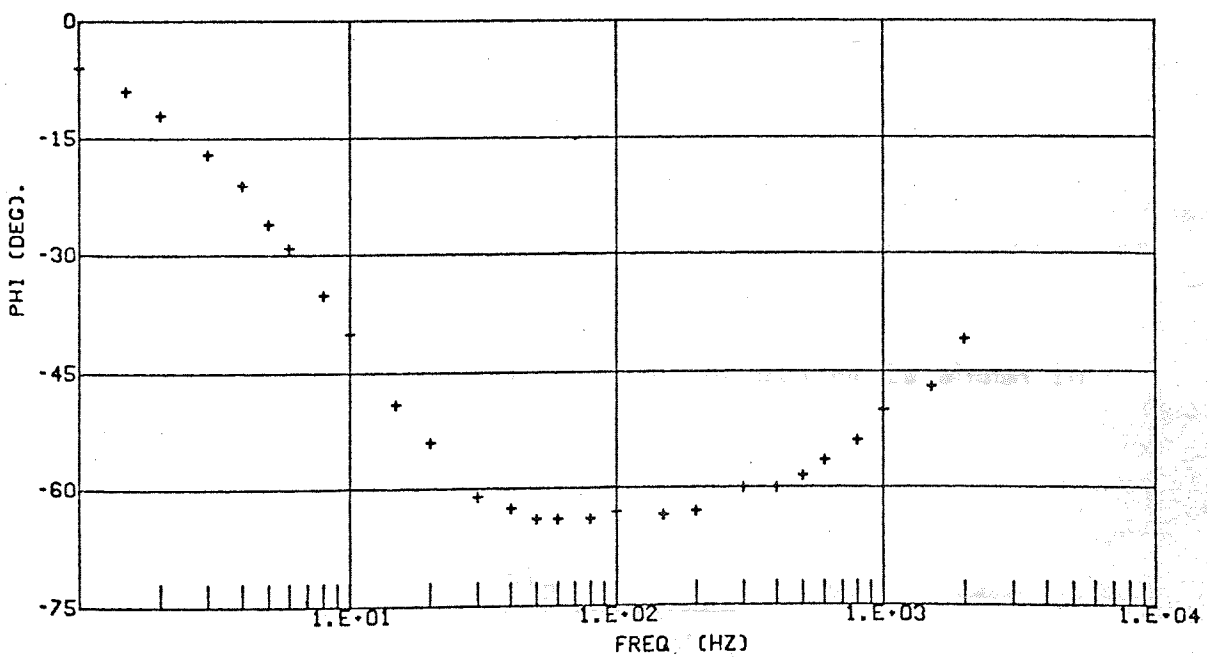


FIGURE 5.4 Stator V/I Phase Response (4.0 A p-p)

discrete current level, can be adequately described by a two-pole, one-zero function. The transfer between current and flux is therefore described by a one-pole, one-zero function. Consider a linear model of the stator circuit, for fixed amplitude current perturbations, to be represented as shown in Figure 5.5, with volt drops as shown.

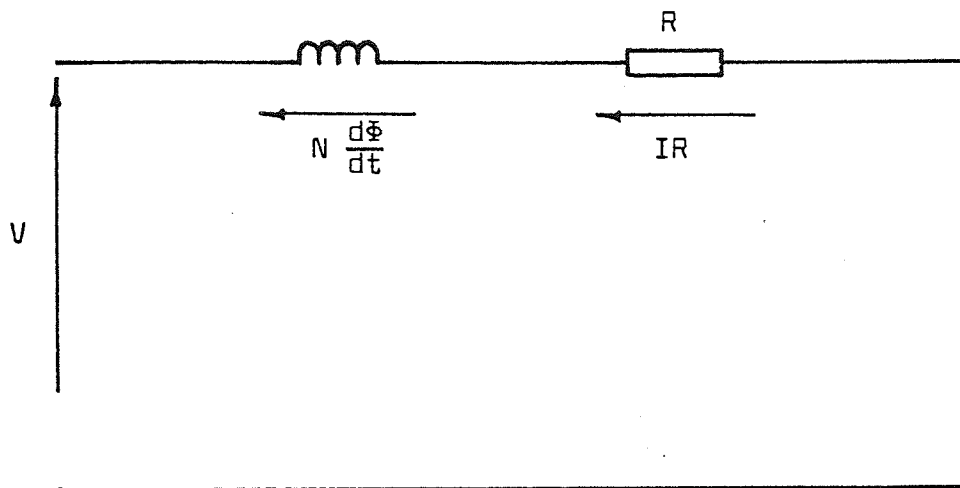


FIGURE 5.5 Circuit Representation of Stator

Let the transfer between current and flux be :-

$$\frac{\Phi(s)}{I(s)} = K \frac{(1 + sT_1)}{(1 + sT_2)}$$

A transfer function block diagram of the system is shown in Figure 5.6 which leads to :-

$$\frac{I(s)}{V(s)} = \frac{1 + sT_2}{R + s(RT_2 + KN) + s^2KNT_1}$$

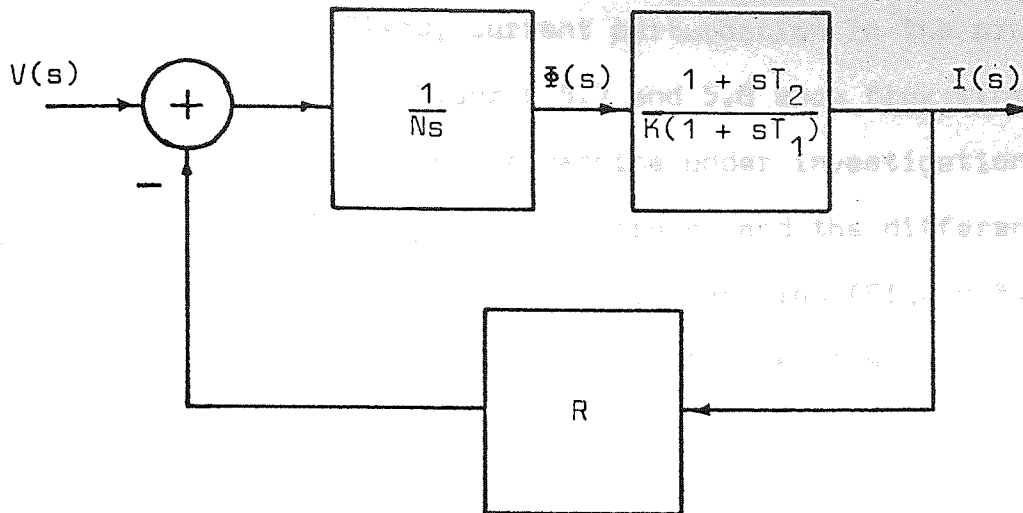


FIGURE 5.6 Block Diagram Representation of Stator

$$\text{and } \frac{\Phi(s)}{V(s)} = \frac{K(1 + sT_1)}{R + s(RT_2 + KN) + s^2KNT_1} \quad \text{5.1}$$

The measured frequency response between voltage and current is normalised to zero dB at zero frequency. The transfer function for the normalised frequency domain measurements is thus:-

$$\frac{I(j\omega)}{V(j\omega)} = \frac{(1 + j\omega T_2)}{1 + j\omega(T_2 + \frac{KN}{R}) - \omega^2 \frac{KN}{R} T_1} \quad \text{5.2}$$

The constant K relates steady-state flux to current. The factor KN is the flux linkage per ampere and is thus the inductance L in henrys.

5.4 Prediction of Transfer Function

Estimation of the transfer function directly from frequency

response data will yield poor results if the parameters are obtained at a small, fixed, current perturbation in the presence of magnetic hysteresis. Figures 5.7 and 5.8 show flux linkages plotted against current for the machine under investigation. The presence of hysteresis is demonstrated and the difference in average inductance for high (Figure 5.7) and low (Figure 5.8) current perturbations is clear. In the figures the scales for flux linkages and current are such that the average inductance is calculated from

$$L = 6.4 \times \text{average slope of loop} \quad \text{mH}$$

Thus, from Figure 5.7, at a peak-to-peak current perturbation of 3.8 A, the average inductance is 12.8 mH and, from Figure 5.8, at a peak-to-peak current perturbation of 0.17 A, the average inductance is 7.76 mH.

It is clear that, due to hysteresis and saturation, the transfer between voltage and flux is dependent upon the amplitude of the reversal of stator current. In order that these non-linearities are taken into account, in addition to eddy current effects, it is necessary to obtain frequency response data over the machine's working range of current amplitudes. The transfer function can then be used to represent the non-linear effects by obtaining current dependent time constants.

The transfer function between voltage and current can be determined, from the frequency response data, using computational curve fitting techniques presented by Levy²⁸, Sanathanan and Koerner²⁹, and Payne³⁰. However, since the dominant pole is mainly dependent upon the L/R time constant, which can be

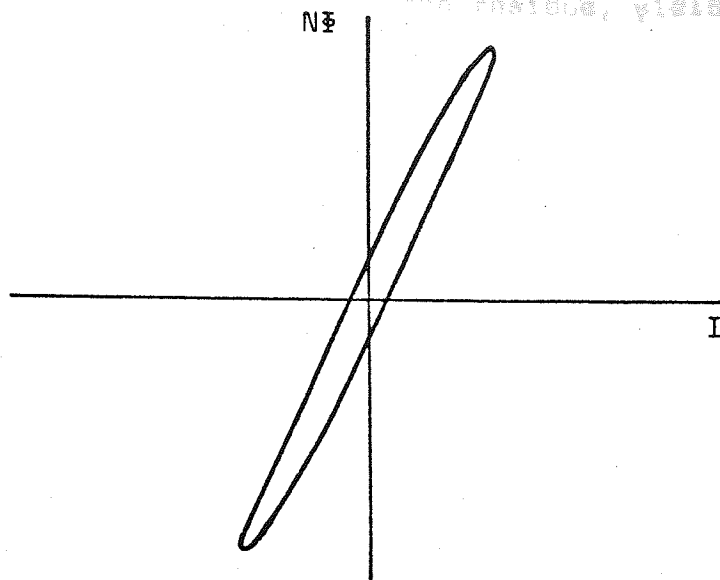


FIGURE 5.7 Flux Linkage-Current Loop (3.8 A p-p)

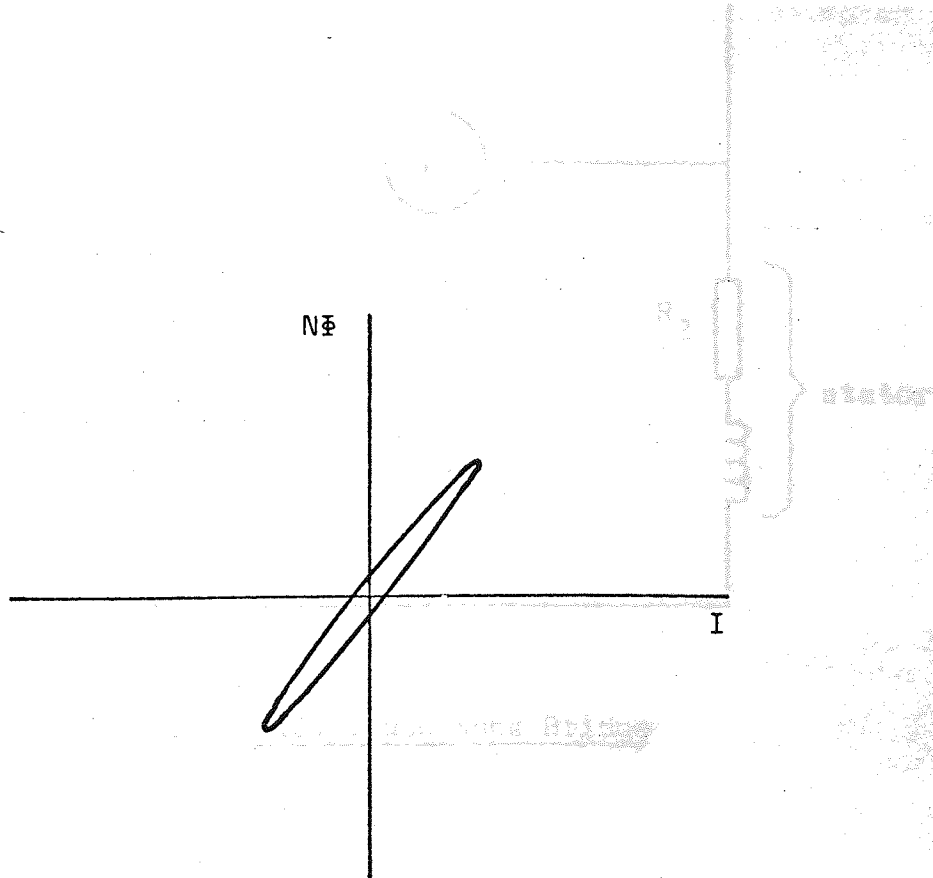


FIGURE 5.8 Flux Linkage-Current Loop (0.17 A p-p)

determined with reasonable accuracy by inductance and resistance measurements, it has been found that a technique based upon the subtraction of the dominant pole from the frequency response and then fitting a transfer function to the residue, yields superior results.

5.4.1 Measurement of inductance

A d.c. inductance bridge, using the method due to Jones¹⁹ is set up as shown in Figure 5.9.

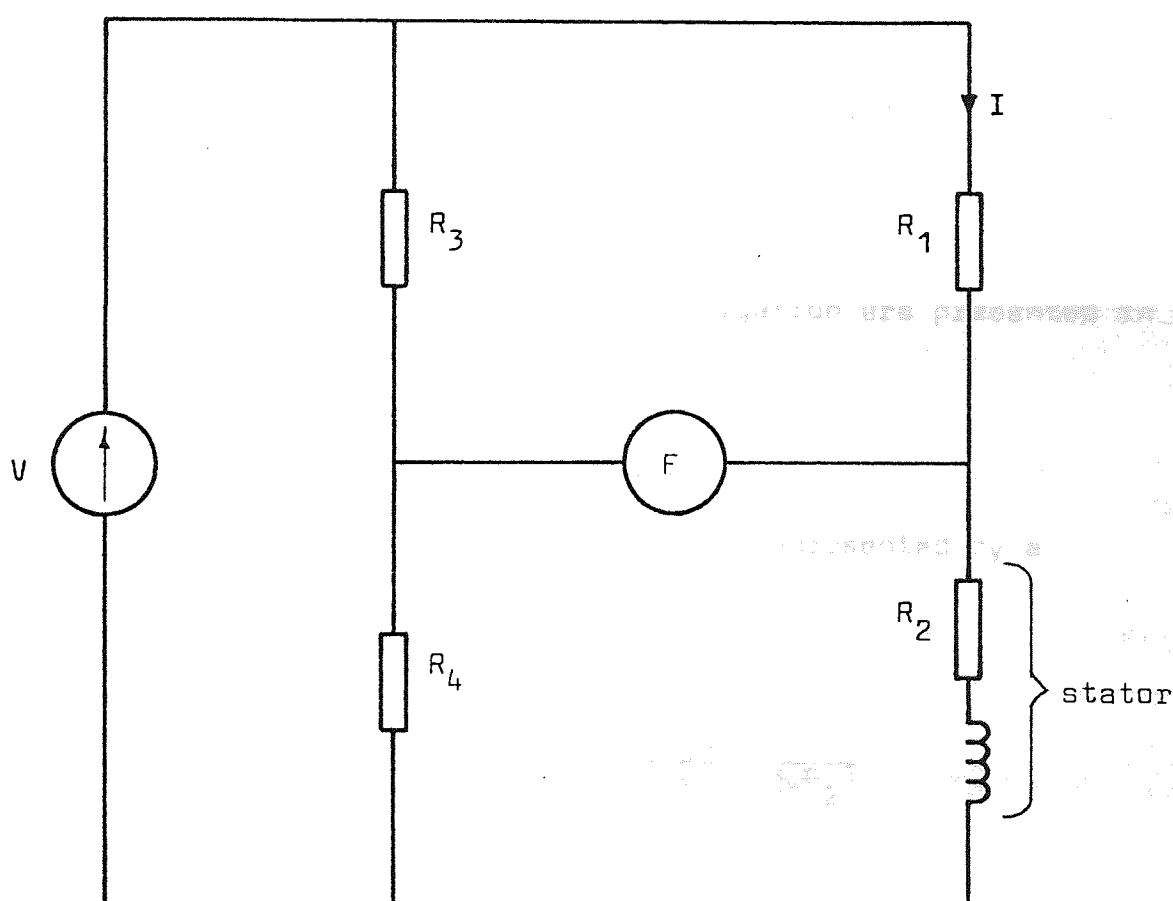


FIGURE 5.9 D.C. Inductance Bridge

The bridge is balanced in the steady state, by adjustment of resistors R_1 , R_3 and R_4 in such a way that the fluxmeter is

presented with the correct damping resistance. The voltage V is reversed and the corresponding fluxmeter deflection noted. The average inductance, at various current perturbations, is calculated from the bridge equation :-

$$L = \frac{C \alpha}{I} \frac{R_3 + R_4}{R_3} \text{ henrys}$$

Where :-

C = fluxmeter scale factor (Wb/division)

α = total change in fluxmeter scale reading (divisions)

I = total change of current (amps)

The results for the machine under investigation are presented in Figure 5.10.

5.4.2 Determination of time constants

Let each, measured, frequency response be represented by a one-zero, two-pole transfer function

$$\frac{I(j\omega)}{V(j\omega)} = \frac{1 + j\omega Z}{(1 + j\omega P_1)(1 + j\omega P_2)}$$

$$= \frac{1 + j\omega Z}{1 + j\omega(P_1 + P_2) - \omega^2 P_1 P_2}$$

equating coefficients with equation 5.2

$$P_1 = Z + \frac{L}{R} - P_2 \quad \text{-----} \quad 5.3$$

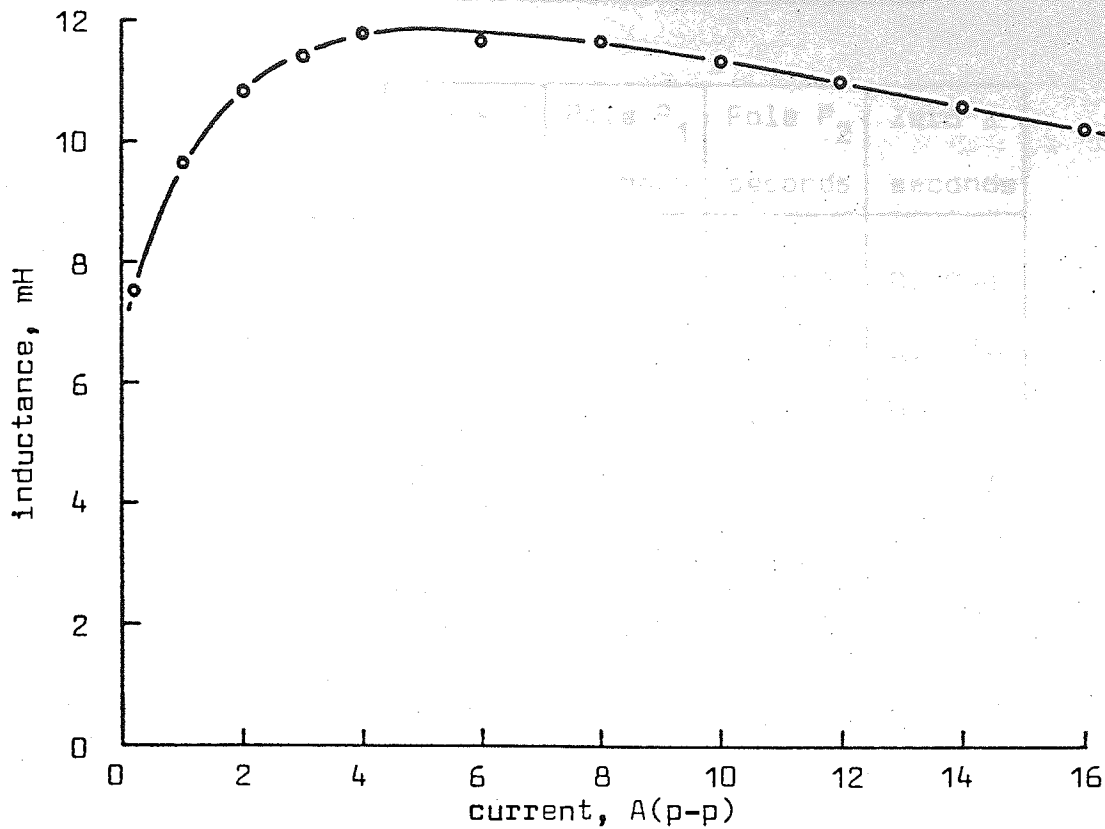


FIGURE 5.10 Average Inductance as a Function of Peak-to-Peak Current

and

$$T_1 = \frac{P_1 P_2 R}{L} \quad 5.4$$

The transfer function is evaluated by subtracting the dominant pole, P_1 , from the frequency response and evaluating the zero and second pole from the residue. The procedure is iterated to satisfy equation 5.3 using $P_1 = L/R$ as an initial guess. Time constant T_1 is calculated from equation 5.4. The results, for the machine under investigation, are summarised in Table XVI.

TABLE XVI Summary of Transfer Function

Phase I A (p-p)	Phase L mH	Phase R ohms	Pole P ₁ seconds	Pole P ₂ seconds	Zero Z seconds
0.1	7.10	0.788	0.0100	0.0008	0.0018
0.2	7.50	0.686	0.0117	0.0007	0.0014
0.4	8.14	0.686	0.0126	0.0006	0.0014
1.0	9.60	0.682	0.0148	0.0006	0.0013
1.5	10.3	0.713	0.0150	0.0004	0.0010
2.0	10.8	0.705	0.0158	0.0004	0.0009
3.0	11.4	0.727	0.0161	0.0003	0.0008
4.0	11.8	0.708	0.0173	0.0006	0.0012
6.0	11.7	0.697	0.0174	0.0005	0.0011
8.0	11.7	0.720	0.0168	0.0005	0.0011

5.5 Calculation of Transient Current and Flux

Equations 5.1 and 5.2 are used to calculate the transient flux and current in response to a voltage forcing function. The results presented in Table XVI show that time constants T_1 and T_2 can be considered independent of current with little loss of accuracy. On the other hand, the inductance (KN) must be calculated on the basis of the magnitude of the current perturbation in use. For this purpose a function is fitted to the variation of average inductance with current magnitude. Digital simulation of the transfer function is described in Chapter 6.

5.6 Conclusions

The transfer function between the voltage applied to the stator winding and the magnetic flux in the stator-rotor air gap is not, in general, a simple, linear, first order function with only winding inductance and resistance as determining factors. Eddy currents, hysteresis and saturation effects cause the transfer to be more complex with consequent difficulties in identification and simulation. Inductance measurement techniques should recognise the effects of these non-linearities as they can cause the result to be a very poor estimate of the true value.

Eddy current effects can be approximated by assuming that the transfer between current and flux can be adequately described by a linear, one-zero, one-pole function at specific current levels. The time constants of the function can be made current dependent to account for non-linear effects. The results (Table XVI) have shown, however, that the time constants can be assumed to be independent of current amplitude with little loss of accuracy. If this is generally true an economy is possible in the identification method in that only one frequency-response measurement is needed.

Hysteresis and saturation effects can be approximated by representing the inductance as the average slope of the flux linkage-current loop at specific current amplitudes. Such measurements are conveniently made by employing a d.c. inductance bridge. The transfer between voltage and flux is represented by a linear, one-zero, two-pole function at fixed values of current amplitude. The time constant due to inductance is made dependent upon the amplitude of the current perturbation passing through the stator windings.

6.1 Introduction

The dynamic performance of a stepping motor is, in general, highly non-linear. In consequence, mathematical models, that adequately describe these non-linearities, are complex and will, in general, require a computing aid to facilitate their solution. Analogue computers, digital computers or a hybrid arrangement can be used in this role.

Nishimura et al.³¹ were the first to report the use of an analogue computer for the simulation of stepping motors although Kuo et al.³² had previously reported the use of analogue methods, on a digital computer, by employing the IBM 360 Continuous System Modelling Program (CSMP). Nishimura et al.³¹ compare analogue computer and digital computer simulation methods. They report that analogue computer simulation produces a much larger error, partly due to the use of piecewise-linear approximations and partly due to drift errors. Singh³³ asserts that analogue computer simulation is practical only for single-step performance studies since, for multi-stepping, the initial conditions at the beginning of each new step have to be reset, making the procedure extremely tedious. However, Nishimura et al.³¹ seem to have been successful in this respect by employing two identical analogue circuits. One circuit is used to solve the differential equations for one pulse period and the other to solve the equations for the next. At the end of a pulse period the final values of the active circuit are supplied as the initial values of the other circuit to start the next simulation period.

Many examples of the use of digital computers, to solve mathematical models of the stepping motor, can be found in the literature (25,31-36). The use of CSMP is common but, as concluded by Singh³³, the use of FORTRAN provides greater flexibility since stepping motor systems are inherently digital in nature and thus require simulation of switching operations. These operations can be programmed, very easily, in FORTRAN. Moreover, the program efficiency of a FORTRAN simulated system is superior to the program efficiency of the same system simulated in CSMP.

The major non-linearities inherent in the stepping motor and drive have been taken into account in the modelling. The resulting complexity of the simulation render analogue methods unsuitable and therefore simulation by digital computer, using the FORTRAN programming language, is chosen to provide predictions of system performance.

A block diagram of the stepping motor and drive is used as the basis of the digital simulation. The function blocks, and the links between them, are translated into computer software. In general the functional blocks are written as subroutines, or parts of subroutines, with linking being achieved by calls to the subroutines from a main program or subprogram (see Appendix A).

6.2 Digital Simulation

Digital simulation of the stepping motor and drive is achieved by converting, where necessary, the mathematical and functional models of its sub-systems to a form that is suitable for digital solution. These digital representations of the sub-system

functions are then incorporated into a digital computer program which provides software links between the simulated sub-systems. The simulation package is written in FORTRAN IV and implemented on a PDP-9/15 digital computer. Further details of the simulation software can be found in Appendices A and B.

A block diagram of the stepping motor and drive is presented in Figure 6.1.

The notation used in the block diagram is as follows :-

N_r	number of rotor teeth
θ_e	rotor angle (electrical) (rad)
θ_m	rotor angle (mechanical) (rad)
ω_r	angular velocity of rotor (rad/s)
J	total inertia on motor shaft (kg m^2)
B	viscous friction coefficient of motor and load (N m s)
T_f	coulomb friction torque of motor and load (N m)
T	torque developed by the motor (N m)
V_a	voltage applied to 'a' phase winding (V)
V_b	voltage applied to 'b' phase winding (V)
e_{b_a}	generated e.m.f. in 'a' phase (V)
e_{b_b}	generated e.m.f. in 'b' phase (V)
I_a	current in 'a' phase winding (A)
I_b	current in 'b' phase winding (A)
k	current feedback factor (R_1) (ohms)
Φ_a	flux in 'a' phase (Wb)
Φ_b	flux in 'b' phase (Wb)
K	steady state Φ/I ratio (Wb/A)
s	Laplace operator

On receipt of an input pulse the two phase drive state generator

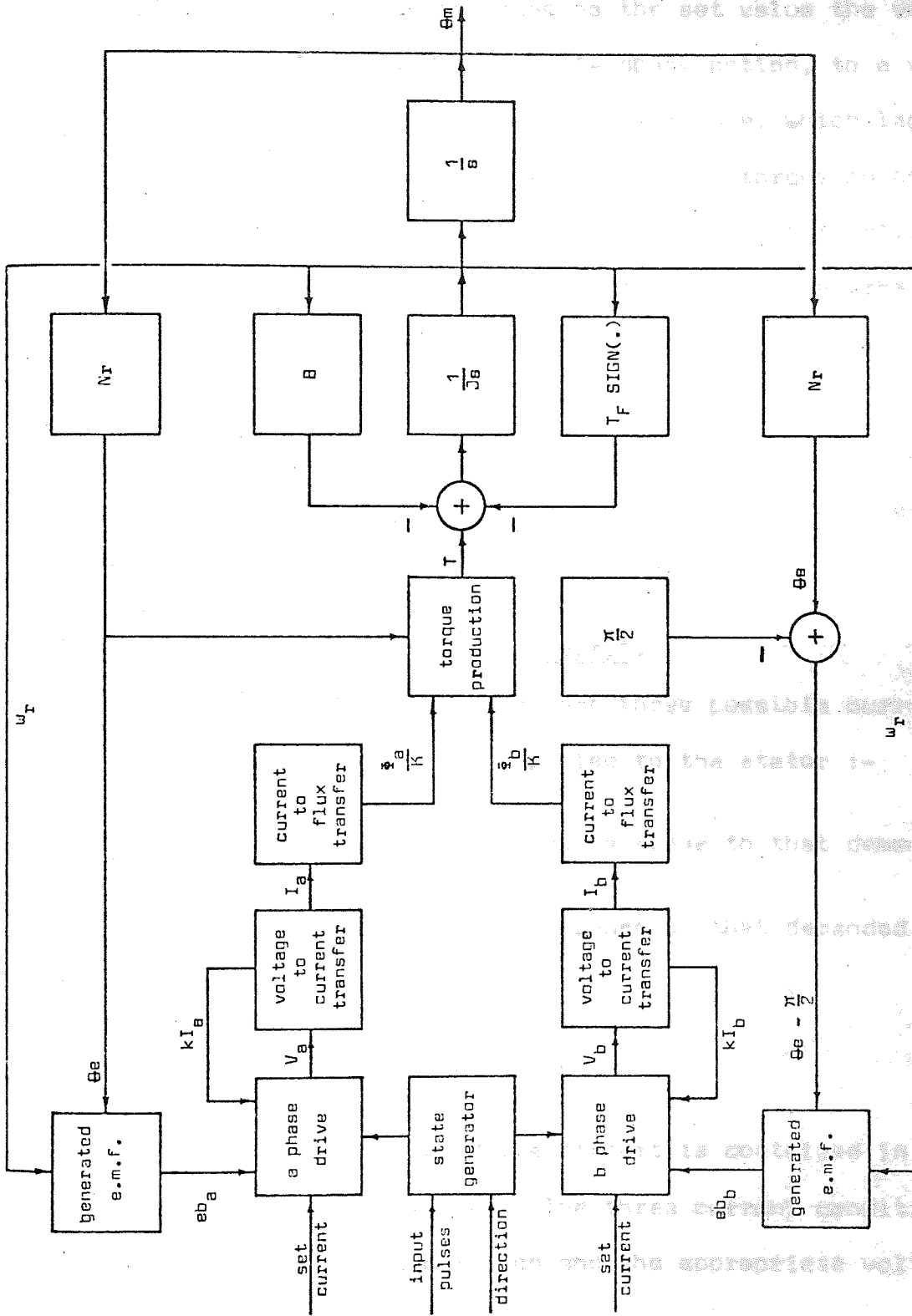


FIGURE 6.1 Block Diagram Model of Hybrid Stepping Motor and Drive

provides the appropriate drive circuit with a demand to reverse the current. The phase voltage is reversed and held at a high value, which is modified by the generated e.m.f. when the rotor is in motion. When the current reaches the set value the voltage applied to the stator is reduced, by feedback action, to a value which maintains the set current. The flux change, which lags the current change due to eddy currents, causes the torque to change from zero. The rotor moves under the constraints of inertia, viscous friction and coulomb friction. The current reversal gives rise to a flux reversal which causes the zero torque position to shift 90 electrical degrees. In general, the values of J , B and T_F are such that the rotor executes a second order type of response, coming to rest 90 electrical degrees from its position before the input pulse was received.

6.2.1 Drive circuit and generated e.m.f.

It is shown in para. 3.4 that there are three possible current conditions governing the voltage applied to the stator :-

- (a) Stator current in the opposite sense to that demanded
- (b) Stator current in the same sense to that demanded but less than the set value
- (c) Stator current at set value

The digital simulation of the drive circuit is contained in Subroutine CURCAL (Appendix A.4). The three current conditions are easily tested in the simulation and the appropriate voltage determined.

The voltage across the stator winding indicated by condition (a) is a high voltage transient, modified by drive circuit action

(para. 3.3), and machine generated e.m.f. The magnitude of the transient is found, by measurement, to be five volts greater than the high voltage supply. The generated e.m.f. is a function of electrical angle and rotor angular velocity and is given by :-

$$e_{b_a} = K_b \omega_r \cos \theta_e$$

The constant, K_b , is found, by measurement, to be :-

$$K_b = 0.334 \text{ V}/(\text{rad s}^{-1})$$

Note that the 'b' phase generated e.m.f. is given by :-

$$e_{b_b} = K_b \omega_r \cos (\theta_e - \pi/2)$$

The displacement between the generated e.m.f.s in each phase is due to the two phase construction of the machine stator. This phase difference is accounted for, in the simulation, by subtracting 90 electrical degrees via the subroutine arguments in the calling subprogram (RECAL2) (Appendix A.3) when calling CURCAL for 'b' phase calculations. The magnitude of the voltage across the stator windings for condition (a) is given by :-

$$V_s = V + 5 - 0.334 \omega_r \cos \theta_e$$

where

V_s = voltage applied to stator winding

V = voltage of supply

The voltage across the stator winding indicated by condition (b) is the supply voltage modified by IR drops and the saturation characteristics of the drive circuit transistors. The circuit resistance is found to be 0.345 ohms and the drive transistors saturation volt drop 2 V. Consequently, the magnitude of the

voltage across the stator winding for condition (b) is given by :-

$$V_s = V - 0.345 I - 2 - 0.334 \omega_r \cos \theta_e$$

where I = phase current

The voltage across the stator winding indicated by condition (c) is that voltage which is required to cause a stator current equal to the set value to flow. The voltage is therefore given by :-

$$V_s = I_s R$$

where I_s = set value of phase current

R = stator resistance

In practice, it is observed that the current overshoots the set value, due, in the main, to the slow slew rate of the operational amplifier in the feedback path. This is accounted for by keeping the voltage in condition (b) for 0.2 ms after the current has reached the set value.

The sign of the stator voltages is determined by the direction of the current demand. The expressions for stator voltage are programmed in FORTRAN using the variables listed in Table XVII.

6.2.2 Voltage to flux transfer

The digital simulation of the transfer between voltage and current and between current and flux is contained in Subroutine CURCAL (Appendix A.4).

It is shown, in para. 5.3, that the transfer between voltage and current, at each discrete current level, can be adequately described by a two-pole, one-zero function. It is necessary, therefore, to represent this function in a form suitable for

TABLE XVII Drive Circuit Simulation Variables

Variable Name	Variable
VEF	Stator Voltage (V)
S	Current direction demand
V	Supply Voltage (V)
OMEGA	Angular Velocity (rad/s)
RTC	Number of Rotor Teeth
THETA	Displacement (rad) (Mechanical)
AMP	Stator Current (A)
TC	Set Current (A)
R	Stator Resistance (ohms)

digital solution. Consider a generalised form of the transfer function to be

$$\frac{v(s)}{u(s)} = \frac{1 + bs}{1 + es + fs^2} \quad \text{6.1}$$

Consider this relationship in the form of state-space equations :-

$$\dot{\underline{x}} = \underline{A}\underline{x} + \underline{B}\underline{u}$$

$$\underline{v} = \underline{C}\underline{x} + \underline{D}\underline{u}$$

the state variables may be defined such that

$$\dot{x}_1 = x_2 + \frac{b}{f} u$$

$$\dot{x}_2 = -\frac{1}{f} x_1 - \frac{e}{f} x_2 + \frac{1}{f} u - \frac{be}{f^2} u$$

$$v = x_1$$

thus, in state-space form

$$\dot{\underline{x}} = \begin{bmatrix} 0 & 1 \\ -\frac{1}{f} & -\frac{e}{f} \end{bmatrix} \underline{x} + \begin{bmatrix} \frac{b}{f} \\ \frac{f - be}{f^2} \end{bmatrix} \underline{u}$$

$$\underline{v} = \begin{bmatrix} 1 & 0 \end{bmatrix} \underline{x}$$

Thus

$$A = \begin{bmatrix} 0 & 1 \\ -\frac{1}{f} & -\frac{e}{f} \end{bmatrix} \quad B = \begin{bmatrix} \frac{b}{f} \\ \frac{f - be}{f^2} \end{bmatrix} \quad C = \begin{bmatrix} 1 & 0 \end{bmatrix}$$

The state transition matrix may be obtained from :-

$$\phi(t) = \mathcal{L}^{-1} (sI - A)^{-1}$$

which leads to :-

$$\phi(t)_{11} = \frac{1}{r_1 - r_2} \left((r_1 + \frac{e}{f}) \exp(r_1 t) - (r_2 + \frac{e}{f}) \exp(r_2 t) \right)$$

$$\phi(t)_{12} = \frac{1}{r_1 - r_2} \left(\exp(r_1 t) - \exp(r_2 t) \right)$$

$$\phi(t)_{21} = -\frac{1}{f} \left(\frac{1}{r_1 - r_2} \right) \left(\exp(r_1 t) - \exp(r_2 t) \right)$$

$$\phi(t)_{22} = \frac{1}{r_1 - r_2} \left(r_1 \exp(r_1 t) - r_2 \exp(r_2 t) \right)$$

Where r_1 and r_2 are the roots

$$r_1 = -\frac{e}{2f} + \sqrt{\frac{e^2}{4f^2} - \frac{1}{f}}$$

$$r_2 = -\frac{e}{2f} - \sqrt{\frac{e^2}{4f^2} - \frac{1}{f}}$$

To solve the equations by digital methods the sampled data form of the state-space equations is used.

$$\underline{x}_{n+1} = F\underline{x}_n + G\underline{u}_n$$

where $F = \phi(h)$

$h =$ time step

$\phi(h) =$ discrete form of state transition matrix

$$G = A^{-1} [\phi(h) - I] B$$

or $G = A^{-1} [F - I] B$

$$A^{-1} [F - I] = \begin{bmatrix} -e & -f \\ 1 & 0 \end{bmatrix} \begin{bmatrix} F_{11} - 1 & F_{12} \\ F_{21} & F_{22} - 1 \end{bmatrix}$$

$$A^{-1} [F - I] = \begin{bmatrix} -e(F_{11} - 1) - fF_{21} & -eF_{12} - f(F_{22} - 1) \\ F_{11} - 1 & F_{12} \end{bmatrix}$$

$$G = \begin{bmatrix} B_{11}(1 - e(F_{11} - 1) - fF_{21}) & B_{21}(1 - eF_{12} - f(F_{22} - 1)) \\ B_{11}(F_{11} - 1) & B_{21}F_{12} \end{bmatrix}$$

The normalised form of the voltage to current transfer function (para. 5.3) is :-

$$\frac{I(s)}{V(s)} = \frac{1 + sT_2}{1 + s(T_2 + \frac{L}{R}) + s^2 \frac{L}{R} T_1} \quad \text{6.2}$$

Comparing coefficients with equation 6.1

$$b = T_2$$

$$e = T_2 + \frac{L}{R}$$

$$f = \frac{L}{R} T_1$$

$$v(s) = I(s)$$

$$u(s) = V(s)$$

Note that equation 6.2 is normalised. The output vector should, therefore, be multiplied by $1/R$ to yield current in amperes.

The transfer function from voltage to current is, in general, current dependent. It is shown in para. 5.5 that time constants T_1 and T_2 can be considered independent of current but the inductance L must be calculated on the basis of the magnitude of the current perturbation used. A polynomial fit to the variation of average inductance with peak current is obtained by the method of least squares. The resulting expression is programmed to yield average inductance as a function of the peak current attained at the last switch.

The discrete form of the state equations for the voltage to current transfer are programmed in FORTRAN using the variables listed in Table XVIII.

It is shown in para. 5.3, that the transfer between current and flux, at each discrete current level, can be adequately described by a one-pole, one-zero function

$$\frac{\Phi}{K}(s) = \frac{1 + sT_1}{1 + sT_2}$$

The state variables may be defined such that

$$\dot{x} = -\frac{1}{T_2} x + \frac{1}{T_2} \left(1 - \frac{T_1}{T_2}\right) I$$

$$\frac{\Phi}{K} = x + \frac{T_1}{T_2} I$$

In the sampled data form

$$\underline{x}_{n+1} = F \underline{x}_n + G \underline{I}_n$$

where

$$F = \phi(h)$$

$$h = \text{time step}$$

$$\phi(h) = \exp\left(-\frac{h}{T_2}\right)$$

$$G = \left(\exp\left(-\frac{h}{T_2}\right) - 1\right) \left(\frac{T_1}{T_2} - 1\right)$$

The discrete form of the state equations for the current to flux transfer are programmed in FORTRAN using the variables listed in Table XIX.

TABLE XVIII Voltage-to-Current Transfer Simulation Variables

Variable Name	Variable
B	$b = T_2$
E	$e = T_2 + \frac{L}{R}$
F	$f = \frac{L}{R} T_1$
TAU1	T_1
TAU2	T_2
SLOPE	L
R	R
ALPHA	r_1
BETA	r_2
EALPH	$\exp(r_1 h)$
EBETA	$\exp(r_2 h)$
BM	B Matrix
FM	F Matrix
AIFI	$A^{-1} [F - I]$
GM	G Matrix
X1	x_1
X2	x_2
AMP	Stator Current

TABLE XIX Current-to-Flux Transfer Simulation Variables

Variable Name	Variable
EX	$\phi(h) = \exp\left(-\frac{h}{T_2}\right)$
STEP1	Time Step = h
TAU2	T_2
X	x
TA	$\frac{T_1}{T_2}$
AMP	Stator Current I
FLUX	Normalised Flux $\frac{\Phi}{K}$

6.2.3 Torque production

Static torque is a complex function of the two phase currents and the electrical displacement angle. Analysis of the static torque displacement characteristic is contained in Chapter 4 and leads to an expression for torque (para. 4.5) which is programmed in FORTRAN in Subroutine TRIGTQ (Appendix A.5). The torque expression contains Fourier components of permeance which are, in general, current dependent. Permeance coefficients as a function of current are investigated in para. 4.6.1. A polynomial fit, to these functions, is obtained by the method of least squares. The resulting expressions are programmed to yield current dependent permeance coefficients.

The calculation of time dependent torque is achieved by computing

the torque with time dependent input parameters. This is achieved by calling the subroutine, at each time step, with updated input arguments. Transient torque is a function of time dependent electrical angle and the two time dependent phase fluxes. In order that the flux unit is compatible with the current used for the steady state solution of torque, the subroutine is called with normalised flux, Φ/K where K is the steady state Φ/I ratio.

6.2.4 Rotor dynamics

The digital simulation of the rotor dynamics is contained in Subroutine RECAL2 (Appendix A.3).

To simulate the dynamics of the stepping motor (Figure 6.1) it is necessary, in the first instance, to solve

$$T = J \ddot{\theta}_m + B \dot{\theta}_m$$

State-space treatment can be applied in a similar manner to that applied to the voltage to current transfer function (equation 6.1). This leads to a sampled data form for the rotor dynamics as follows :-

$$\theta_{m_{n+1}} = \theta_{m_n} + \dot{\theta}_{m_n} \frac{J}{B} (1 - \exp(-\frac{B}{J} h)) + \frac{1}{B} \left(h - \frac{J}{B} (1 - \exp(-\frac{B}{J} h)) \right) T_n$$

$$\dot{\theta}_{m_{n+1}} = \dot{\theta}_{m_n} \exp(-\frac{B}{J} h) + \frac{1}{B} (1 - \exp(-\frac{B}{J} h)) T_n$$

$$\omega_r = \dot{\theta}_m$$

$$h = \text{time step}$$

Coulomb friction T_F is accounted for, in the simulation, by inspecting the sign of ω_r and modifying the input torque accordingly. The discrete form of the state equations for the rotor dynamics are programmed in FORTRAN using the variables listed in Table XX.

TABLE XX Rotor Dynamics Simulation Variables

Variable Name	Variable
SLUG	J
STEP	h
FRIC	B
THETA	θ_m
OMEGA	ω_r
TOR	Torque

6.3 Prediction of Rotor Dynamics

A description of the simulation package, which comprises a main program and five subroutines, is contained in Appendix A. The input variables required by the package are listed in Table XXI and the output parameters available as a function of time are listed in Table XXII.

6.4 Measurement of Rotor Dynamics

The position of the stepping motor output shaft is measured by an eleven bit, Gray coded encoder. The encoder is interfaced

TABLE XXI Input Variables Required for Simulation

Variable	Unit
Maximum Current (Set Current)	A
Aiming Voltage (Supply Voltage)	V
Winding Resistance	ohm
Inertia	kg m ²
Friction (Viscous Friction Coefficient)	N m s
Frictional Torque (Coulomb Friction)	N m
Number of Rotor Teeth	
Number of Turns per Pole	
Time Step	s
Period as Integer Multiplier of Time Step	
Number of Steps to be Computed	

TABLE XXII Simulation Output Parameters

Parameter	Unit
Displacement	Degrees (Electrical)
Angular Velocity	rad/s (Mechanical)
Torque	N m
Current (A Phase)	A
Flux (A Phase)	mWb

to the PDP-9/15 digital computer which, on the receipt of an interrupt, is programmed to read the encoder output, convert the output to natural binary and store the result. The program continues in this mode for a prescribed number of interrupt pulses. The results may then be outputted to the graph plotter where, by knowing the frequency of the interrupts, they are plotted against time. Alternatively the results can be saved by outputting to paper punch.

6.5 Typical Results

The predictions are obtained using the input data listed in Table XXIII, unless otherwise stated.

TABLE XXIII Simulation Input Data

Variable	Value
Winding Resistance	0.606 ohms
Inertia	0.000448 kg m ²
Friction	0.028 N m s
Frictional Torque	0.002 N m
Number of Rotor Teeth	42
Number of Turns per Pole	40
Time Step	0.0002 s

A set of results are presented (Figures 6.2, 6.3 and 6.4) which predict the stepping motor performance when subjected to a single step demand with the drive circuit high voltage supply set to

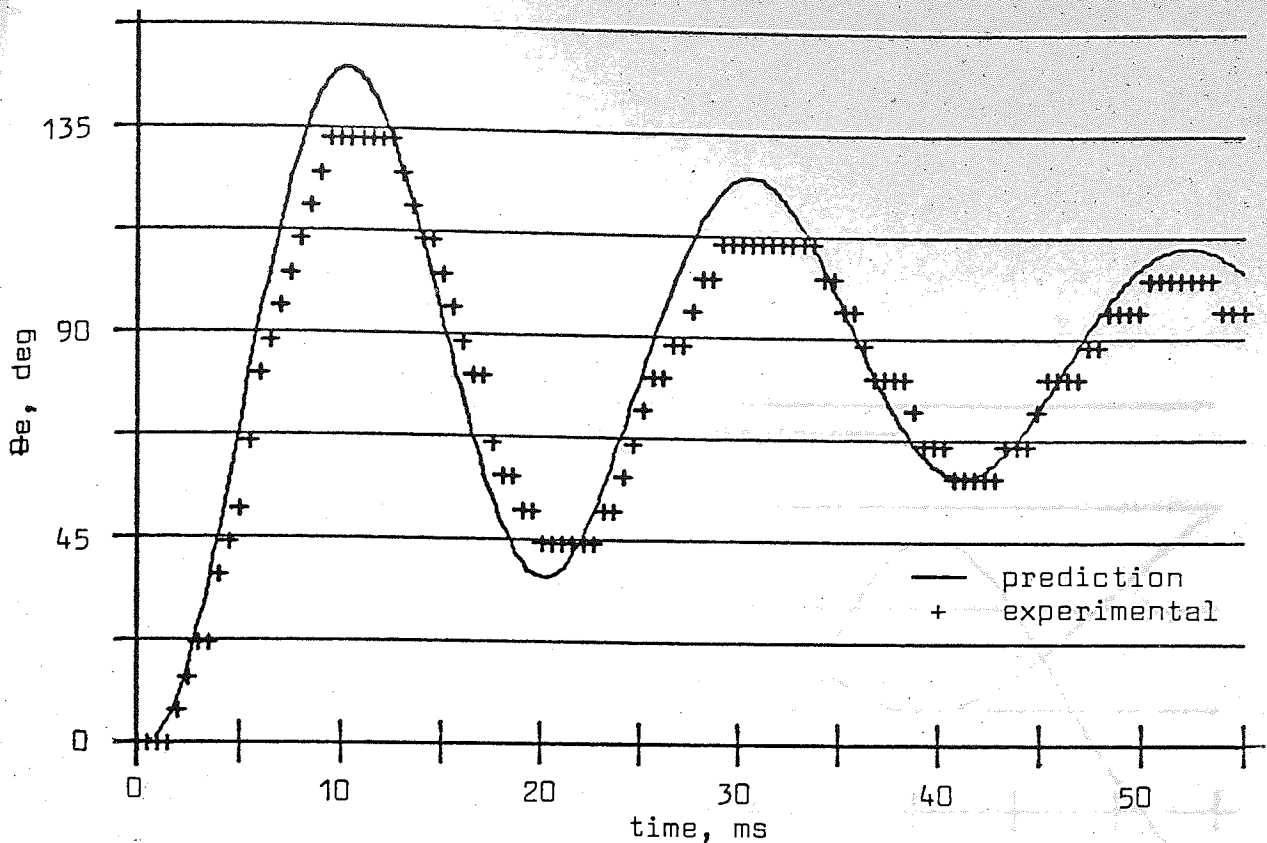


FIGURE 6.2 Single Step Response of Unloaded Rotor
 High Voltage On, Set Current 2 A

40 volts and the current demand set at 2 A. Figure 6.2 shows the predicted displacement with the experimental result superimposed, Figure 6.3 shows the corresponding prediction of the torque with the displacement included as reference and Figure 6.4 shows the corresponding prediction of the 'a' phase current and flux.

The results presented in Figures 6.5 and 6.6 compare the 6 A single step transient predictions, obtained with the drive circuit high voltage supply set to 40 volts, with the predictions obtained with the drive circuit high voltage supply disconnected and the low voltage supply set to 12 volts. Figure 6.5 shows the predicted displacements and Figure 6.6 the predicted torques.

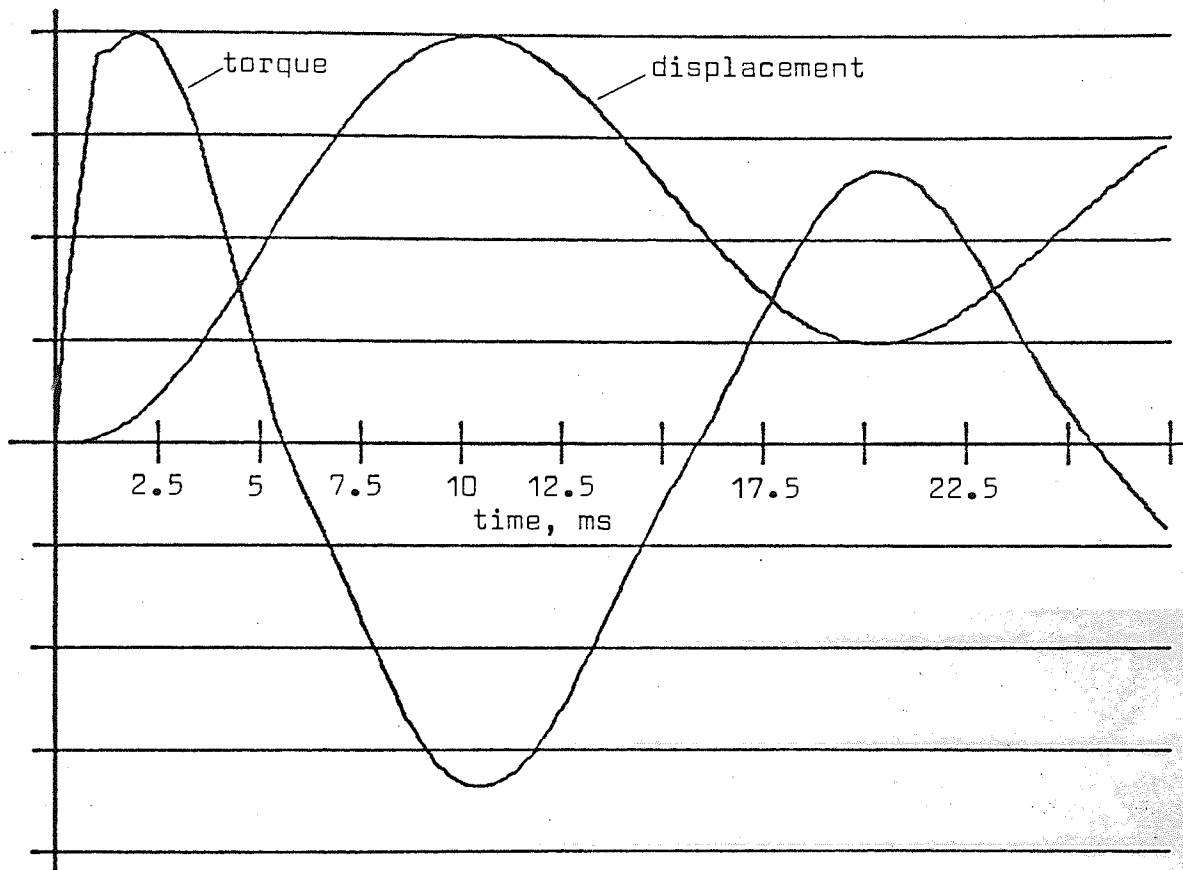


FIGURE 6.3 Prediction of Torque and Displacement

in Response to a Single Step Demand

High Voltage On, Set Current 2 A, Rotor Unloaded

Scales: Displacement = 37.2 deg(elec)/div

Torque = 0.363 N m/div

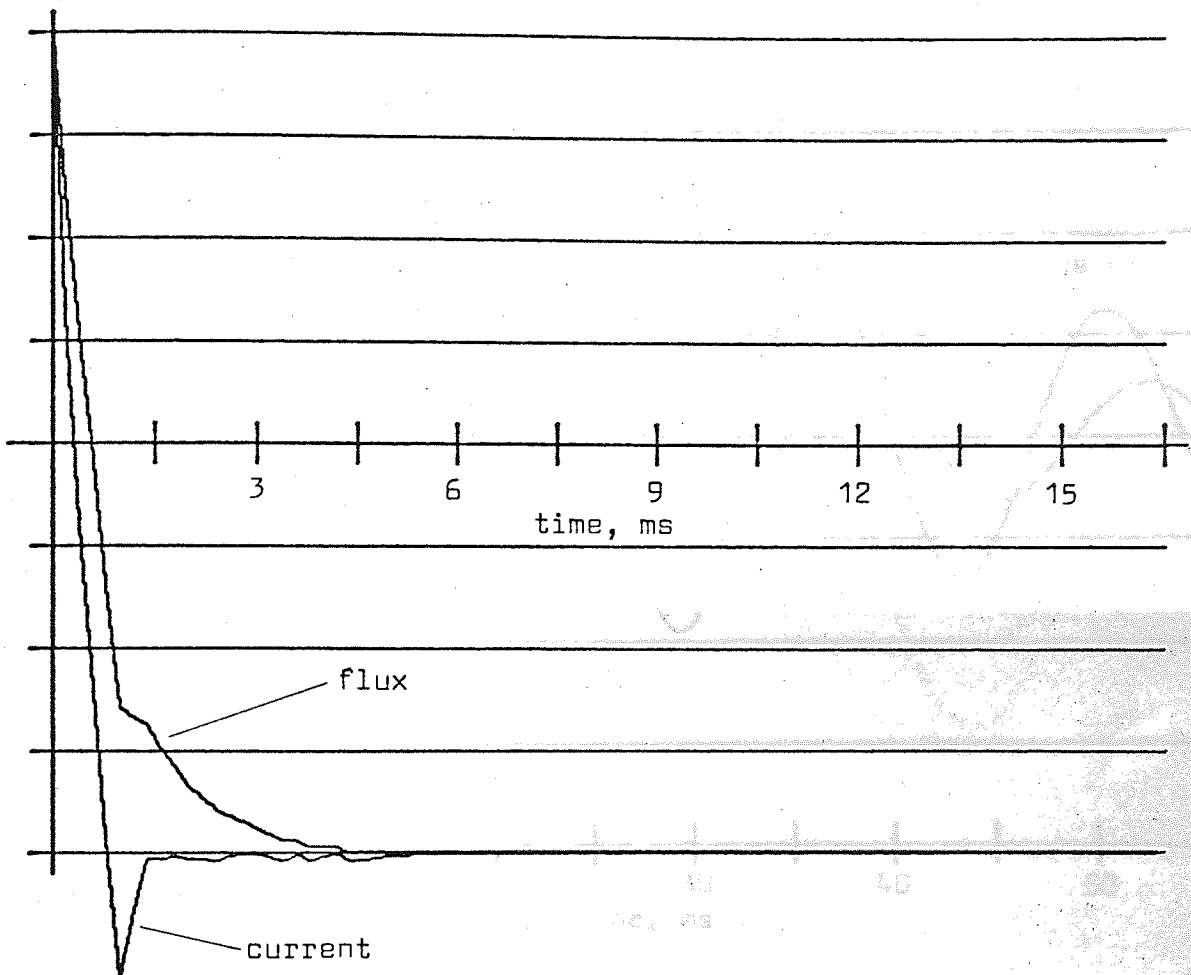


FIGURE 6.4 Prediction of 'a' Phase Current and Flux

in Response to a Single Step Demand

High Voltage On, Set Current 2 A, Rotor Unloaded

Scales: Current = 0.5 A/div

Flux = 0.0373 mWb/div

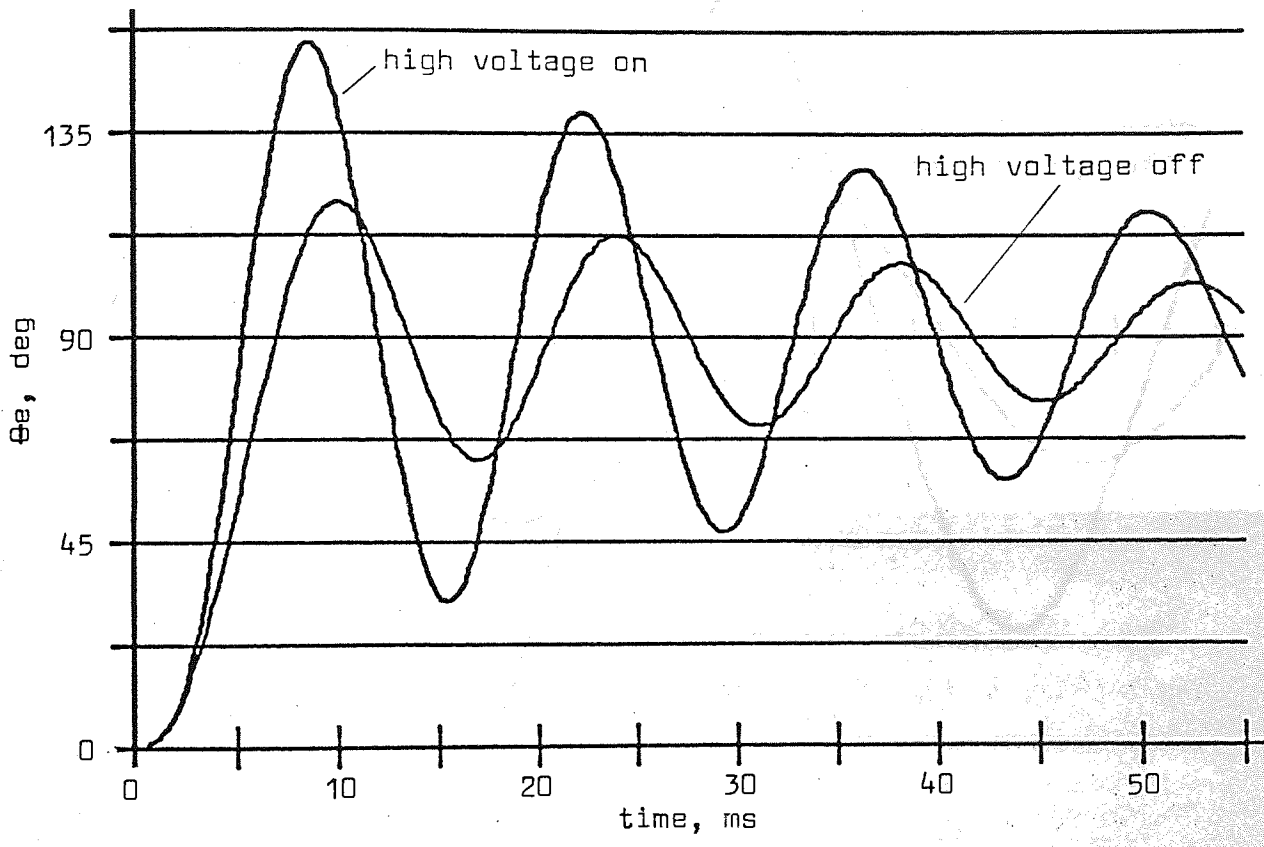


FIGURE 6.5 Predictions of Single Step Response
of Unloaded Rotor
 Set Current 6 A

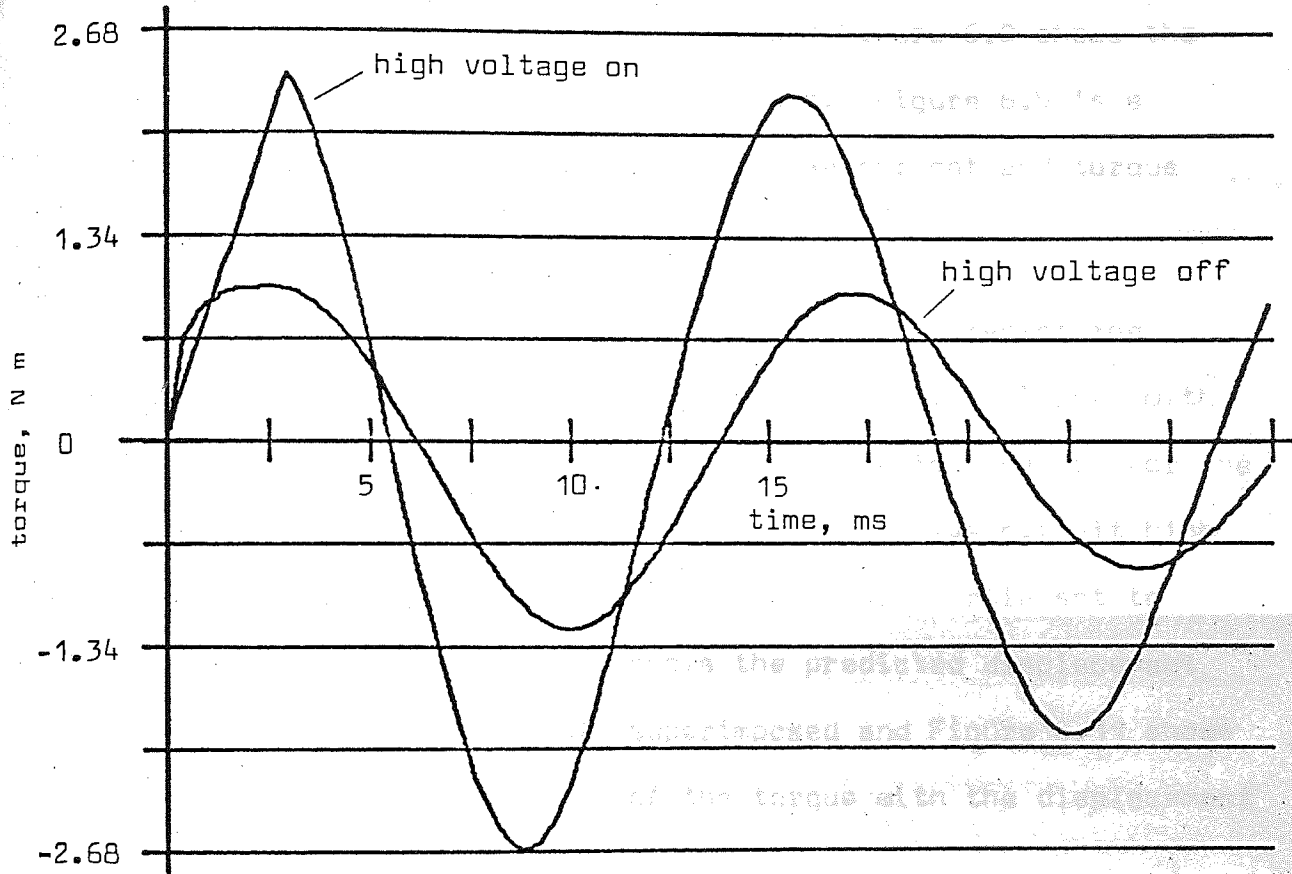


FIGURE 6.6 Predictions of Torques in Response to a Single Step Demand

Set Current 6 A, Rotor Unloaded

Results are presented in Figures 6.7 and 6.8 which compare predictions of the stepping motor performance made with, and without, eddy current time constants. The predictions are for the 6 A single step transient response with the drive circuit high voltage supply disconnected and the low voltage supply set to 12 volts. Figure 6.7 shows the predicted displacements with the experimental result superimposed and Figure 6.8 shows the corresponding predictions of the torques. Figure 6.9 is a prediction of the corresponding 'a' phase current and torque with eddy current time constants included.

The results presented in Figures 6.10 and 6.11 predict the stepping motor performance when the output shaft is loaded with inertia equal to the rotor inertia. The predictions are for the 4 A single step transient response with the drive circuit high voltage supply set to 40 volts and the total inertia set to 0.000916 kg m^2 . Figure 6.10 shows the predicted displacement with the experimental result superimposed and Figure 6.11 shows the corresponding prediction of the torque with the displacement included as reference.

Multi-stepping results are presented in Figures 6.12 to 6.15. The current demand is set at 4 A and the step rate at 50 steps per second. Figures 6.12 and 6.13 show the results for the high voltage supply set to 40 volts. Figure 6.12 shows the predicted displacement with the experimental results superimposed and Figure 6.13 shows the corresponding prediction of the torque. Figures 6.14 and 6.15 present the results for the high voltage supply disconnected and the low voltage supply set to 12 volts. Figure 6.14 shows the predicted displacement with the experimental results superimposed and Figure 6.15 shows the corresponding prediction of torque.

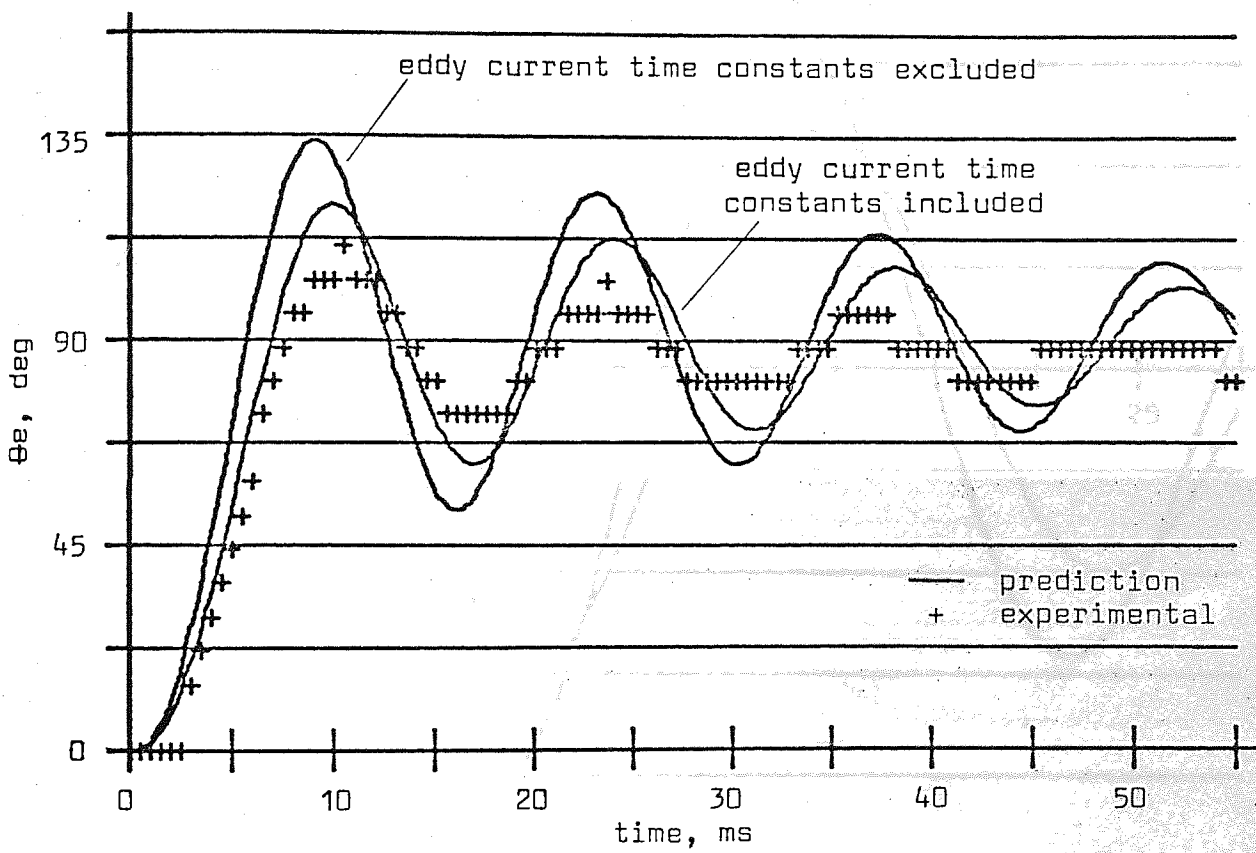


FIGURE 6.7 Single Step Response of Unloaded Rotor

High Voltage Off, Set Current 6 A

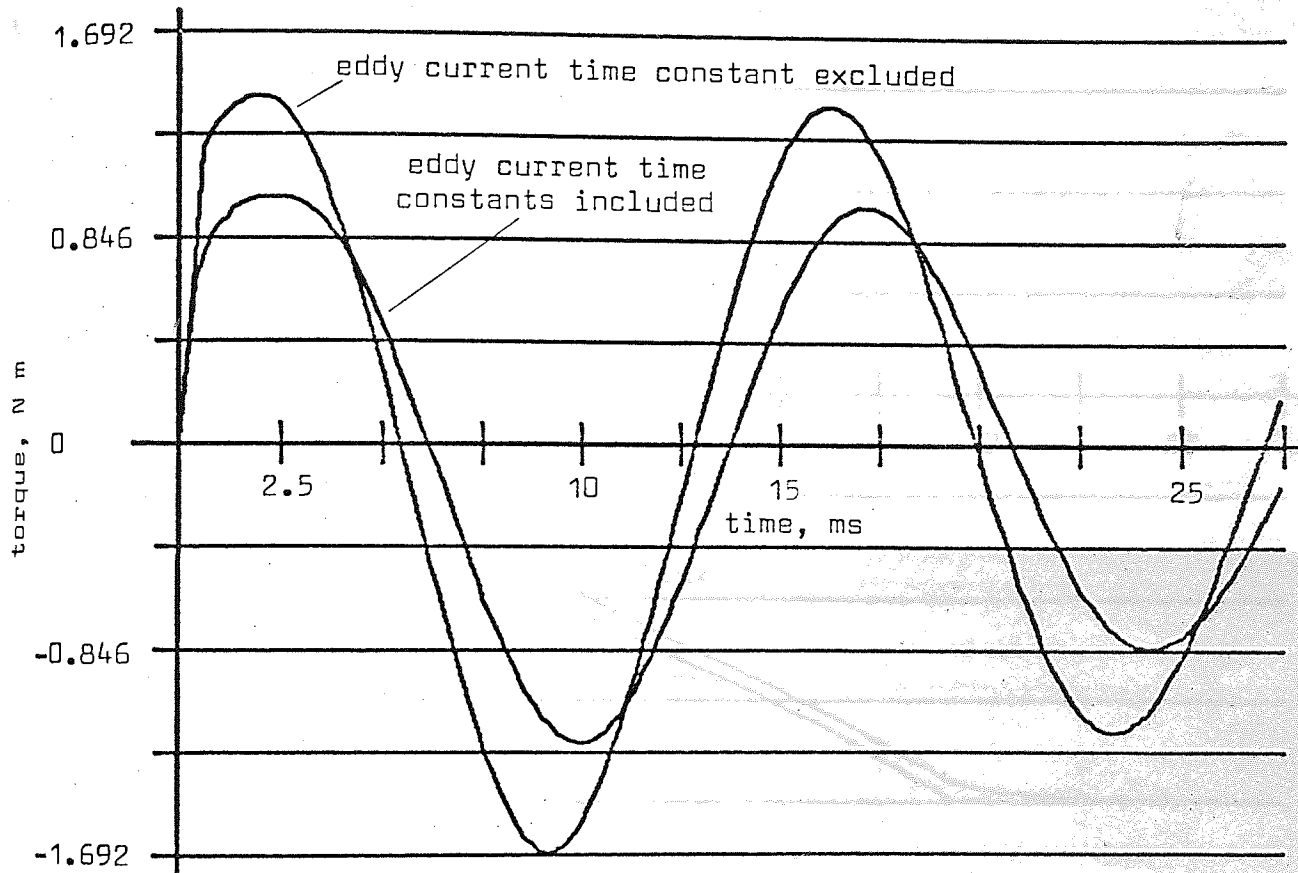


FIGURE 6.8 Predictions of Torque in Response to a
Single Step Demand ω_r , Set Current 6 A
 High Voltage Off, Set Current 6 A, Rotor Unloaded

Flux = 0.1 mWb

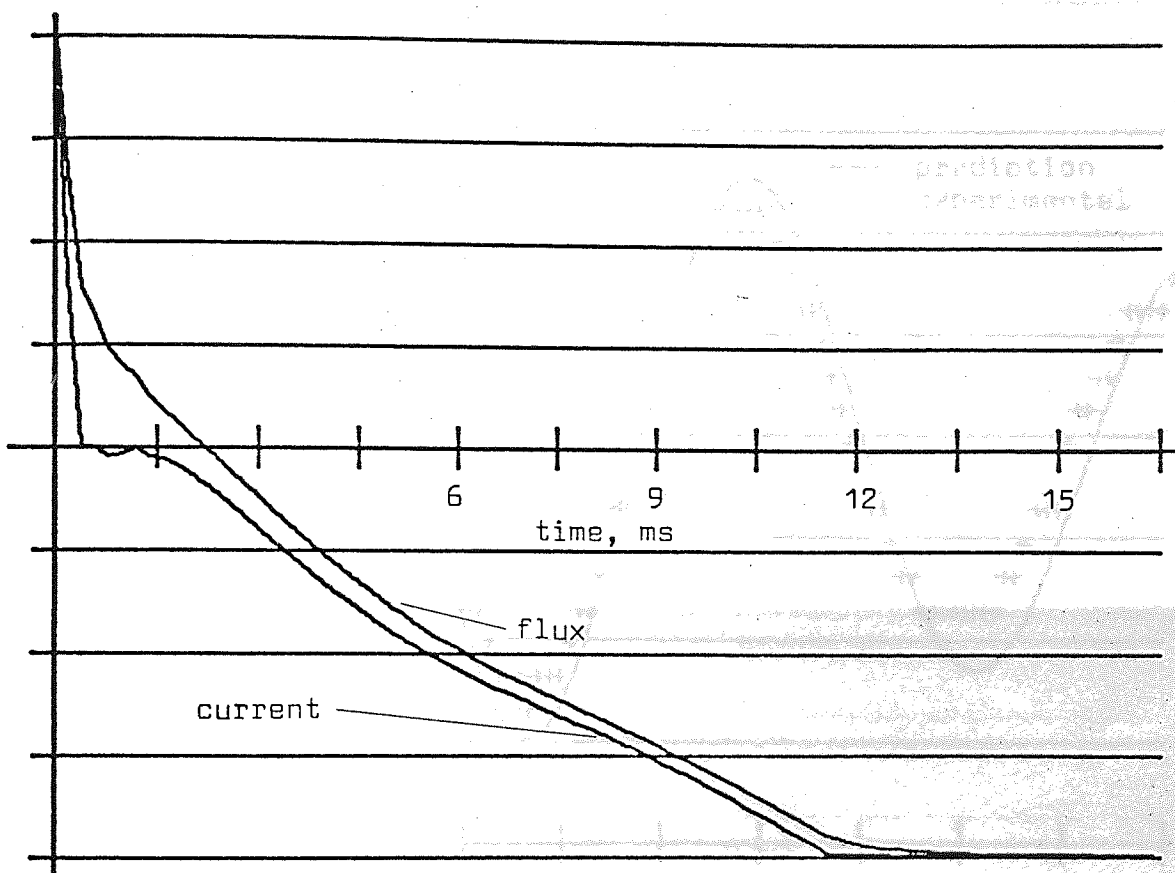


FIGURE 6.9 Prediction of 'a' Phase Current and Flux
in Response to a Single Step Demand

High Voltage Off, Set Current 6 A

Scales: Current = 0.15 A/div

Flux = 0.1 mwb/div

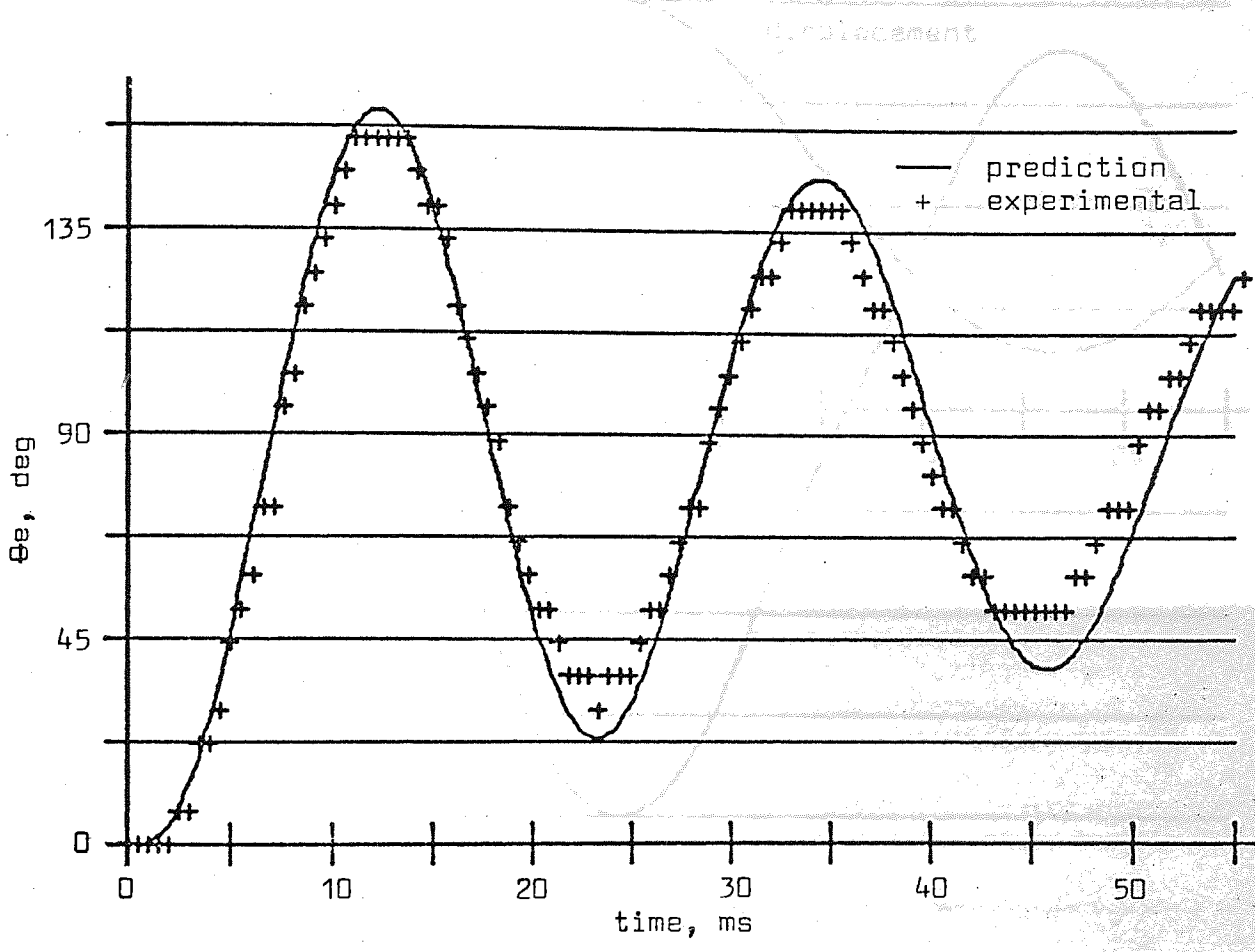


FIGURE 6.10 Single Step Response of Loaded Rotor

High Voltage On, Set Current 4 A
 Total Inertia = 0.000916 kg m²
 Displacement = 40.4

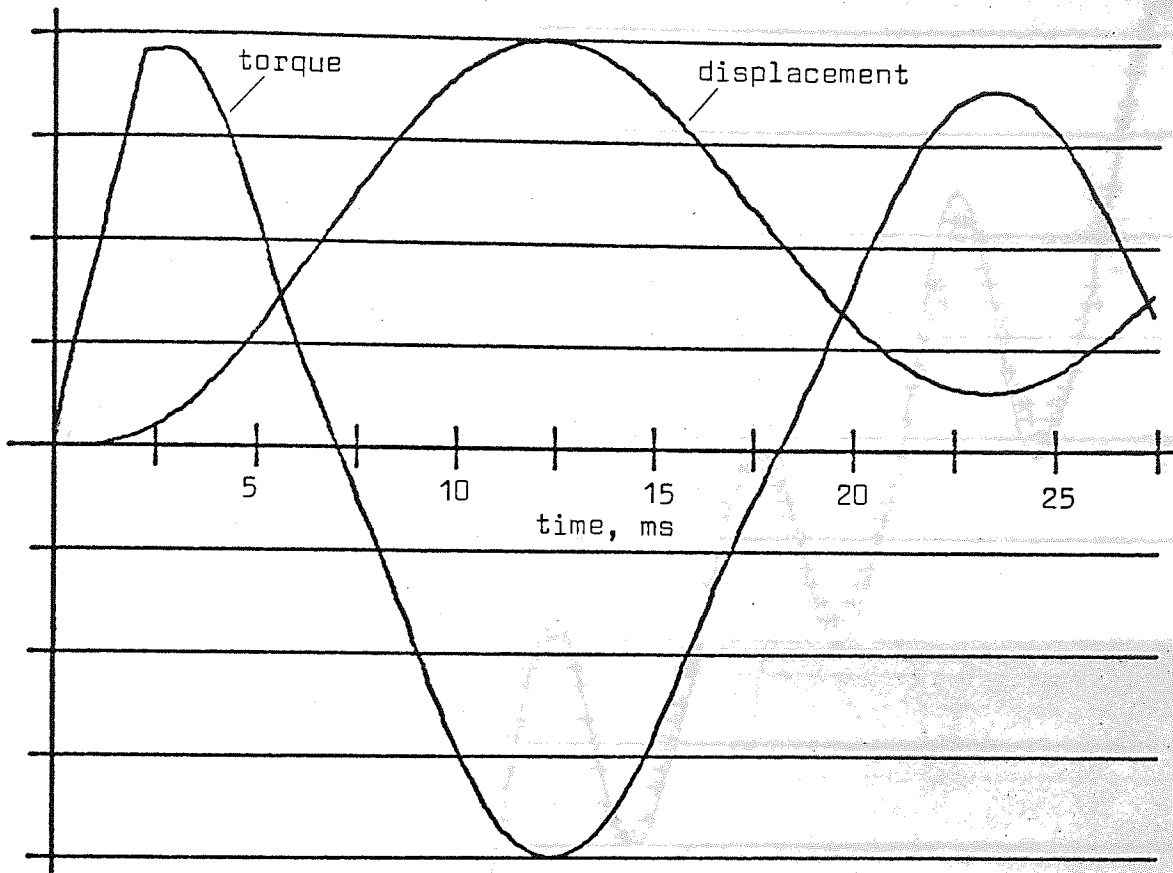


FIGURE 6.11 Prediction of Torque and Displacement

in Response to a Single Step Demand

High Voltage On, Set Current 4 A,

Total Inertia = 0.000916 kg m^2

Scales: Displacement = $40.4 \text{ deg(elec)/div}$

Torque = 0.59 N m/div

time, ms

Multi-Stepping Response of

50 e.p.s., High Voltage On

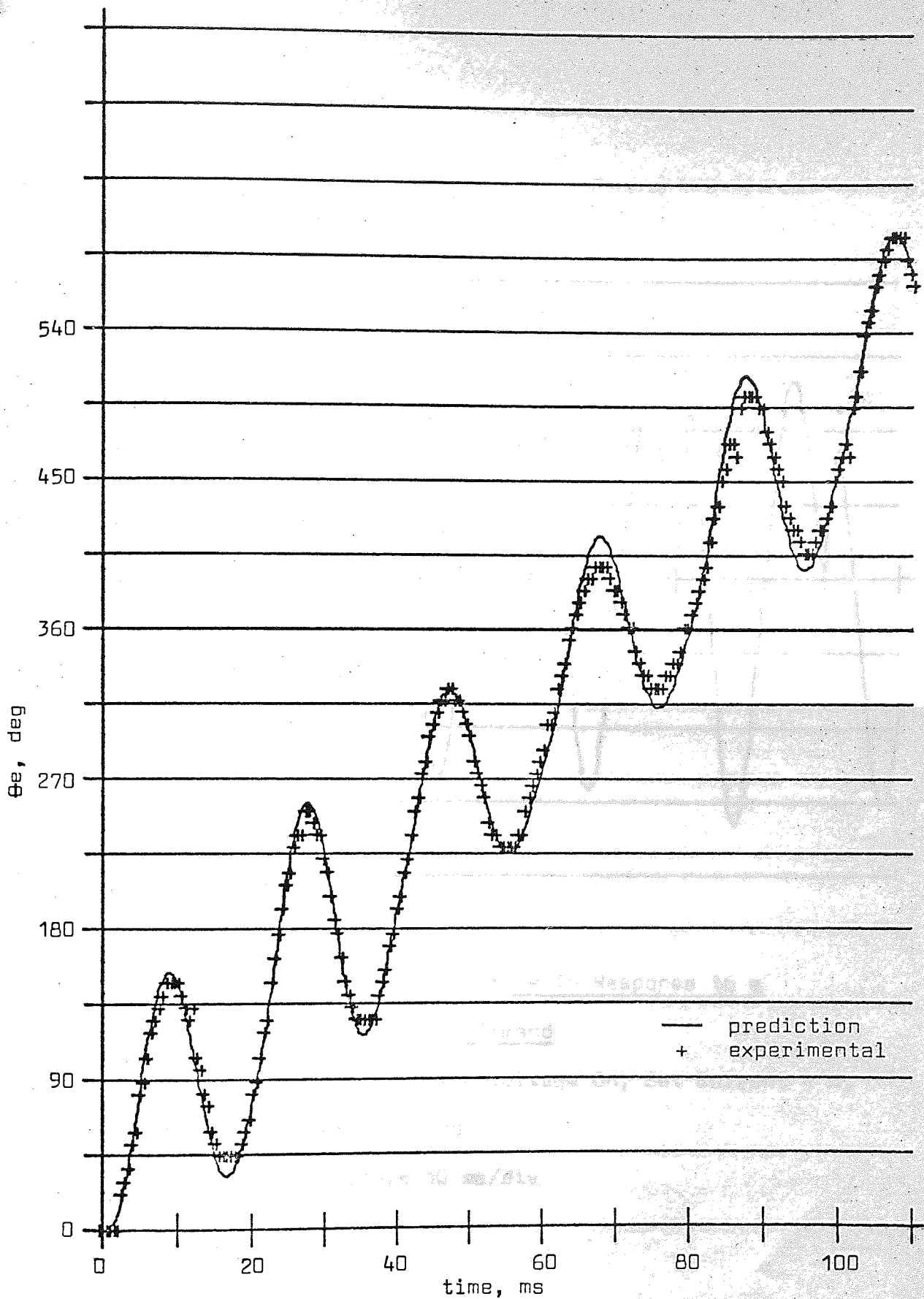


FIGURE 6.12 Multi-Stepping Response of Unloaded Rotor

50 s.p.s., High Voltage On, Set Current 4 A

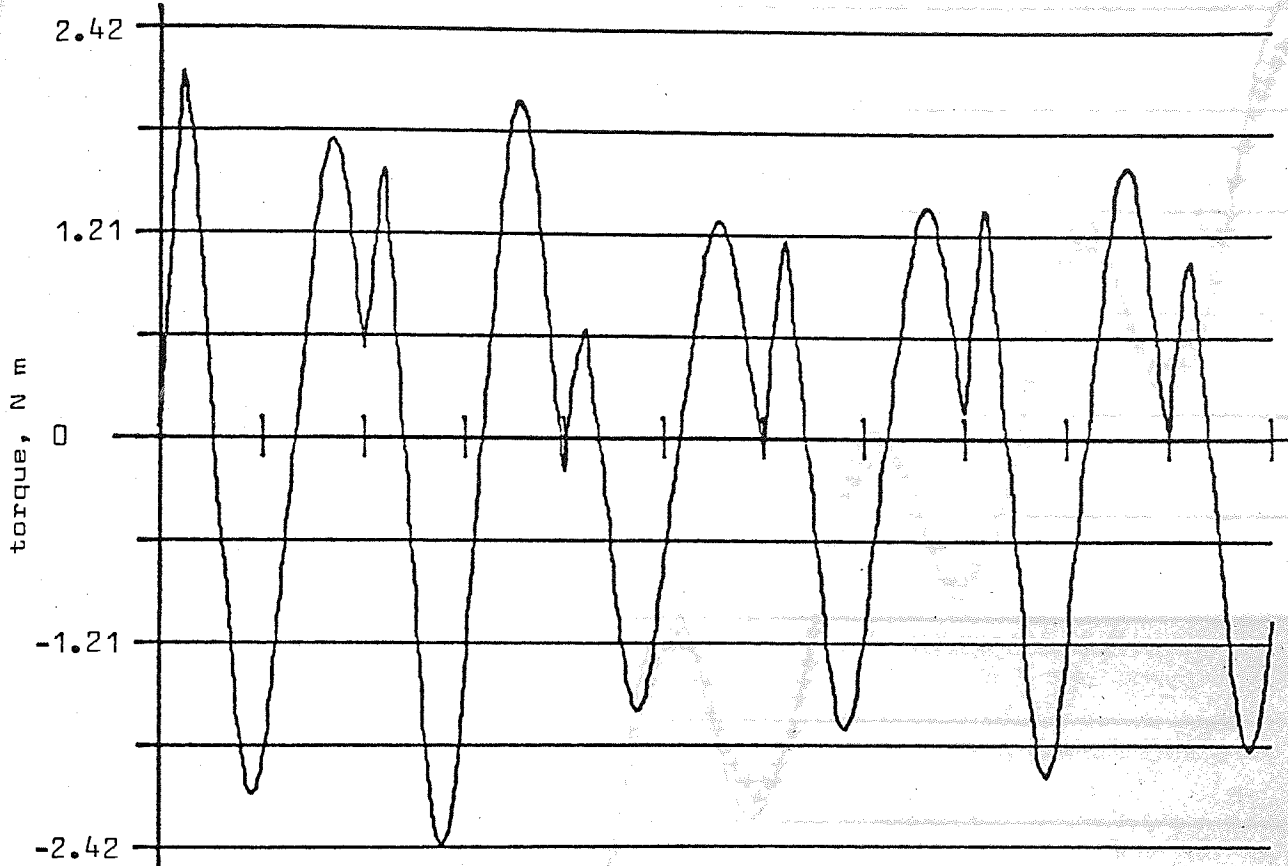


FIGURE 6.13 Prediction of Torque in Response to a Multi-Stepping Demand

50 s.p.s., High Voltage On, Set Current 4 A,
Rotor Unloaded

Time Scale 10 ms/div

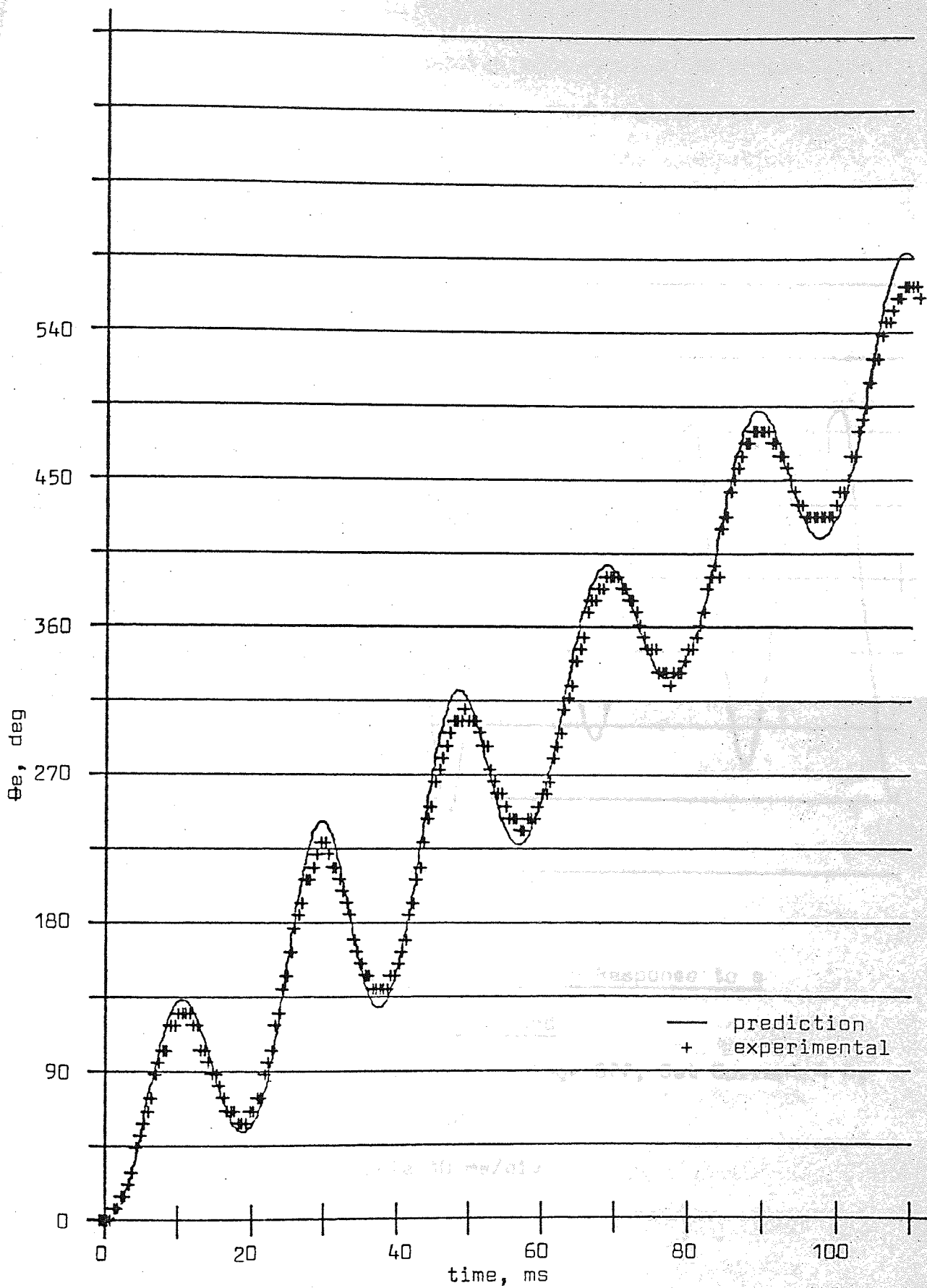


FIGURE 6.14 Multi-Stepping Response of Unloaded Rotor

50 s.p.s., High Voltage Off, Set Current 4 A

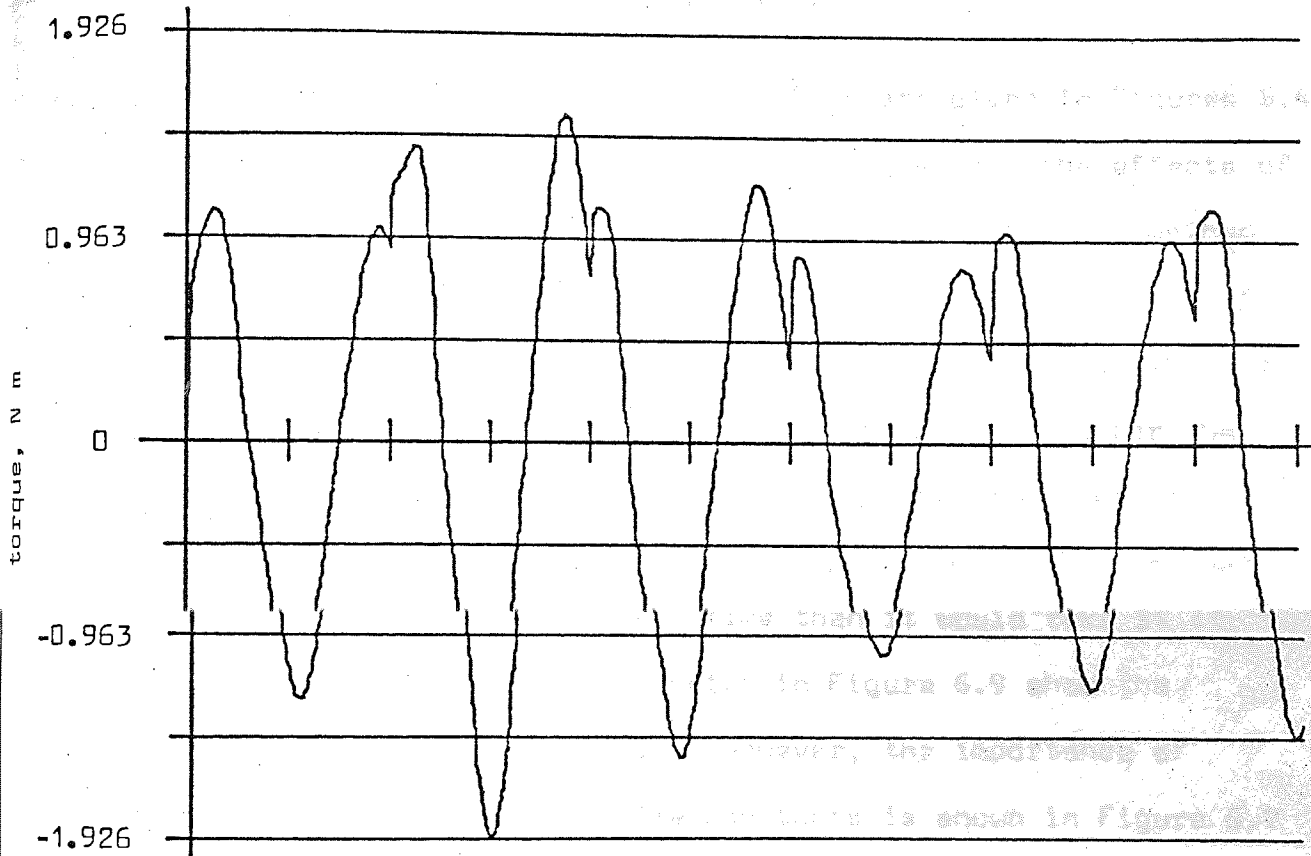


FIGURE 6.15

Prediction of Torque in Response to a
Multi-Stepping Demand

50 s.p.s., High Voltage Off, Set Current 4 A,
Rotor Unloaded

Time Scale 10 ms/div

6.5.1 Discussion

A sample of the results of stepping motor and drive simulations is presented by Figures 6.2 to 6.15. Such a sample is included to give an indication of the capability of the simulation package and to demonstrate its accuracy by comparing predicted and measured results of rotor dynamics.

Predictions of switch on current and flux are given in Figures 6.4 and 6.9. The results presented by Figure 6.4 show the effects of high voltage forcing and illustrate that, even with this method of drive, the eddy current time constant is important since, if current is the control parameter, the forcing is removed when it reaches its set value leaving the flux without forcing for the remainder of its change. It is of interest to note that the current overshoot predicted in Figure 6.4 is beneficial in that it establishes the flux in less time than it would take if it were absent. The results presented in Figure 6.9 show the predicted flux lag to be small. However, the importance of including the eddy current time constants is shown in Figure 6.7 where, the prediction of displacement with the time constants excluded is shown to be less accurate, when compared to the measured response, than when eddy current time constants are included. Figure 6.8 shows that the main cause for predicting a response with an initial rise which is too rapid, with eddy current time constants excluded, is that the prediction of the initial torque is much too high.

The effects of high voltage forcing are illustrated by the predictions of Figure 6.5 which shows the higher initial acceleration of the rotor and, in consequence, the higher peak overshoot. High voltage forcing produces a much higher peak

torque, as predicted in Figure 6.6, which gives rise to a more oscillatory response of the rotor. Such a response may not, of course, be desirable particularly when multi-stepping. It is for this reason that bilevel and chopper drive circuits generally give rise to more acute stability problems. This situation should be recognised in controller design where high voltage forcing should be used in combination with current control for optimum results. Multi-stepping predictions (Figures 6.12 to 6.15) illustrate again that higher peak torques and a more oscillatory response result from high voltage forcing.

6.6 Conclusions

To achieve reasonable accuracy, when predicting the dynamic performance of a stepping motor and drive, it is necessary to take account of the major non-linearities. This gives rise to a complex simulation which is only tractable with a computational aid. A digital simulation is proposed using the FORTRAN programming language. This offers both accuracy and computational efficiency.

It is shown that the mathematical and functional models of the stepping motor sub-systems can be represented by a digital simulation. Some types of non-linearities are approximated by making certain parameters, where necessary, dependent upon current and flux and updating the values of the parameters at each time step. Other types of non-linearity are represented by switching the value of certain parameters as a result of inspecting the value of other parameters. The resulting digital simulation is considered to be a powerful method of non-linear analysis.

The simulation yields predictions of displacement, for various input and loading conditions, which are shown to be reasonably accurate by comparison with the measured result. The requirement for the inclusion of eddy current effects is clearly illustrated.

of a stepping motor is that it

the use of an output

system does not, of

However, a large

of the

of the

of the

of the

of the

of the

of the rotor, this

at certain

being made of a

allowing, are a feature

the discrete nature of

which are in excess of the

in uniform motion. The

such that the average

of mechanics. This

of the time resulting in

are reduced by a

operation this can be

voltage or current, or an

7 CONTROL ASPECTS

7.1 Open-Loop

One of the major advantages of a stepping motor is that its output shaft may be positioned without the use of an output transducer and external feedback. Such a system does not, of course, adapt to unpredictable load changes. However, a large percentage of stepping motor applications involve fixed or predictable loads (37). An early contribution on the subject of the open-loop stepping motor was made by Bailey 38,39,40. He provides many examples of applications that are ideally suited to the open-loop stepping motor such as celestial trackers and drone controls.

The major difficulty of open-loop operation is due to the under-damped single step response of the rotor. This response gives rise to instabilities, or resonances, at certain stepping rates due, in the main, to step demands being made at a time when the rotor velocity is negative.

Oscillations in velocity, whilst slewing, are a feature of open-loop operation. They result from the discrete nature of the torque demand and peak torques which are in excess of the value required to keep the rotor in uniform motion. The rotor must, therefore, execute a motion such that the average torque is that required by the laws of mechanics. This demands that the torque is negative for part of the time resulting in oscillations in motion. Velocity oscillations are reduced by a reduction in peak torque demand. In normal operation this can be achieved by a reduction of voltage or current, or an increase in step rate.

The stator electrical time constant is responsible for the decrease in peak torque as the step rate increases. Kuo⁴¹ has observed that stable slow speed operation can be achieved by reducing the control voltage although he does not offer a reason for this behaviour.

The subject of damping has been given considerable attention in the literature (9,13,42,43,44). The object of this attention is to reduce resonance problems and velocity oscillation problems to a minimum. Kuo and Singh⁴² have contributed a comprehensive paper on the topic which covers viscous-inertia dampers, damping by electronic switching schemes and damping by modification of motor parameters. Damping methods which are not subject to controller action, such as viscous friction, inertia, viscous-inertia, electro-magnetic and eddy current, offer little advantage. These methods can reduce the settling time with the penalty, however, of an inevitable reduction in the speed of response thus limiting the acceleration of the rotor. If a reduction in the speed of response is acceptable then a decrease in settling time is often quite satisfactorily achieved, without recourse to elaborate damping methods, by using a less efficient drive circuit to provide a slow increase of stator current.

Electro-magnetic and eddy current methods lend themselves to the possibility of controller intervention to provide damping when necessary. Such methods are capable of achieving maximum accelerations with the suppression of the unwanted results of a lightly damped response when required. Other methods in this category are electronic back phasing (13) and delayed last step (13,42). Modification of machine parameters, to provide an inherent increase in damping, is not satisfactory since the speed

of response is sacrificed. It is preferable to provide a machine which has a lightly damped response, thus maximising the acceleration, and then to rely on controller action for any damping that is required.

For successful open-loop control an accurate system model is required in order that a controller may be designed to meet the system specification. It may be attractive to modify the machine in such a way that it behaves in a well defined manner, for example, by adding viscous-inertia dampers, but this usually results in abandoning beneficial characteristics of the machine resulting in an unsatisfactory system. Microprocessors offer the possibility of controlling a stepping system, in open-loop, by software implemented control schemes or by a combination of hardware and software control devices (45,46). Micro-stepping schemes (47,48) can be implemented to improve system accuracy and stability.

7.2 Closed-Loop

All closed-loop control schemes presented in the literature (49-55) use some method to determine when to apply the next position demand pulse. This is usually achieved by a slotted disc mounted on the output shaft with the number of slots normally equal to the number of steps per revolution of the motor. Photo-electric sensors are usually employed to provide the feedback pulses as the disc rotates between the sensors and a light source. The electrical angle that the step demand is in advance of the actual rotor position is known as the lead angle and may be adjusted by mechanical alignment of the sensors or by more elaborate methods. Under such a scheme the rotor moves at a velocity dependent upon

the drive circuit set current, lead angle and load conditions. The feedback method is a form of electronic commutation which causes the motor to satisfy the laws of mechanics by regulating its angular velocity.

Fredriksen^{49,50} was the first to propose closing the loop between the shaft position and input step demand by sensing discrete rotor angles with opto-electronic devices operating on a slotted disc coupled to the rotor shaft. Kuo et al.⁵¹ consider the effects of mechanical adjustment of lead angle and, in a later contribution, Kuo⁵² proposes pulse injection schemes to switch from acceleration to deceleration, and lead angle control by time-delayed feedback. Lead angle control, by such a method, is difficult since the angle is a function of both the time delay and the rotor angular velocity.

The main advantages offered by the closed-loop stepping motor are that it is load adaptive and, since it is not constrained to a particular stepping rate, its angular velocity is non-oscillatory. Its behaviour is similar to a d.c. motor and for applications where these characteristics are desirable it is often argued that a d.c. motor with shaft encoder is superior. Recent developments, however, in the field of closed-loop control of stepping motors without feedback encoders (53,54,55), may give the stepping motor the advantage in the closed-loop role. Feedback without encoders is achieved by stator current or voltage waveform sensing since these waveforms contain positional information.

7.3 Conclusions

The major advantage of a stepping motor is exploited when

operated in open-loop. Difficulties of this mode of operation can be minimised by controller design based upon an accurate system model. In order to maximise system performance it is, in general, preferable to modify the system response by controller intervention than by changing the inherent motor characteristics by fixed damping arrangements. Software implemented control schemes are feasible using microprocessors which offer the possibility of implementing sophisticated control schemes that are cost effective. In roles that demand the characteristics offered by the closed-loop stepping motor, d.c. motors, with shaft encoders, may offer a superior solution.

8 CONCLUSIONS

8.1 General

For successful performance predictions of a stepping motor system a comprehensive, non-linear, model is required. Such a model must take account of the effects of drive circuit characteristics, a non-linear torque displacement characteristic, eddy currents, stator inductance and generated e.m.f. Simplified and linearised models have a limited use since valid results are confined to small deviations about the null after a mechanical disturbance of the rotor. The comprehensive model gives rise to a complex simulation which is only tractable with a computational aid. A digital simulation is proposed using the FORTRAN programming language. This offers both accuracy and computational efficiency.

The performance of a stepping motor system is largely dependent upon the drive circuit employed to power the motor. For high speed, high efficiency systems it is necessary to use a bipolar circuit of either the bilevel or chopper type, switched by a two phase drive state generator.

For a given machine, the time constant and copper losses of the stator winding are independent of the number of turns in the winding space. Power losses in the drive circuit, on the other hand, are inversely proportional to the number of stator turns. It is shown that the overdrive voltage, in bilevel and chopper circuits, gives little advantage when it exceeds a level of ten times the rated stator voltage. For high system efficiency, therefore, stator windings should be wound with as many turns as possible consistent with not exceeding the voltage breakdown

characteristics of the drive transistors at ten times overdrive.

For accurate simulations of rotor dynamics, when full step demands are made, it is essential that the torque applied to the rotor is capable of accurate prediction. Linear torque displacement characteristics, sinusoidal approximations and direct addition of phase torques are poor models of the formulation of static torque. Physical considerations of torque production lead to the mathematical model proposed by Chai⁴ which predicts results that are observable in practice. A proposed development of this model has enhanced accuracy, due to the inclusion of extra Fourier components of permeance, and has the advantage that it can be used to predict static torque for any combination of phase currents. The prediction of dynamic torque is achieved by using time dependent displacement and normalised flux in place of steady state displacement and current. Normalised flux is defined such that it is compatible with the current used in the static case.

It is shown that the permeance coefficients, estimated from the measured static torque displacement characteristics have expected values, and compare favourably with permeance parameters estimated directly from the machine geometry. The estimation of the permeance coefficients directly from the machine geometry is shown to be feasible when the effects of magnetic saturation are minimal.

For the type of solid rotor machine investigated it is shown that the transfer function between stator voltage and air gap flux is not a simple, linear, first order function defined by stator resistance and inductance. Eddy currents, hysteresis and

saturation effects cause the transfer to be more complex with consequent difficulties in identification and simulation.

Eddy current effects can be approximated by assuming that the transfer between current and flux can be adequately described by a linear, one-zero, one-pole function. On the other hand, due to the effects of hysteresis and saturation, the inductance must be represented as a non-linear function of current. This is accomplished by defining the inductance as the average slope of the flux linkage-current loop at specific current amplitudes.

The transfer between voltage and flux is represented by a linear, one-zero, two-pole function at fixed values of current amplitude. The non-linearity is approximated by causing the inductance to be dependent upon the amplitude of the current perturbation passing through the stator windings.

It is shown that frequency response methods, in combination with average inductance measurements at specific current amplitudes, can, by using complex curve fitting techniques, yield linearised functions for the transfer between voltage and flux at specific current amplitudes.

It is shown that the mathematical and functional models of the stepping motor sub-systems can be represented by a digital simulation. Some types of non-linearities are approximated by making certain parameters, where necessary, dependent upon current and flux and updating the values of the parameters at each time step. Other types of non-linearity are represented by switching the value of certain parameters as a result of inspecting the value of other parameters. The resulting digital simulation is considered to be a powerful method of non-linear analysis.

8.2 Suggestions for Further Work

It is considered that an investigation into methods of estimating the effects of magnetic saturation upon the permeance coefficients will be useful. It is possible that by artificially increasing the air gap measurement, when calculating the permeance displacement characteristic, reasonable results can be obtained. It is likely that the factor by which the air gap is multiplied, for a given degree of saturation, will be established empirically. The inclusion of saturation effects will enable optimum tooth to valley ratios to be determined and will make feasible the estimation of the static torque displacement characteristic, from the machine geometry, at all levels of excitation.

The effects of a more realistic model of saturation and hysteresis on stepping motor performance predictions will be of interest. The representation of the non-linearity, to take account of its memory characteristic, together with the calculation of incremental inductance at each time step, may contribute to superior predictions of system performance.

Closing the loop between output position and input step demand does not, in general, offer any advantage over a d.c. motor with shaft encoder. It is considered, however, that closing the loop between shaft position and current demand will preserve the desirable characteristics of the open-loop stepping motor with the advantage that the system will be load adaptive and well damped.

Open-loop operation using microprocessor based controllers is an area where much useful work is possible. A system, based upon

look-up tables generated by the simulation program, and incorporating micro-stepping routines for enhanced stability and accuracy would seem to be a useful area of research.

APPENDICES

A SIMULATION SOFTWARE

A.1 Introduction

The stepping motor and drive is simulated by converting the mathematical and functional models of its sub-systems into digital computer software and then programming links to provide a simulation of the complete system. The simulation package is written in FORTRAN IV and implemented on a PDP-9/15 digital computer which has 24 k of core store supported by magnetic tape backing store. The simulations of the sub-systems are written in the form of subroutines which are called via a main program. This program links the subroutines to provide the overall system simulation. Other subroutines are provided which may be called by the user to provide outputs to the graph plotter and teletype if required. The program structure offers maximum flexibility to the user. The main object of the simulation is that it shall be employed in an interactive design role. A graphics display terminal will enhance this capability.

In accordance with the practice of the Digital Equipment Corporation (DEC) 'oh' and 'zero' are distinguished by writing 'zero' as \emptyset in all program flow charts, descriptions and listings.

A.2 Main Program

The listing of the main program is not included since its function is straightforward and is therefore adequately described with the

aid of the flow chart presented in Figures A.1 to A.7.

Stepping motor and drive data, the time interval to be used, when solving the discrete form of the system equations, and the total time to be simulated, are requested via the teletype. Subroutine RECAL2 is called which calculates the output parameters at each time step for the total simulation time. When this task is complete the results are returned to the main program in array form. The parameters that are available for output and their array names are given in Table XXIV.

TABLE XXIV Parameters Available as Outputs

Array Name	Output Parameter
THET	Displacement (rad) (Mechanical)
OMEG	Angular Velocity (rad/s) (Mechanical)
TORQUE	Torque (N m)
CUR	A Phase Current (A)
AFLUX	A Phase Flux (Wb)

The main program now calls Subroutine PLOTGR which allows the user to select the size of graph required and the X and Y co-ordinate marker intervals. When the graph axis and markers are plotted the subroutine returns to the main program with the graph size information. These data are required if the results are to be automatically scaled. The user may select automatic scaling, in which case the selected output parameter is scaled to fit the graph area; alternatively, the user may select to input a scale factor from the teletype.

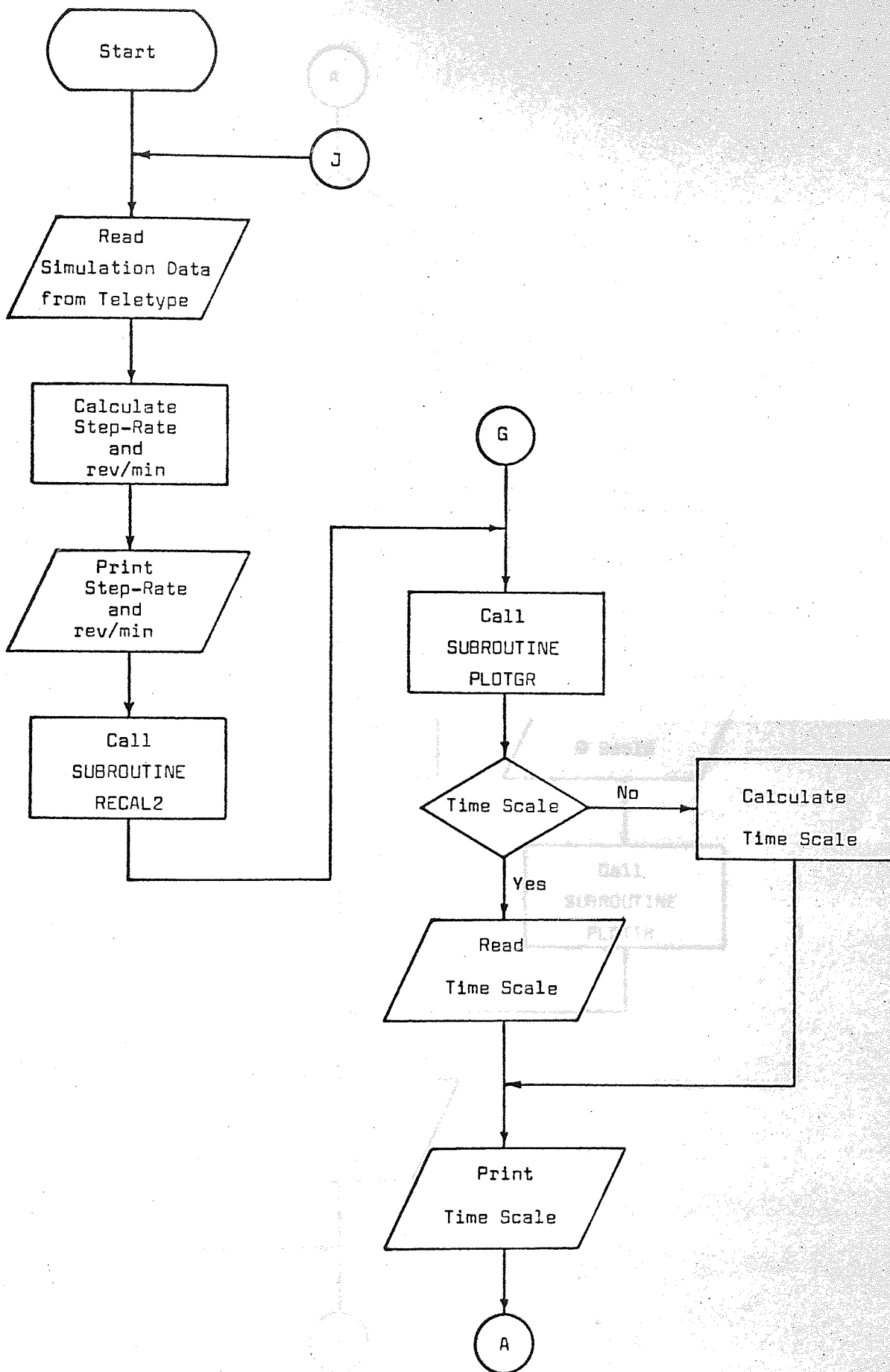


FIGURE A.1 Main Program Flow Chart - Part 1

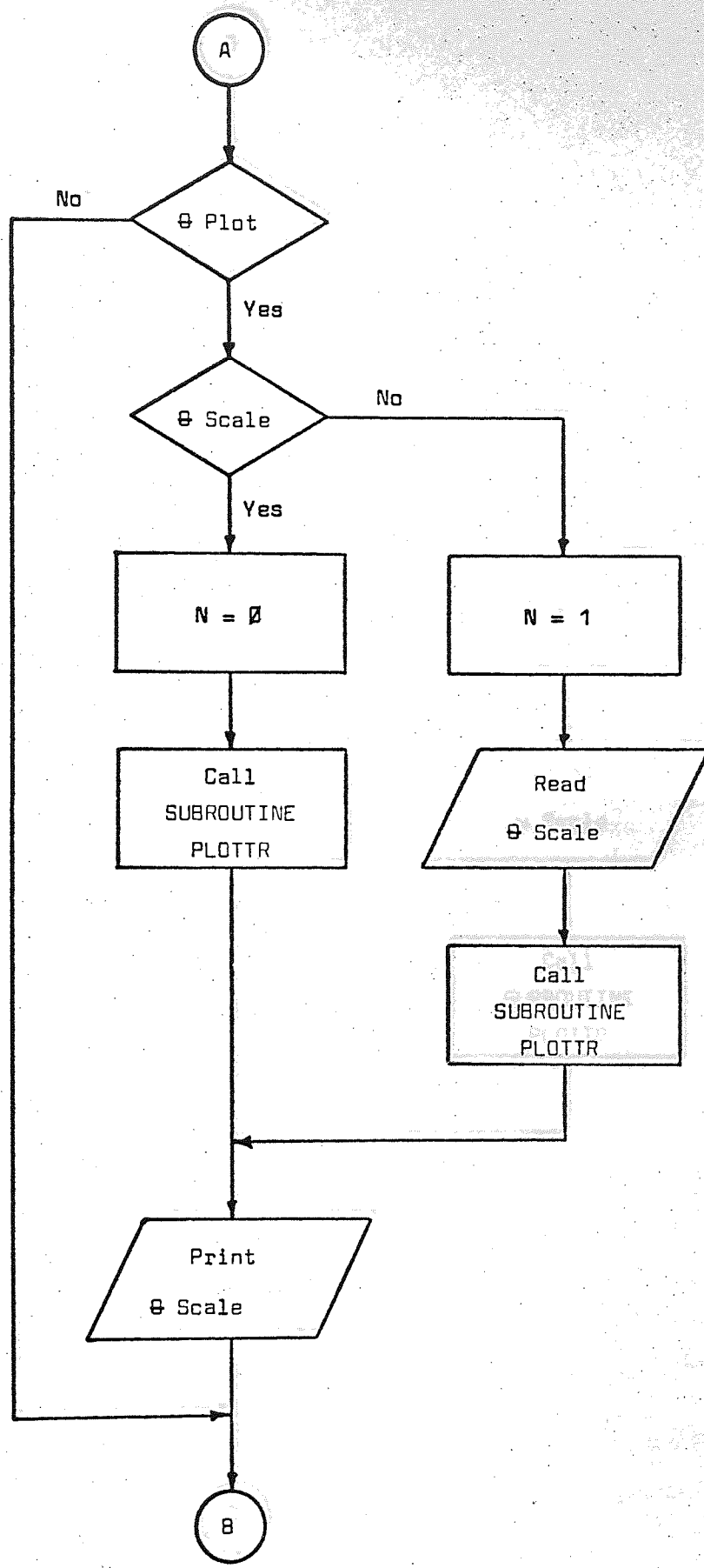


FIGURE A.2 Main Program Flow Chart - Part 2

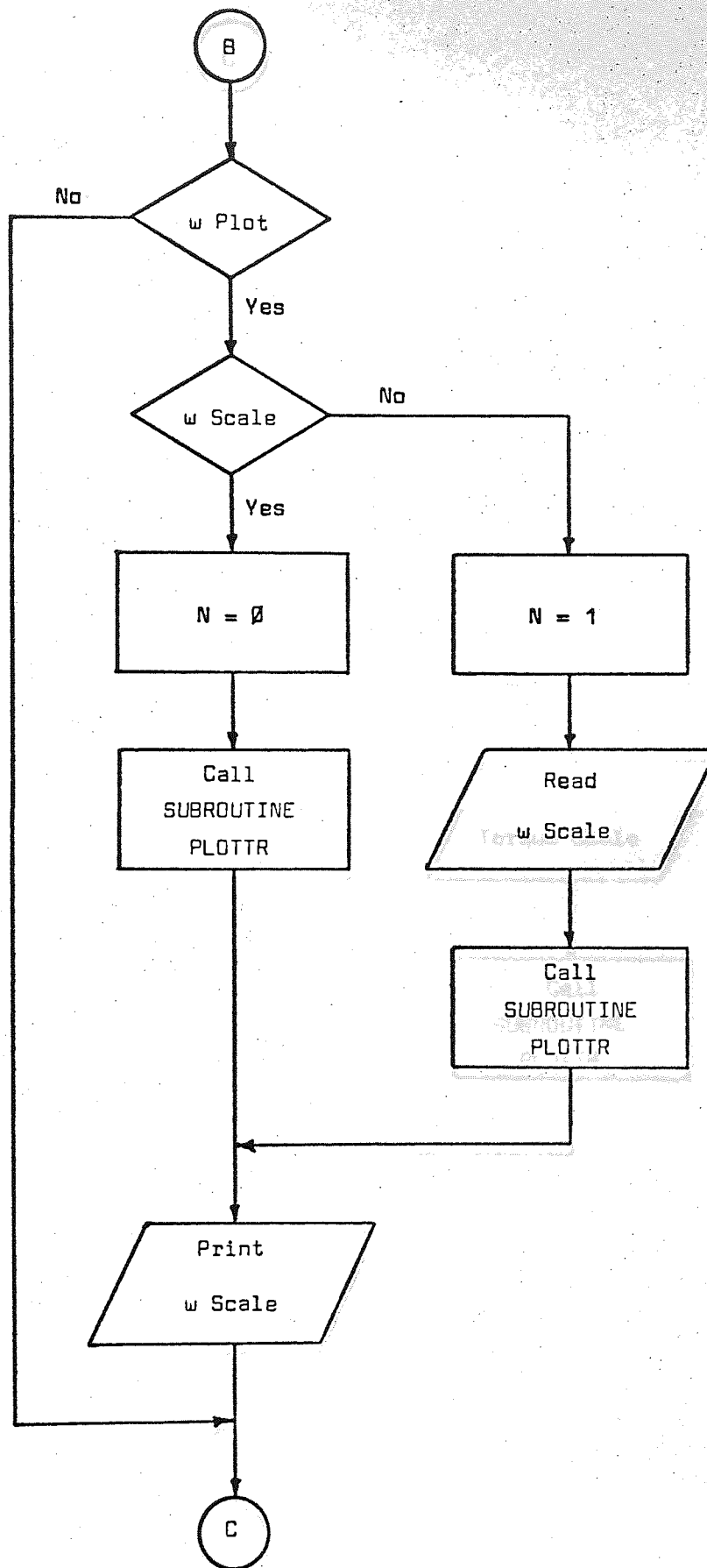


FIGURE A.3 Main Program Flow Chart - Part 3

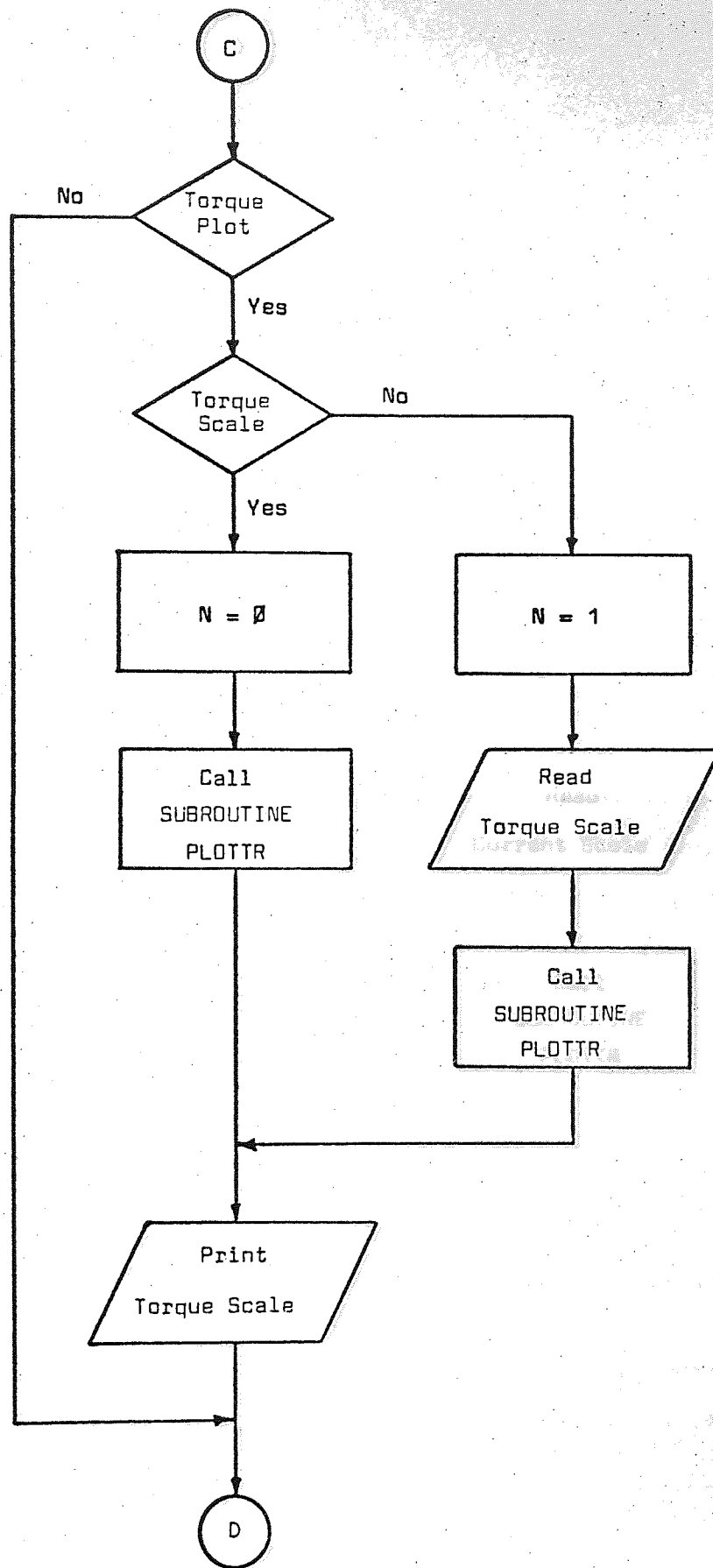


FIGURE A.4 Main Program Flow Chart - Part 4

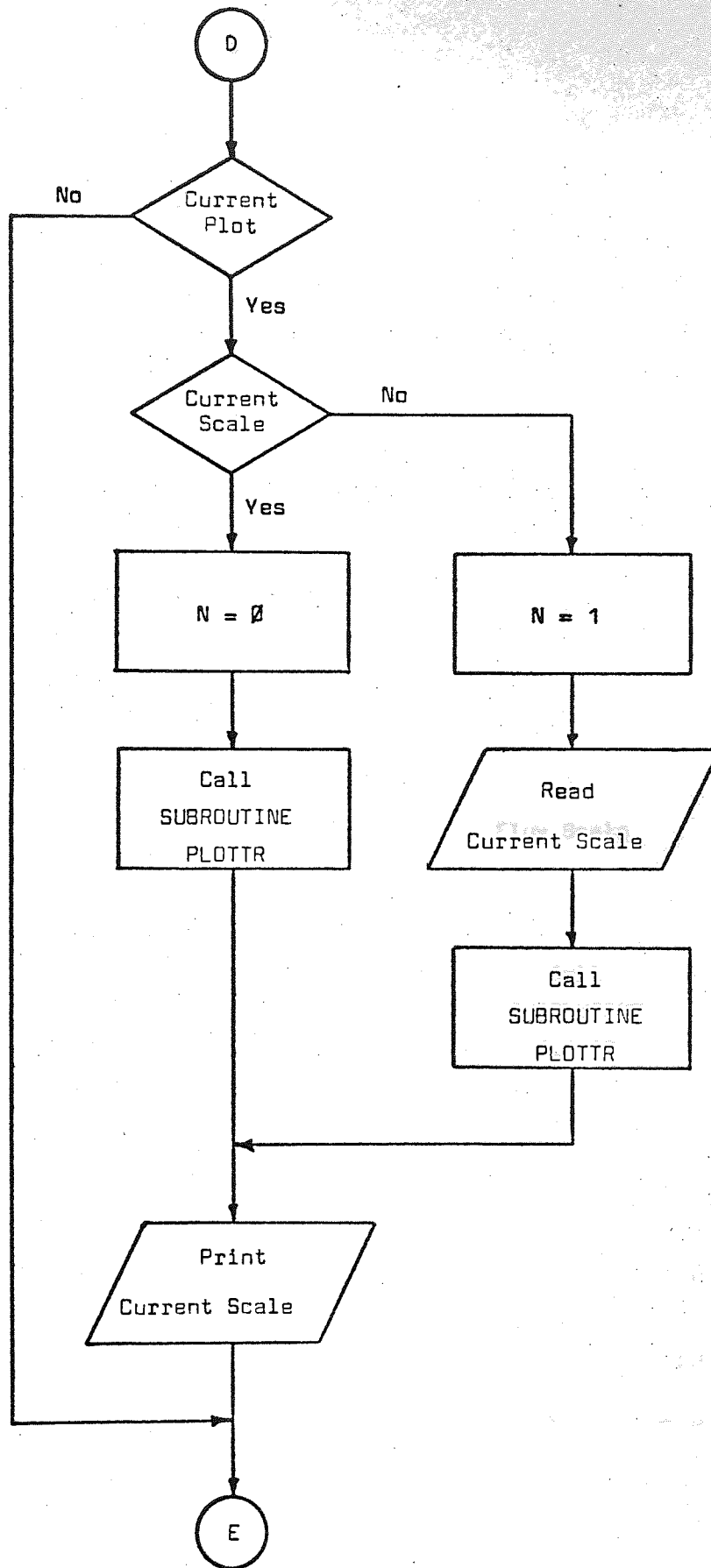


FIGURE A.5 Main Program Flow Chart - Part 5

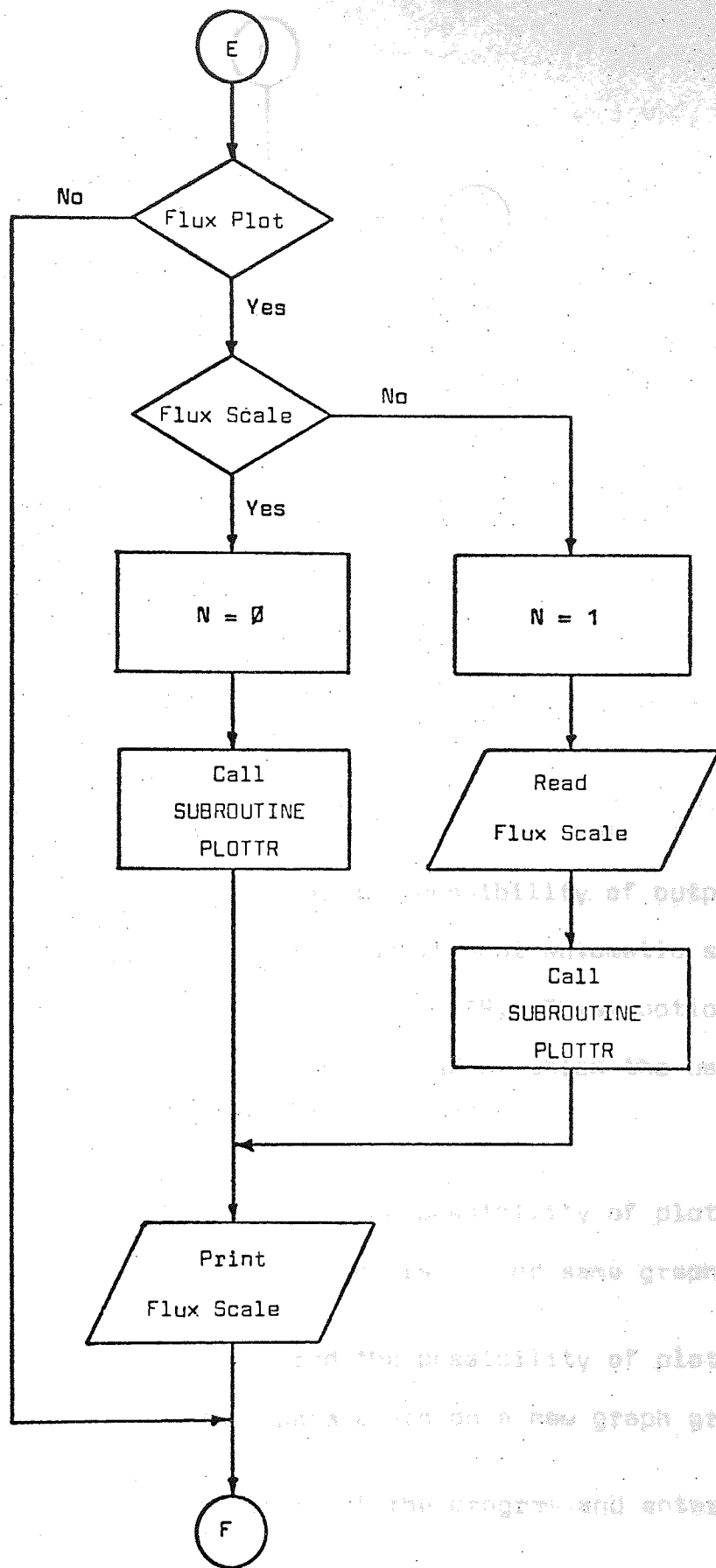


FIGURE A.6 Main Program Flow Chart - Part 6

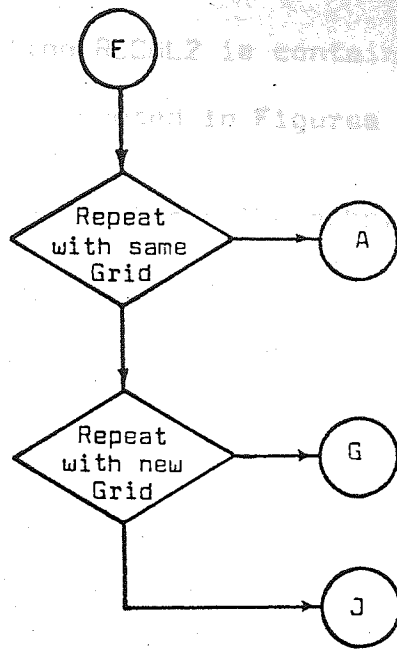


FIGURE A.7 Main Program Flow Chart - Part 7

The main program offers the user the possibility of outputting a set of calculated results, with or without automatic scaling, to the graph plotter via Subroutine PLOTTR. These options are offered on all five output parameters after which the user may select to :-

- (i) Return to be offered the possibility of plotting the five output parameters on the same graph grid.
- (ii) Return to be offered the possibility of plotting the five output parameters on a new graph grid.
- (iii) Return to the start of the program and enter new data.

A.3 Subroutine RECAL2

The listing of Subroutine RECAL2 is contained in Appendix B.1 and the flow chart is presented in Figures A.8 and A.9.

Variables are transferred between the subprogram and the main program via two COMMON statements; RES and REC2. The variables contained in these statements are listed in Tables XXV and XXVI respectively.

The object of the subprogram is to calculate the output parameters (Table XXIV) from the input data (Table XXVI), at discrete time steps, for the total simulation time requested and to return these results, in array form (Table XXV), to the main program. Subroutine CURCAL and TRIGTQ are called from the subprogram to enable values of current, flux and torque to be calculated at each time step.

Variables are initialised such that the initial conditions at the start of the simulation are :-

- (i) A phase current negative at a magnitude equal to the maximum value.
- (ii) B phase current positive at a magnitude equal to the maximum value.
- (iii) Rotor displacement at 45 electrical degrees.
- (iv) Rotor angular velocity at zero.

Subroutine CURCAL is called twice for initialisation. On the first call 'a' phase values are initialised and on the second call 'b' phase values are initialised. Subroutine TRIGTQ is then

TABLE XXV COMMON Statement RES

Variable Name	Variable
CUR (Array)	A Phase Current (A)
THET (Array)	Displacement (rad) (Mechanical)
AFLUX (Array)	A Phase Flux (Wb)
OMEG (Array)	Angular Velocity (rad/s) (Mechanical)
TORQUE (Array)	Torque (N m)

TABLE XXVI COMMON Statement REC2

Variable Name	Variable
T	Maximum Current (A)
FRIC	Viscous Friction Coefficient (N m s)
STEP	Time Step (s)
SLUG	Inertia (kg m ²)
J	Number of Times Steps to be Computed
NB	Switching Period as a Multiple of Time Step
FRIT	Coulomb Friction (N m)
RT	Number of Rotor Teeth
PIM	180.0/π

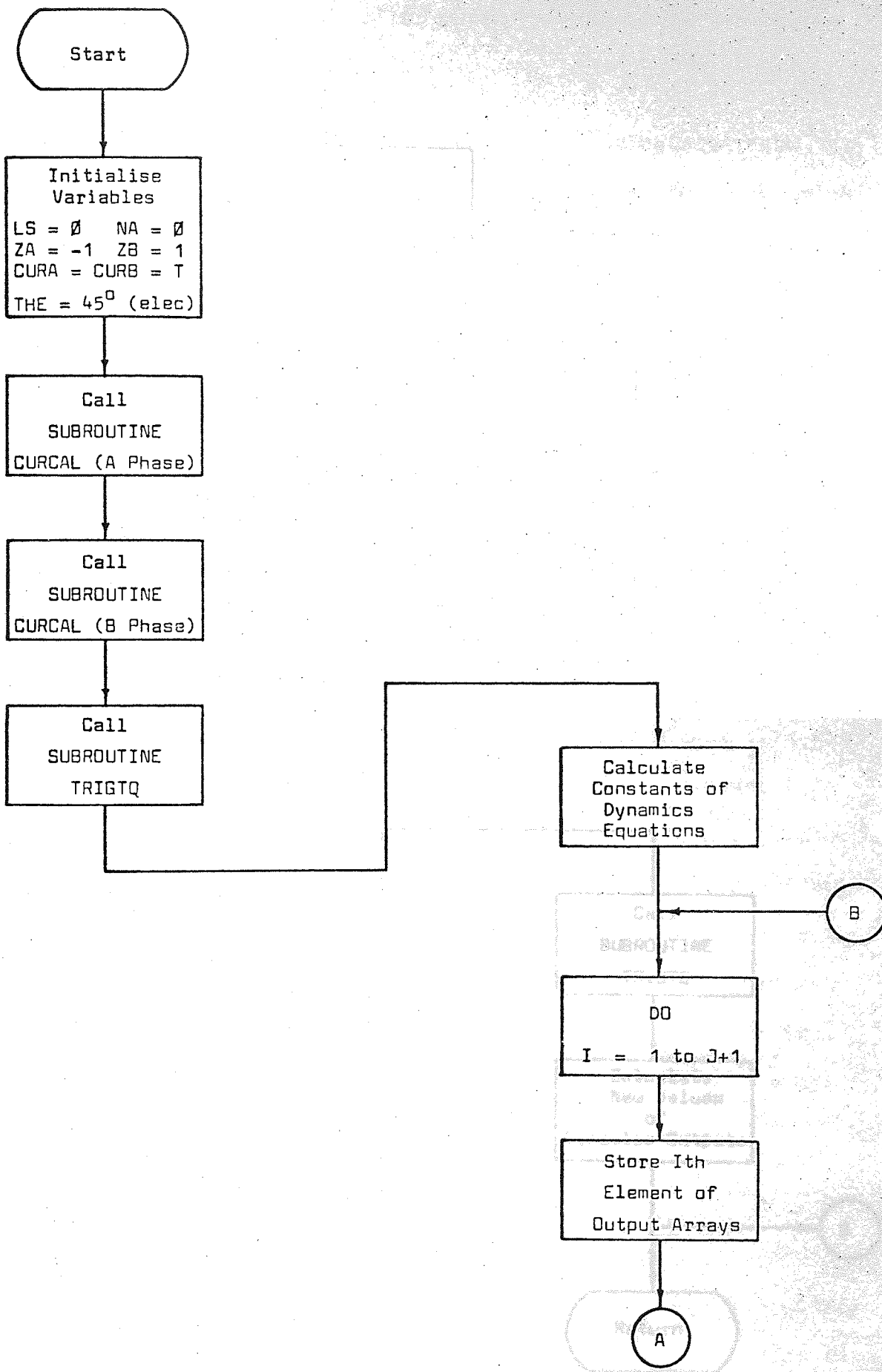


FIGURE A.8 Subroutine RECAL2 Flow Chart - Part 1

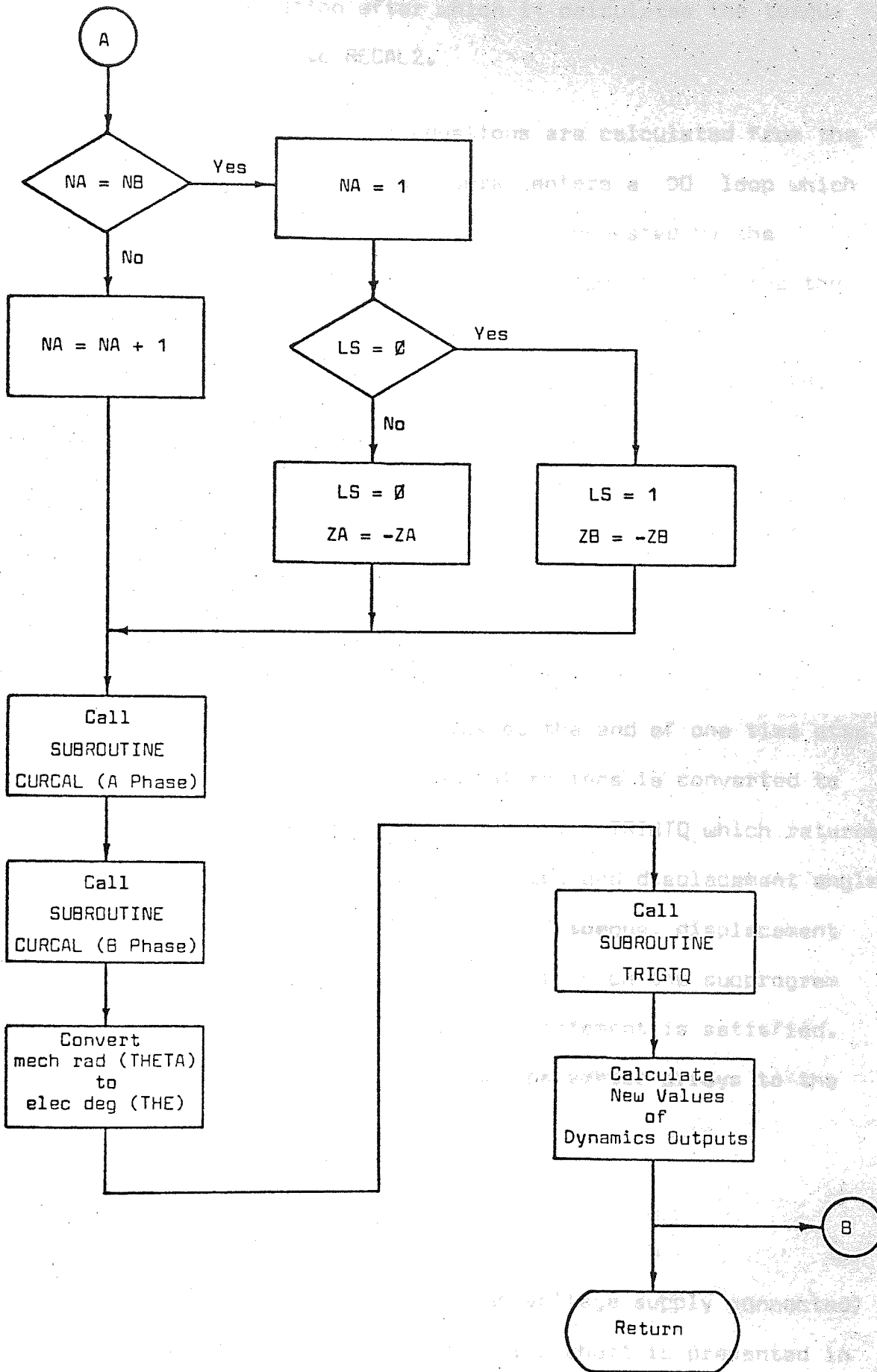


FIGURE A.9 Subroutine RECAL2 Flow Chart - Part 2

called for initialisation after which it calculates the torque and returns its value to RECAL2.

The constants of the dynamics equations are calculated from the input data, after which the subprogram enters a DO loop which is executed for the number of time steps requested by the user (J). Within the DO loop the first operation stores the Ith element of the output parameter arrays (Table XXIV). A current switch point is detected by the condition $NA = NB$. If the condition is satisfied NA is set to 1 and the phase to be switched is then established by testing FLAG LS. The FLAG is then set to switch the other phase at the next switch. The appropriate phase current direction indicator (ZA or ZB) is reversed, after which Subroutine CURCAL is called twice, first for 'a' phase and then for 'b' phase. The subprogram returns the values of phase current and flux at the end of one time step to RECAL2. Displacement in mechanical radians is converted to electrical degrees before calling Subroutine TRIGTQ which returns torque given normalised flux in each phase and displacement angle in electrical degrees. The new values of torque, displacement and angular velocity are calculated after which the subprogram executes a further loop until the DO statement is satisfied. The subprogram then returns the output parameter arrays to the main program.

A.4 Subroutine CURCAL

The listing of Subroutine CURCAL (high voltage supply connected) is contained in Appendix B.2 and the flow chart is presented in Figures A.10 and A.11.

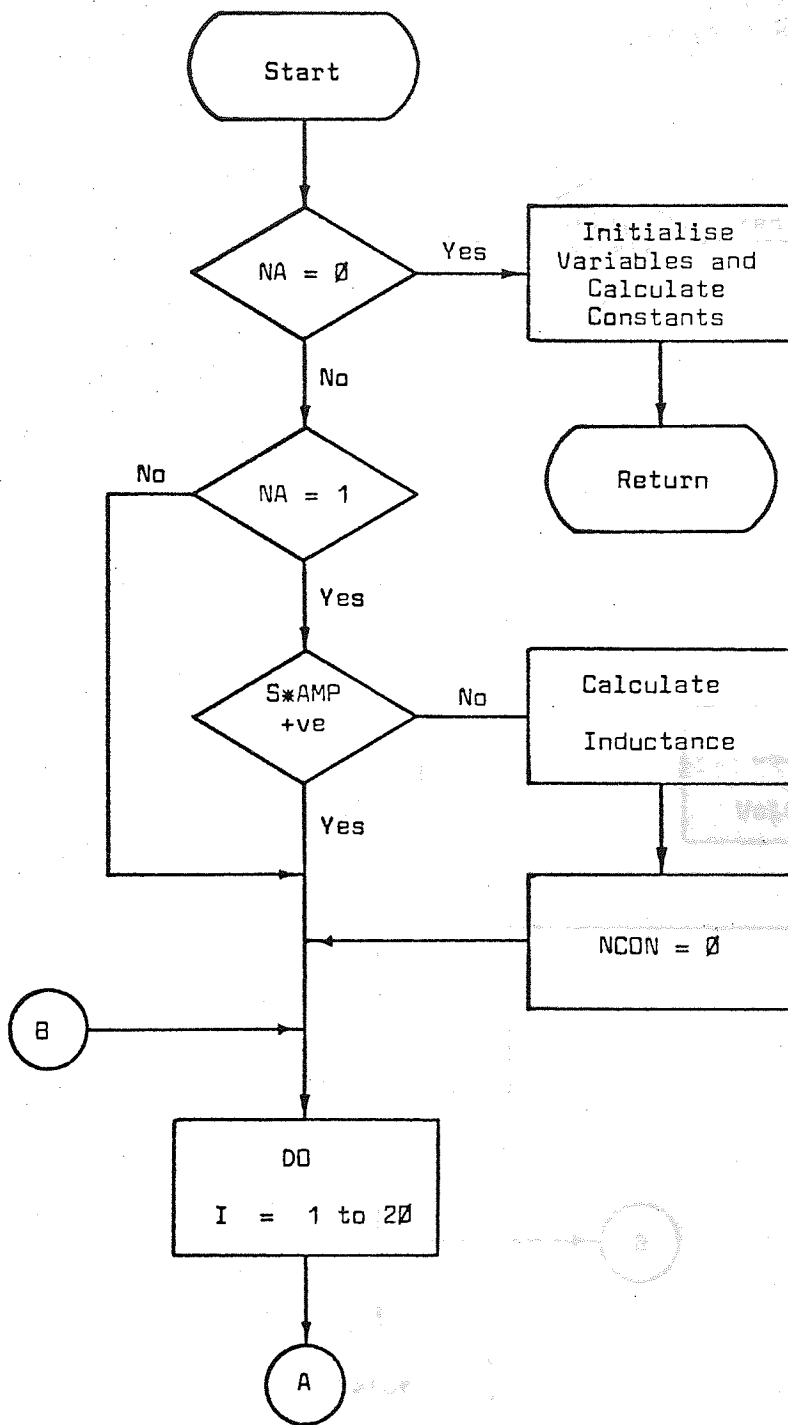


FIGURE A.10 Subroutine CURCAL Flow Chart - Part 1

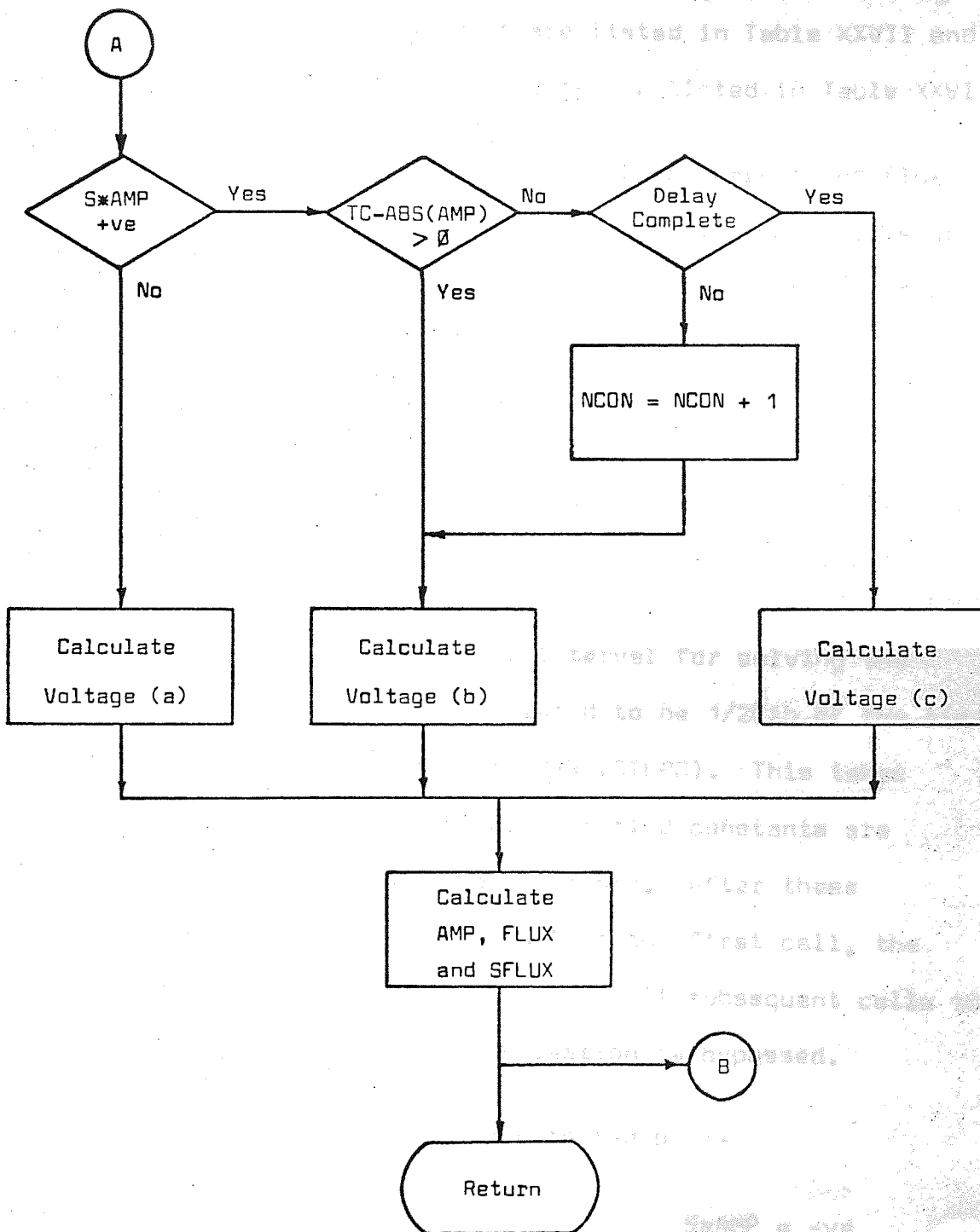


FIGURE A.11 Subroutine CURCAL Flow Chart - Part 2

Variables are transferred between the subprogram and the main program via COMMON statement CURR and between the subprogram and Subroutine RECAL2 by the subprogram arguments. The variables contained in the COMMON statement are listed in Table XXVII and the variables transferred as arguments are listed in Table XXVIII.

The object of the subprogram is to calculate current and flux from the input data (Tables XXVII and XXVIII). The results are returned to Subroutine RECAL2 at each time step. Drive circuit simulation is included with the effects of machine generated e.m.f. being taken into account.

The first call to the subroutine, for a particular phase, is detected by $NA = \emptyset$. The voltage to flux equations are initialised, parameters entered as data are defined and constants are calculated. The discrete time interval for solving the voltage to flux equations is calculated to be 1/20th of the time step entered via COMMON statement CURR (STEP). This takes account of the fact that the electrical time constants are smaller than the mechanical time constants. After these preliminary calculations, carried out at the first call, the subprogram returns to Subroutine RECAL2. At subsequent calls to the subroutine ($NA \neq \emptyset$) the initialisation is bypassed.

A demand for current switching is detected by :-

$NA = 1$ and $S*AMP = -ve$

If these conditions are met, the average inductance is calculated on the basis of the value of current attained at the last switch and the delay counter is set to zero.

A DO loop is entered which is executed 20 times before the

TABLE XXVII COMMON Statement CURR

Variable Name	Variable
V	Supply Voltage (V)
R	Stator Resistance (ohms)
TC	Maximum Current (A)
STEPC	Time Step (s)
TURNS	Number of Turns per Pole
RTC	Number of Rotor Teeth

TABLE XXVIII Subroutine CURCAL Arguments

Variable Name	Variable
OMEGA	Angular Velocity (rad/s)
THETA	Displacement (rad) (Mechanical)
AMP	Current (A)
S	Current Direction Demand
NA	Switch Status
X1, X2, X	States of State Space Equations
FLUX	Normalised Flux (Φ/K) (A)
SFLUX	Flux (Wb)
NCON	High Voltage Overshoot Time Counter

results for current and flux are returned to RECAL2. The results are, therefore, returned at every main program time step. Within the DO loop the voltage to flux state equations are solved. It is necessary, therefore, to determine the magnitude and direction of the voltage forcing function. There will be three possible conditions :-

- (a) High voltage transient, due to current reversal, modified by machine generated e.m.f.
- (b) Voltage of drive circuit supply modified by circuit IR drops, saturation characteristics of drive transistors and machine generated e.m.f.
- (c) Voltage limited to yield set current.

Condition (a) is indicated by the current being in the opposite sense to that demanded ($S*AMP = -ve$).

Condition (b) is indicated by the current being in the same sense to that demanded ($S*AMP = +ve$) but less than the set value ($ABS(AMP) < TC$).

Condition (c) is indicated by the current being in the same sense as that demanded ($S*AMP = +ve$), it being equal to, or greater than, the set value ($ABS(AMP) \geq TC$) and the delay time being complete. ($NCON \geq NDELAY$)

A.4.1 Subroutine derivatives

Two derivatives of Subroutine CURCAL have been written :-

- (i) LVCAL
- (ii) LRCAL

LVCAL simulates the drive circuit with high voltage supply disconnected.

LRCAL is a modified version of LVCAL changed to reduce the eddy current time constants to zero.

Descriptions of these derivatives have not been included, since the changes involved are minor.

A.5 Subroutine TRIGTQ

The listing of Subroutine TRIGTQ is contained in Appendix B.3 and the flow chart is presented in Figure A.12.

Variables are transferred between the subprogram and the main program via COMMON statement TRIG and between the subprogram and Subroutine RECAL2 by the subprogram arguments. The variables contained in the COMMON statement are listed in Table XXIX and the variables transferred as arguments are listed in Table XXX.

The object of the subprogram is to calculate torque from normalised flux in each phase and displacement angle in electrical degrees. The calculations are performed at each time step and the results returned to Subroutine RECAL2.

The first call to the subroutine is detected by $NA = \emptyset$. Parameters entered as data are defined and constants are determined. Permeance coefficients are then calculated. At subsequent calls to the subroutine ($NA \neq \emptyset$) the initialisation is bypassed and the permeance coefficients calculated directly.

To prevent a division by zero in the ATAN2 routine ABS(FA) is

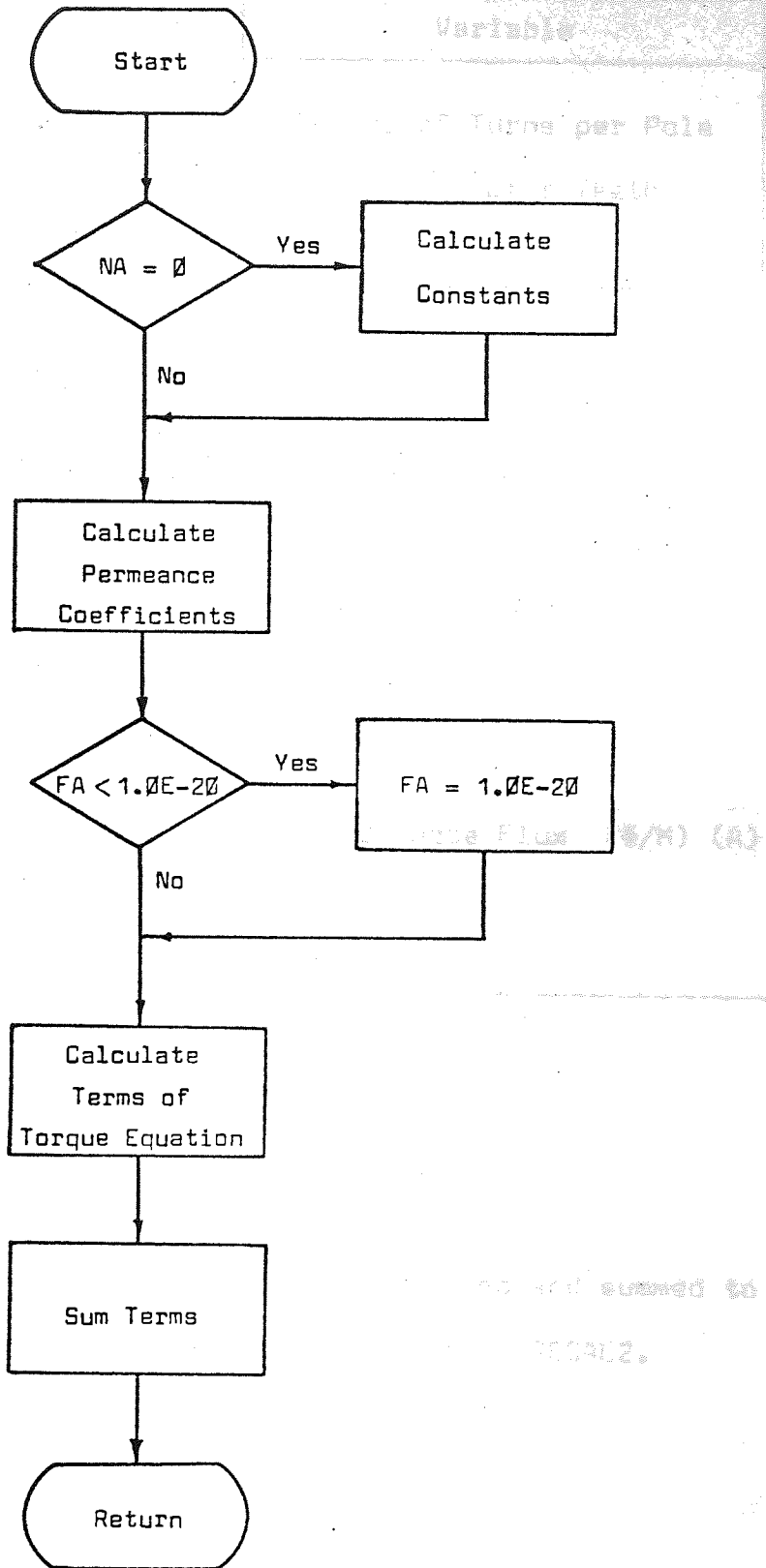


FIGURE A.12 Subroutine TRIGTQ Flow Chart

TABLE XXIX COMMON Statement TRIG

Variable Name	Variable
TURNT	Number of Turns per Pole
RTT	Number of Rotor Teeth
PI	π

TABLE XXX Subroutine TRIGTQ Arguments

Variable Name	Variable
ANG	Displacement Angle (deg) (Electrical)
FA	Normalised A Phase Flux (Φ/K) (A)
FB	Normalised B Phase Flux (Φ/K) (A)
TQ	Torque (N m)
NA	Switch Status

not allowed to be less than $1.0E-20$.

Terms of the torque equation are calculated and summed to yield torque which is then returned to Subroutine RECAL2.

A.6 Subroutine PLOTGR

The listing of Subroutine PLOTGR is not included since the subprogram is dependent upon non-standard software written for a specific graph plotter. The subprogram flow chart is presented in Figures A.13 and A.14.

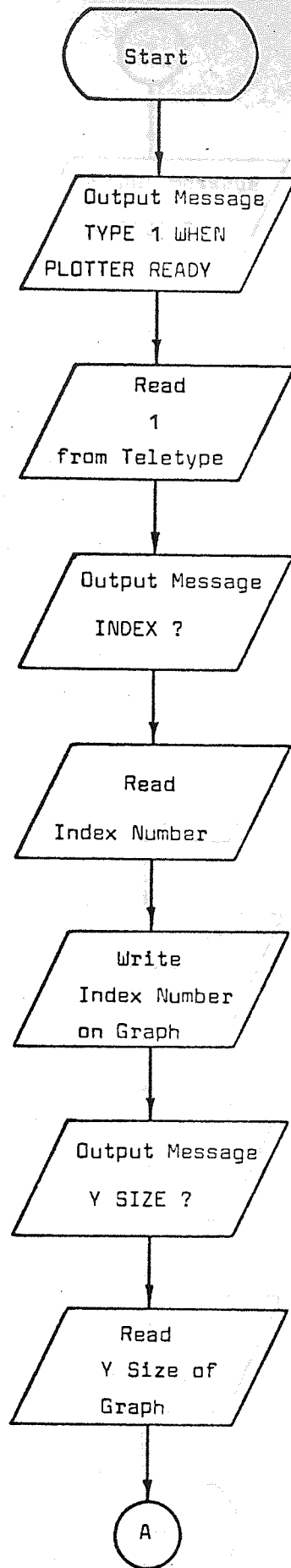


FIGURE A.13 Subroutine PLOTGR Flow Chart - Part 1

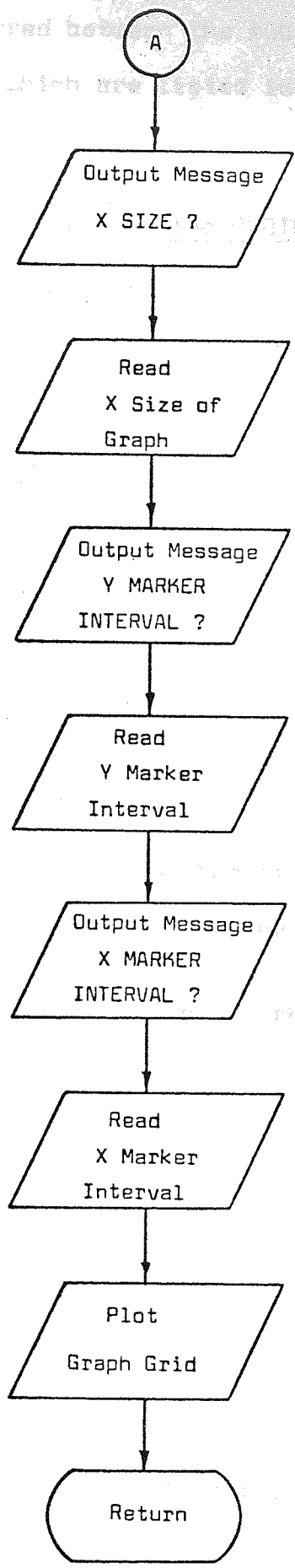


FIGURE A.14 Subroutine PLOTGR Flow Chart - Part 2

Variables are transferred between the subprogram and the main program via arguments which are listed in Table XXXI.

TABLE XXXI Subroutine PLOTGR Arguments

Variable Name	Variable
YS	Size of Graph in Y Direction (inches)
XS	Size of Graph in X Direction (inches)

The objects of the subprogram are :-

- (i) To halt the main program until the graph plotter is made ready.
- (ii) To request an index number from the user and plot that number on the graph sheet.
- (iii) To request graph size and marker information from the user.
- (iv) To plot the graph grid.
- (v) To return the graph size information to the main program.

A.7 Subroutine PLOTTR

The listing of Subroutine PLOTTR is not included since the subprogram is dependent upon non-standard software written for a specific graph plotter. The subprogram flow chart is presented in Figure A.15.

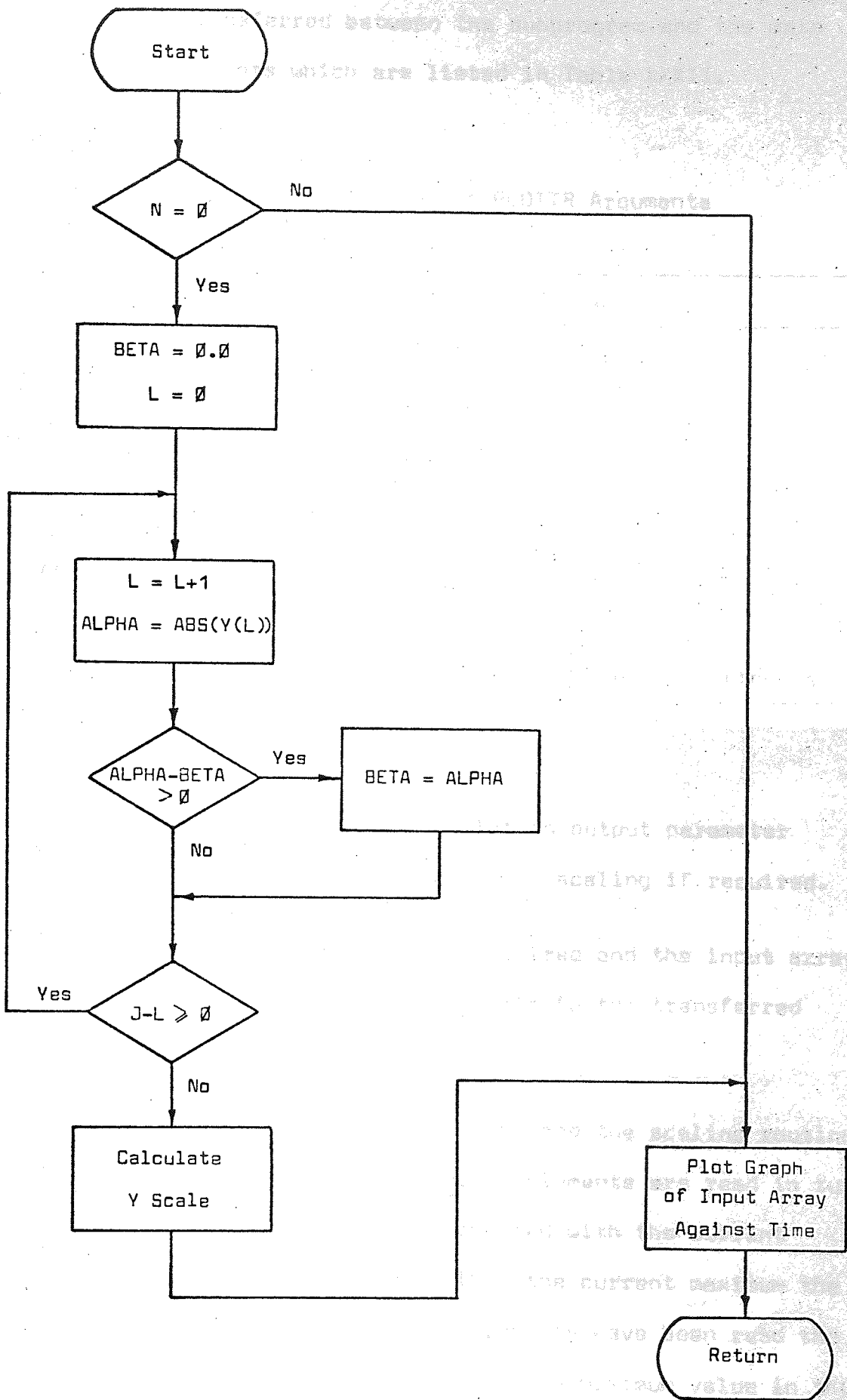


FIGURE A.15 Subroutine PLOTTR Flow Chart

Variables are transferred between the subprogram and the main program via arguments which are listed in Table XXXII.

TABLE XXXII Subroutine PLOTTR Arguments

Variable Name	Variable
Y (Array)	Output Parameter
J	Number of Time Steps Computed
YSCALE	Y Co-ordinate Scale
STEP	Time Step (s)
XSCALE	X Co-ordinate Scale
N	Automatic Scaling Flag
YS	Size of Graph in Y Direction (inches)

The object of the subprogram is to plot an output parameter against time and to provide automatic Y scaling if required.

If $N \neq \emptyset$ automatic scaling is not required and the input array is plotted against time using a Y scale factor transferred from the main program.

If $N = \emptyset$ automatic scaling is required and the scaling routine is entered. The output parameter array elements are read in turn and the absolute value of each is compared with the current maximum. If an element is greater than the current maximum the maximum value is updated. When all elements have been read the Y scale factor is calculated such that the maximum value in the array just fills the graph space.

B PROGRAM LISTINGS

B.1 Subroutine RECAL2

C SUBROUTINE TO CALCULATE THE TIME RESPONSES OF A HYBRID STEPPER MOTOR
C OPERATED IN TWO PHASE
C

```
SUBROUTINE RECAL2  
COMMON/RES/CUR(800), THET(800), AFLUX(800), OMEG(800), TORQUE(800)  
COMMON/REC2/T, FRIC, STEP, SLUG, J, NB, FRIT, RT, PIM  
LS=0  
NA=0  
CURA=T  
CURB=T  
ZA=-1.0  
ZB=1.0  
OMEGA=0.0  
DIC=45.0/(PIM*RT)  
THETA=DIC
```

C CONVERT MECHANICAL RADIAN TO ELECTRICAL DEGREES

```
THE=THETA*RT*PIM  
CALL CURCAL(OMEGA, THETA, CURA, ZA, NA, X1A, X2A, XA, FLUXA, SFLUXA, NCONA)  
CALL CURCAL(OMEGA, THETA-90.0/(PIM*RT), CURB, ZB, NA, X1B, X2B, XB,  
IFLUXB, SFLUXB, NCONB)  
CALL TRIGTQ(THE, FLUXA, FLUXB, TOR, NA)  
A=EXP(-(FRIC*STEP/SLUG))  
D=(1.0-A)/FRIC  
C=SLUG*D  
EM=(STEP-C)/FRIC  
DO 5 I=0, J  
K=I+1  
CUR(K)=CURA  
AFLUX(K)=SFLUXA  
THET(K)=THETA-DIC  
OMEG(K)=OMEGA  
TORQUE(K)=TOR  
IF(NB-NA)1,1,2  
2 NA=NA+1  
GOTO 3  
1 NA=1  
IF(LS)6,6,7  
7 LS=0  
ZA=-ZA  
GOTO 3  
6 LS=1  
ZB=-ZB  
3 CALL CURCAL(OMEGA, THETA, CURA, ZA, NA, X1A, X2A, XA, FLUXA, SFLUXA, NCONA)  
CALL CURCAL(OMEGA, THETA-90.0/(PIM*RT), CURB, ZB, NA, X1B, X2B, XB,  
IFLUXB, SFLUXB, NCONB)  
THE=THETA*RT*PIM  
CALL TRIGTQ(THE, FLUXA, FLUXB, TOR, NA)  
TOR=TOR-SIGN(FRIT, OMEGA)  
THETA=THETA+OMEGA*C+TOR*EM  
OMEGA=OMEGA*A+TOR*D  
5 CONTINUE  
RETURN
```


B.2 Subroutine CURCAL

```
C SUBROUTINE TO CALCULATE THE CURRENT AND FLUX TIME RESPONSE OF A
C HYBRID STEPPER MOTOR USING A 2 POLE 1 ZERO MODEL FOR THE TRANSFER
C BETWEEN INPUT VOLTAGE AND FLUX
C
C THE SUBROUTINE INCLUDES DRIVE CIRCUIT MODELLING
C (HV SUPPLY CONNECTED) AND SUBTRACTION OF MACHINE GENERATED EMF
C
C MACHINE AND DRIVE CIRCUIT PARAMETERS ARE INCLUDED AS DATA IN THIS
C SUBROUTINE. APPLICATION TO OTHER MACHINES AND DRIVE CIRCUITS WILL
C REQUIRE THESE PARAMETERS TO BE RE-DEFINED
C
      SUBROUTINE CURCAL(OMEGA, THETA, AMP, S, NA, X1, X2, X, FLUX, SFLUX, NCON)
      COMMON/CURR/V, R, TC, STEPC, TURNS, RTC
      IF(NA)7,7,8
      P2=0.00050
      TAU2=0.001
      RR=1.0/R
      SLOPE=0.71804462E-2+0.401609E-2*TC-0.94805687E-3*TC*TC
      1+0.62407058E-4*TC*TC*TC
      TAU1=(TAU2+SLOPE*RR-P2)*P2*R/SLOPE
      TA=TAU1/TAU2
      STEP1=0.05*STEPC
      X1=AMP*R
      X2=-(AMP*R*R)/SLOPE
      X=AMP*(1.0-TA)
      B=TAU2
      FLUX=AMP
      SFLUX=SLOPE*FLUX/(4.0*TURNS)
      NDELAY=IFIX(0.0002/STEP1)
      NCON=NDELAY
      RETURN
8      IF(NA-1)9,9,10
9      IF(S*AMP)13,10,10
13     TCA=ABS(AMP)
      SLOPE=0.71804462E-2+0.401609E-2*TCA-0.94805687E-3*TCA*TCA
      1+0.62407058E-4*TCA*TCA*TCA
      SRR=SLOPE*RR
      NCON=0
```

FORM PRODUCED BY A ...
... LACY PHASE ...

... WHICH ARE INCLUDED
... WILL

```
10 DO 2 I=1,20
    IF(S*AMP)3,4,4
    IF(TC-ABS(AMP))1,1,6
1   IF(NDELAY-NCON)11,11,12
12  NCON=NCON+1
    GOTO 6
11  VEF=S*TC*R
    GOTO 5
6   VEF=S*(V-(0.345*ABS(AMP)+2.0))-0.334*OMEGA*COS(RTC*THETA)
    GOTO 5
3   VEF=S*(V+5.0)-0.334*OMEGA*COS(RTC*THETA)
5   E=TAU2+SRR
    F=SRR*TAU1
    RF=1.0/F
    ERF=E*RF
    BRF=B*RF
    C=ERF*0.5
    D=SQRT(C*C-RF)
    ALPHA=-C+D
    BETA=-C-D
    A1=1.0/(ALPHA-BETA)
    EALPH=EXP(ALPHA*STEP1)
    EBETA=EXP(BETA*STEP1)
    FM11=A1*((ALPHA+ERF)*EALPH-(BETA+ERF)*EBETA)
    FM12=A1*(EALPH-EBETA)
    FM21=-RF*FM12
    FM22=A1*(ALPHA*EALPH-BETA*EBETA)
    BM11=BRF
    BM21=RF-ERF*BRF
    AIFI11=(-E*(FM11-1.0))-F*FM21
    AIFI12=-E*FM12-F*(FM22-1.0)
    AIFI21=FM11-1.0
    AIFI22=FM12
    GM11=AIFI11*BM11+AIFI12*BM21
    GM21=AIFI21*BM11+AIFI22*BM21
    X1P=X1
    X1=FM11*X1+FM12*X2+GM11*VEF
    X2=FM21*X1P+FM22*X2+GM21*VEF
    AMP=X1*RR
    EX=EXP(-(STEP1/TAU2))
    X=EX*X+(EX-1.0)*(TA-1.0)*AMP
    FLUX=X+TA*AMP
    SFLUX=SLOPE*FLUX/(4.0*TURNS)
2   CONTINUE
    RETURN
```

B.3 Subroutine TRIGTQ

C SUBROUTINE TO CALCULATE THE TORQUE PRODUCED BY A 2 PHASE HYBRID
 C STEPPER MOTOR GIVEN NORMALISED FLUX IN EACH PHASE AND DISPLACEMENT
 C ANGLE IN ELECTRICAL DEGREES
 C
 C THE CALCULATION IS BASED UPON MACHINE PARAMETERS WHICH ARE INCLUDED
 C AS DATA IN THIS SUBROUTINE. APPLICATION TO OTHER MACHINES WILL
 C REQUIRE THESE PARAMETERS TO BE RE-DEFINED
 C

```

SUBROUTINE TRIGTQ(ANG,FA,FB,TQ,NA)
COMMON/TRIG/TURNT,RTT,PI
IF(NA)3,3,4
3  PIR=PI/180.0
   RTTU=RTT*TURNT
   RTTU2=RTTU*TURNT
   PM=2.01E-7
   FM=6534.0
4  FABM=AMAX1(ABS(FA),ABS(FB))
   P0=(1.5159467+0.15325632*FABM-0.1857418E-1*FABM*FABM)*1.0E-6
   P0=P0-4.76E-9*ABS(FA*FB)
   P1=(0.80703295-0.34234272E-2*FABM-0.59586366E-2*FABM*FABM)*1.0E-6
   P2=(-0.10406602+0.10975104*FABM-0.30528913E-1*FABM*FABM+
10.23493571E-2*FABM*FABM*FABM)*1.0E-6
   P3=(0.28826619E-1+0.48555131E-3*FABM-0.43535661E-3*FABM*FABM)
1*1.0E-6
   P4=(0.12075269E-3+0.12320862E-2*FABM-0.60792603E-3*FABM*FABM
1+0.53025976E-4*FABM*FABM*FABM)*1.0E-6
   RANG=ANG*PIR
   SSQ=(FA*FA+FB*FB)
   RTSSQ=SQRT(SSQ)
   IF(ABS(FA)-1.0E-20)1,1,2
1  FA=1.0E-20
2  SHANG=ATAN2(FB,FA)
   RANGN=RANG-SHANG
   RANGP=RANG+SHANG
   A3=SIN(4.0*RANG)
   A11=P0*P0
   A1=RTTU2/A11
   A2=2.0*A1*P4*PM*FM*RTSSQ*A3/TURNT
   A4=COS(RANGN)
   A5=RTTU2*SSQ
   A6=RTTU*PM*FM*RTSSQ
   A7=A1*A3*(P4+P4)
   A10=RANG+RANG+RANG+SHANG
   A8=COS(A10)
   A9=P1/(P0+P0)
   A12=P1*A4
   A13=-4.0*A3*P4
   TM4=-((P2+P2)*RTTU2*(FA*FA-FB*FB)*SIN(RANG+RANG)
   TM8=P1*A9*A5*SIN(RANGN+RANGN)
   TM911=P1*P3/P0*A5*(A3*2.0+SIN(RANGP+RANGP))
   TM12=1.5*P3*P3/P0*A5*SIN(A10+A10)
   TM13=-A6*A9*SIN(RANGN)
   TM14=-1.5*A6*P3/P0*SIN(A10)
   TM1=-A12*A12*A7*SSQ
   TM2=-P3*P3*A7*A8*A8*SSQ
   TM3=-RTT*PM*PM*FM*FM/(A11+A11)*A3*P4
   TM5=A13*A5
   TM6=A13*A1*A4*P1*P3*SSQ*A8
   TM7=A2*A12
   TM10=A2*P3*A8
   TQ=TM1+TM2+TM3+TM4+TM5+TM6+TM7+TM8+TM911+TM10+TM12+TM13+TM14
RETURN
  
```

REFERENCES

- 1 PROCTOR, J.: 'Stepping motors move in', Production Engineering, 1963, 34, pp.74-78
- 2 THOMAS, A.G., and FLEISCHAUER, J.F.: 'The power stepping motor - a new digital actuator', Control Engineering, 1957, 4, pp.74-81
- 3 SNOWDON, A.E., and MADSEN, E.W.: 'Characteristics of a synchronous inductor motor', Trans. Am. Inst. Elec. Eng., 1962, 81, pp.1-5
- 4 CHAI, H.D.: 'Magnetic circuit and formulation of static torque for single-stack permanent magnet and variable reluctance step motors', Proceedings of the Incremental Motion Control Systems and Devices Symposium, University of Illinois, USA, 1973, pp.E-1 - E-18
- 5 O'DONOHUE, P.J.: 'Transfer function for a stepper motor', Control Engineering, 1961, 8, pp.103-104
- 6 KIEBURTZ, R.B.: 'The step motor - the next advance in control systems', IEEE Trans., 1964, AC-9, pp.98-104
- 7 ROBINSON, D.J., and TAFT, C.K.: 'A dynamic analysis of magnetic stepping motors', ibid., 1969, IECI-16, pp.111-125

- 8 PICKUP, I.E.D., and TIPPING, D.: 'method of predicting the dynamic response of a variable reluctance stepping motor', Proc. IEE, 1973, 120, (7), pp. 757-765
- 9 HUGHES, A., and LAWRENSON, P.J.: 'Electromagnetic damping in stepping motors', *ibid.*, 1975, 122, (8), pp. 819-824
- 10 BELING, T.E.: 'Permanent magnet step motors', Theory and Applications of Step Motors, (KUD, B.C., West, 1974), pp. 206-251
- 11 BELING, T.E.: 'High power output from a pm stepping motor', Proceedings of the Incremental Motion Control Systems and Devices Symposium, University of Illinois, USA, 1976, pp. I-1 - I-9
- 12 BELING, T.E.: 'Some effects of drive systems on stepping motor resonances', Proceedings of the International Conference on Stepping Motors and Systems, University of Leeds, England, 1976, pp. 125-131
- 13 MAGINOT, J., and OLIVER, W.: 'Step motor drive circuitry and open loop control', Proceedings of the Incremental Motion Control Systems and Devices Symposium, University of Illinois, USA, 1974, pp. B-1 - B-39
- 14 KORDIK, K.S., and SENICA, K.M.: 'Step motor selection', *ibid.*, 1974, pp. J-1 - J-26
- 15 LAWRENSON, P.J., HUGHES, A., and ACARNLEY, P.P.: 'Improvement and prediction of open-loop starting/stopping rates of stepping motors', Proc. IEE, 1977, 124, (2), pp. 169-172

- 16 JOHNSON,R.C.,and STEELE,M.E.: 'Some aspects of inverter driven closed loop stepping motor systems',Proceedings of the International Conference on Stepping Motors and Systems, University of Leeds,England,1974,pp.113-128
- 17 BAILEY,S.J.: 'Incremental servos,part II,operation and analysis',Control Engineering,1960,7,Dec.,pp.97-102
- 18 SINGH,G.: 'Mathematical modeling of step motors',Proceedings of the Incremental Motion Control Systems and Devices Symposium,Part 1,University of Illinois,USA,1972,p.60
- 19 JONES,C.V.: 'Unified theory of electrical machines', (Butterworths,1967),pp.21-23
- 20 CHAI,H.D.: 'Permeance model and reluctance force between toothed structures',Proceedings of the Incremental Motion Control Systems and Devices Symposium,University of Illinois, USA,1973,pp.K-1 - K-12
- 21 JONES,A.L.: 'Permeance model and reluctance force between toothed structures',ibid.,1976,pp.H-1 - H-8
- 22 CHAI,H.D.: 'Technique for finding permeance of toothed structures of arbitrary geometry',Proceedings of the International Conference on Stepping Motors and Systems, University of Leeds,England,1976,pp.31-37
- 23 HARRINGTON,R.F.: 'Field computation by moment method', (MacMillan,1968)

- 24 HARRINGTON, R.F., et al.: 'Computation of Laplacian potentials by an equivalent source method', Proc. IEE, 1969, 116, (10), pp. 1715-1720
- 25 SINGH, G., KUO, B.C., and MARION, R.: 'Dynamic modeling of permanent-magnet step motors', Proceedings of the Incremental Motion Control Systems and Devices Symposium, University of Illinois, USA, 1975, pp. E-1 - E-12
- 26 KORDIK, K.S.: 'Step motor inductance measurements', *ibid.*, 1975, pp. C-1 - C-10
- 27 PICKUP, I.E.D., and TIPPING, D.: 'Prediction of pull-in rate and settling-time characteristics of a variable-reluctance stepping motor and effect of stator-damping coils on these characteristics', Proc. IEE, 1976, 123, (3), pp. 213-219
- 28 LEVY, E.C.: 'Complex-curve fitting', IRE Trans., 1959, AC-4, pp. 37-43
- 29 SANATHANAN, C.K., and KOERNER, J.: 'Transfer function synthesis as a ratio of two complex polynomials', IEEE Trans., 1963, AC-8, pp. 56-58
- 30 PAYNE, P.A.: 'An improved technique for transfer function synthesis from frequency response data', *ibid.*, 1970, AC-15, pp. 480-483

- 31 NISHIMURA, M., MURAKAMI, Y., and KODAMA, Y.: 'Dynamic characteristics of a step motor represented as a nonlinear discrete time system', Elec. Eng. in Japan, 1971, 91, (2), pp. 101-109
- 32 KUO, B.C., SINGH, G., and YACKEL, R.: 'Modeling and simulation of a stepping motor', IEEE Trans., 1969, AC-14, pp. 745-747
- 33 SINGH, G.: 'Computer simulation of step motor systems', Theory and Applications of Step Motors, (KUO, B.C., West, 1974), pp. 106-119
- 34 PIERCE, B.D.: 'Sampled data modeling of stepper servos', Electromechanical Design, 1973, July, pp. 14-21
- 35 HUGHES, A., LAWRENSEN, P.J., STEELE, M.E., and STEPHENSON, J.M.: 'Prediction of stepping motor performance', Proceedings of the International Conference on Stepping Motors and Systems, University of Leeds, England, 1974, pp. 67-76
- 36 TRAMPOSCH, H.: 'Computer simulation of the bifilar-wound permanent-magnet step motor', Proceedings of the Incremental Motion Control Systems and Devices Symposium, University of Illinois, USA, 1975, pp. D-1 - D-14
- 37 KENT, A.J.: 'A step-motor controller for closed-loop investigation', ibid., 1975, pp. G-1 - G-15
- 38 BAILEY, S.J.: 'Incremental servos, part I, stepping vs stepless control', Control Engineering, 1960, 7, Nov., pp. 123-127

- 39 BAILEY,S.J.: 'Incremental servos,part III,how they've been used',*ibid.*,1961,8,Jan.,pp.85-88
- 40 BAILEY,S.J.: 'Incremental servos,part V,interlocking steppers',*ibid.*,1961,8,May,pp.116-119
- 41 KUO,B.C.: 'Control aspects of step motors',*Theory and Applications of Step Motors*,(KUO,B.C.,West,1974),pp.162-186
- 42 KUO,B.C.,and SINGH,G.: 'Damping methods of step motors',*ibid.*,pp.187-205
- 43 KENT,A.J.: 'An investigation into the use of inertia dampers on step-motors',*Proceedings of the Incremental Motion Control Systems and Devices Symposium,University of Illinois,USA,1973*, pp.G-1 - G-38
- 44 LAWRENSON,P.J.,and KINGHAM,I.E.: 'Viscously coupled inertial damping of stepping motors',*Proc.IEE*,1975,122,(10), pp.1137-1140
- 45 FRUS,J.R.: 'Hybrid computer control and data acquisition of step motors',*Proceedings of the Incremental Motion Control Systems and Devices Symposium,University of Illinois,USA,1973*, pp.S-1 - S-13
- 46 WELLS,B.H.: 'Microprocessor control of step motors',*ibid.*, 1976,pp.S-1 - S-9

- 47 FREDRIKSEN, T.R.: 'Micro-stepping - a new control concept for rotary step motors', *ibid.*, 1975, pp.HH-1 - HH-6
- 48 PRITCHARD, E.K.: 'Mini-stepping motor drives', *ibid.*, 1976, pp.Q-1 - Q-11
- 49 FREDRIKSEN, T.R.: 'Direct digital processor control of stepping motors', *IBM Journal*, 1967, March, pp.179-188
- 50 FREDRIKSEN, T.R.: 'Applications of the closed-loop stepping motor', *IEEE Trans.*, 1968, AC-13, pp.464-474
- 51 KUO, B.C., YACKEL, R., and SINGH, G.: 'Time-optimal control of a stepping motor', *ibid.*, 1969, AC-14, pp.747-749
- 52 KUO, B.C.: 'Closed-loop control of step motors', *Theory and Applications of Step Motors*, (KUO, B.C., West, 1974), pp.252-272
- 53 FERRARIS, P., VAGATI, A., and VILLATA, F.: 'Definition of a nonlinear control technique for dynamic performances improvement of p.m. stepping motors', *Proceedings of the Incremental Motion Control Systems and Devices Symposium*, University of Illinois, USA, 1976, pp.M-1 - M-12
- 54 FRUS, J.R., and KUO, B.C.: 'Closed-loop control of step motors without feedback encoders', *ibid.*, 1976, pp.CC-1 - CC-11
- 55 JUFER, M.: 'Self-synchronization of stepping motors', *Proceedings of the International Conference on Stepping Motors and Systems*, University of Leeds, England, 1976, pp.38-43

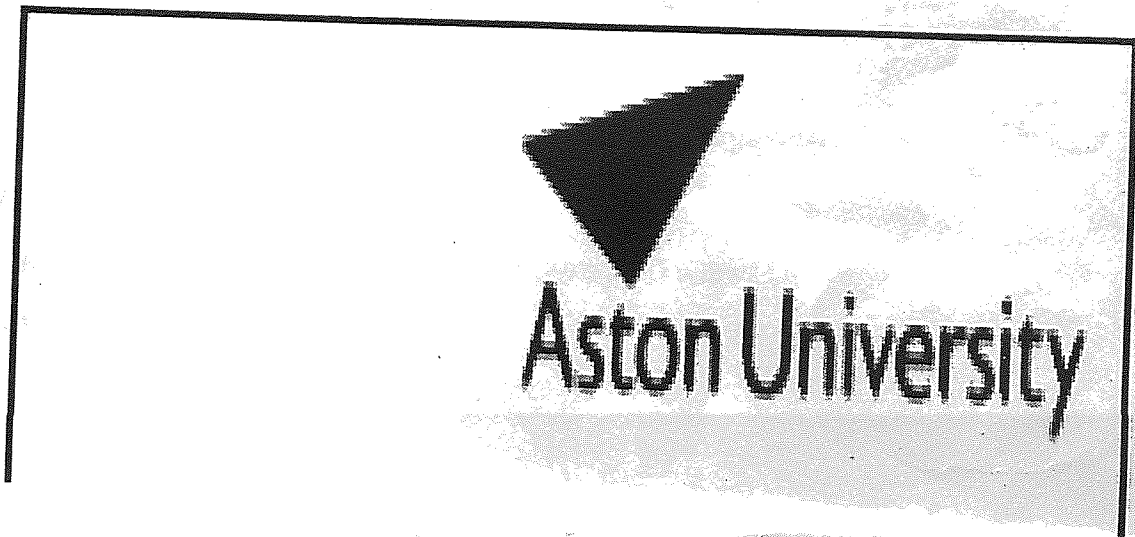
PUBLISHED WORK


MATHEMATICAL MODEL OF A HYBRID STEPPER MOTOR AND DRIVE CIRCUIT

The following publications are deemed to support the application.

1 JOHNSON,R.C.,and JUSTICE,M.: 'Mathematical model of a hybrid stepper motor and drive circuit',Proceedings of the Incremental Motion Control Systems and Devices Symposium, University of Illinois,USA,1975,pp.K-1 - K-14

2 JOHNSON,R.C.,and JUSTICE,M.: 'Transfer function prediction of a hybrid stepper motor',Proceedings of the International Conference on Stepping Motors and Systems,University of Leeds,England,1976,pp.139-149



 Aston University
Content has been removed for copyright reasons